ANALYSIS OF A JOINT DEGENERATION MODEL AND DEGRADABLE CRANIOFACIAL SCREWS IN THE RABBIT TEMPOROMANDIBULAR JOINT

by

Sarah Elizabeth Henderson

B.S. in Biomedical Engineering, Bucknell University, 2008

Submitted to the Graduate Faculty of

Swanson School of Engineering in partial fulfillment

of the requirements for the degree of

Doctor of Philosophy

University of Pittsburgh

2014

UNIVERSITY OF PITTSBURGH

SWANSON SCHOOL OF ENGINEERING

This dissertation was presented

by

Sarah Elizabeth Henderson

It was defended on

July 3, 2014

and approved by

Steven D. Abramowitch, Ph.D., Assistant Professor, Department of Bioengineering

Harvey S. Borovetz, Ph.D., Professor, Department of Bioengineering

Michael S. Gold, Ph.D., Professor, Department of Anesthesiology

Scott Tashman, Ph.D., Associate Professor, Department of Orthopaedic Surgery

Dissertation Director: Alejandro J. Almarza, Ph.D., Assistant Professor, Departments of Oral Biology and Bioengineering

ANALYSIS OF A JOINT DEGENERATION MODEL AND DEGRADABLE CRANIOFACIAL SCREWS IN THE RABBIT TEMPOROMANDIBULAR JOINT

Sarah Elizabeth Henderson, Ph.D.

University of Pittsburgh, 2014

To reduce the impact of temporomandibular joint (TMJ) disorders (TMDs), the primary goals are to eliminate pain and restore joint function. However, with the limitations of current treatment options reaching these goals remains elusive. Limitations of current approaches include diagnostic evaluation, missing the early signs of the disease, and recurring pain. There is also difficulty with device fixation, permanent metals implanted, and device life expectancy. To begin addressing some of these limitations and goals, the specific aims of this dissertation focused on the use of altered joint occlusion to gain a better understanding of a TMD model using fibrocartilage, pain, and joint kinematic assessments and testing magnesium as a biodegradable screw in the craniofacial region. From the altered occlusion model, a connection between the compressive properties of TMJ condylar fibrocartilage after 6 weeks of altered loading and changes in histology was observed. Behavioral and anatomical pain assessment results were consistent with an increase in nociceptive signaling, while changes in excitability and action potential waveform were consistent with compensatory changes of TMJ afferents for an overall increase in afferent drive associated with joint degeneration. With the development of the kinematic assessment for the TMJ, repeatable measurements for both translations and movement paths were found for both the incisors and the motion of the condyle relative to the fossa in rabbits. An overall decrease in the range of joint motion was observed at the incisors and in the joint space, with the altered occlusion model. These results suggest a change in joint

occlusion, leads to condylar damage, which may contribute to pain associated with at least some forms of TMJ disease. Craniofacial bone remodeling occurred around two magnesium alloy screw types, indicating the promise of using magnesium alloys for craniofacial devices. Due to the essential function of the TMJ for everyday living, the knowledge gained in this dissertation will provide a better understanding of TMDs and improve treatment options.

TABLE OF CONTENTS

LIST OF TABLES

LIST OF FIGURES

PREFACE

I would like to start by thanking my Ph.D. advisor Dr. Alejandro Almarza. His patience, guidance, friendship, and mentorship over the past six years have been invaluable. I also want to thank everyone who has been associated with the TMJ Labs and the Center for Craniofacial Regeneration during my time here at Pitt for their friendship and support. There are too many people to name here, but I appreciate each and every one. The one person I would like to specifically acknowledge is Mauro Tudares, for all his help with the animals; without him these projects would have been much harder to complete. I would also like to thank all of my committee members for their guidance over the years on various aspects of my projects: Dr. Abramowitch, Dr. Borovetz, Dr. Gold, and Dr. Tashman. I would like to acknowledge all of the co-authors on my publications for their contributions to this work.

I would also like to acknowledge my funding sources, without which I would not have been able to complete the work necessary for this dissertation. The funding sources include an NIH T-32 training grant for Biomechanics in Regenerative Medicine under grant number T32 EB003392, support from the NSF Engineering Research Center on Revolutionizing Metallic Biomaterials under grant number 0812348, the University of Pittsburgh Research Fund, and the University of Pittsburgh School of Dental Medicine.

Lastly, but perhaps most importantly, I would like to acknowledge my family and friends for their support. They have helped to keep me sane and focused through the ups and downs of

grad school. I would especially like to thank my parents, Linda and Randy, for their unconditional love and support not only through my years here at Pitt, but throughout my entire life. I would also like to thank my brothers Matt, Mark, and Daniel for being there when I needed some sibling love, support, and friendship. To all of my friends, and especially Ben – thank you for everything!

1.0 INTRODUCTION

1.1 MOTIVATION

Pain associated with temporomandibular disorders (TMDs) impacts 3 to 7% of the adult population [24], lowering the quality of life for those who suffer and imposing a significant financial burden on society in the form of health care costs, disability and lost productivity. Even with the multitude of associated signs and symptoms and epidemiological studies presenting large numbers of cases, there is still a large gap in knowledge with the identification and treatment of TMDS. Life can become difficult for those severely affected by a TMD; daily activities such as talking, laughing, yawning and eating can become very painful, and personal life and work often suffer [48, 85, 115]. Currently, there are no consistently effective interventions for TMD pain relief devoid of deleterious side effects. Thus, the need for effective ways to reduce the impact of these disorders is significant.

The long term goal of this research is to reduce the impact of TMDs through pain elimination and restoring joint function. Limitations of current treatment options include lack of a long term solution, recurring pain, missing the early signs of the disease, diagnostic limitations, and difficulty with fixation and permanent metals. Improving diagnostic methods to determine the presence of TMD earlier would allow treatments to begin sooner and possibly limit the number of patients needing total joint reconstruction. Three-dimensional joint kinematics could

be one method developed for earlier diagnosis and evaluation of interventions, allowing for a better understanding of the function of normal diseased joints.

A number of preclinical models have been used to increase our understanding of TMD pain and facilitate identification of novel therapeutic approaches. These preclinical models have primarily focused on quantifying the amount of pain that may be associated with a particular insult to the temporomandibular joint (TMJ) or its related structures. We suggest, however, that because these models fail to encompass critical features of the clinical syndrome, effective therapeutics remain an elusive goal. That is, while TMD pain may be associated with an array of underlying problems, it has unique temporal features that have been missed in all pre-clinical models. Most critically, the fact that TMD pain resolves on its own in a significant fraction of patients has not been adequately explored. Answering the question of why some patients get better while others go on to develop chronic TMD pain is likely to provide critical insight into the etiology of TMDs. The relationship between the extent of degeneration and the manifestation of pain needs to be explained. To begin to address these issues, we have developed an altered occlusion model of TMD in the rabbit that enables control over the timing between the onset and resolution of the pain.

Recently, magnesium alloys have been more closely studied as a potential biomaterial for degradable implants. Current investigations of magnesium alloys as scaffold material demonstrate great promise for the biological application of this metal to regenerate both hard and soft musculoskeletal tissues [21, 37, 39, 40, 50, 51, 59, 61, 69, 73, 74, 78, 93, 127, 128, 137-140, 150-154, 156-159, 163, 167, 168], which is valuable due to the necessity for engineering degradable craniofacial implants. Craniofacial implants, such as plates and screws, are used in

procedures such as osteotomies, bone graft stabilization during reconstructions, and for trauma reconstruction [133]. However, it was unknown how Mg behaves in the craniofacial region.

As an initial step towards achieving these goals, the specific aims of this dissertation focus on the use of a mechanical change in occlusion to gain a better understanding of a TMD model through fibrocartilage, pain, and joint kinematic assessments and testing Mg as a biodegradable screw in the craniofacial region.

1.2 SPECIFIC AIMS

Specific Aim 1: Determine the compressive properties and the biochemical content and distribution of degenerated rabbit TMJ fibrocartilage (disc and condylar fibrocartilage) from altered occlusion, as compared to native tissue.

Purpose: Understand TMJ fibrocartilage degeneration occurring after 6 weeks of splint placement by unconfined compression testing of the TMJ disc, compression testing to a certain force of the condylar cartilage, measuring the DNA content, glycosaminoglycan (GAG) content and total collagen content of both the disc and condylar cartilage, and histology to determine the distribution of cells, GAG, and collagen type II in the TMJ fibrocartilage. *Hypothesis:* Abnormal occlusion will cause a decrease in compression properties due to a decrease in GAG content when compared to normal condylar fibrocartilage.

Specific Aim 2: Determine the presence of pain in a rabbit with altered occlusion.

Purpose: Adapt current pain models and evaluations from small rodents to the rabbit model. Pain will be assessed through behavioral, anatomical, and physiological methods.

Changes in nociceptive threshold are assessed with a mechanical probing of the TMJ region. C-Fos in the nucleus caudalis are assessed with standard anatomical immunohistochemical techniques. Finally, retrogradely labeled TMJ afferents are studied with patch clamp electrophysiological techniques. *Hypothesis:* Abnormal occlusion will increase hypersensitivity in the area surrounding the TMJ and increase the excitability of neurons innervating the TMJ.

Specific Aim 3: Determine the functional kinematic implications of TMJ degeneration caused by altered occlusion.

Purpose: To develop and use high-resolution 3D dynamic imaging of joint function as a non-invasive approach to identify impact of the presence of fibrocartilage degeneration and joint hypersensitivity. These systems can determine the relative motion of the articulating surfaces (arthrokinematics) and the travel path of the mandible. *Hypothesis:* There will be a decrease in superior-inferior incisor and joint translation after splint placement for 6 weeks.

Specific Aim 4: Compare magnesium and magnesium alloy screws to stainless steel screws by assessing biocompatibility, integrity, and strength in a rabbit mandible.

Purpose: To analyze the degradation properties of pure Mg and magnesium alloy AZ31 screws in craniofacial bone through micro-CT and histology, to determine pull out strength of the magnesium screws from a standardized material, and to compare them to similarly sized stainless steel screws. *Hypothesis:* The AZ31 magnesium alloy screws will degrade slower than the pure magnesium screws.

1.3 ORGANIZATION OF DISSERTATION

The following chapters provide essential background information on the TMJ and TMDs and a comprehensive description of the experiments performed to fulfill the specific aims of this dissertation. Chapter 2.0 provides background information to bring together all of the information presented herein and provides a deeper understanding to the motivation behind the research in this dissertation. The chapter begins with an overview of the TMJ and TMDs. Then the chapter goes through the diagnosis and treatment options. Finally the chapter covers some information on animal models used to study TMDs, as well as some research techniques that can be applied to the TMJ. After the background is established, Chapters 3-7 focus on the experiments and results of the aforementioned aims.

Chapter 3.0 focuses on the assessments of the TMJ fibrocartilage after induction of altered occlusion in rabbits, and reports on Specific Aim 1. The TMJ disc and condylar fibrocartilage are tested in compression and the biochemical content and distribution are determined and compared in experimental and control animals.

Chapter 4.0 focuses on the pain analysis of the rabbit altered occlusion model, and reports on Specific Aim 2. The pain response of rabbits to the splints is measured through behavioral, anatomical, and electrophysiological assessments. The assessments are adapted from small rodent models such as mice and rats to the rabbit.

Chapter 5.0 focuses on the development of a kinematic analysis for the rabbit TMJ and addresses the development part of Specific Aim 3. The dynamic function of the rabbit TMJ is assessed through non-invasive three-dimensional skeletal kinematics. Repeatable measurements in distances and movement paths are determined in both the joint space and at the incisors.

Chapter 6.0 focuses on the kinematic analysis of the rabbit altered occlusion model and reports on the experimental part of Specific Aim 3. TMJ kinematics are assessed on rabbits after six weeks of splinting with the splints removed three days prior and compared to data collected on the same rabbits before splinting. The measurements used for comparison are those that were determined in Chapter 5.0 .

Chapter 7.0 focuses on the degradable metal magnesium and presents the results of Specific Aim 4. This study focuses on implanting two types of magnesium screws into the mandible of rabbits to determine the biocompatibility and the amount of magnesium degradation and bone formation over the course of 12 weeks of implantation. The magnesium screws are compared to stainless steel screws in-vivo and in-vitro. The in-vitro pull out force of the screws is compared and the data are used to validate a finite element model of the screws.

Chapter 8.0 provides an overall discussion of the dissertation. It includes overall conclusions, limitations, and future directions of the work completed for this dissertation.

2.0 BACKGROUND

2.1 THE TEMPOROMANDIBULAR JOINT

The temporomandibular joint (TMJ) is a synovial, bilateral, ginglymo-diarthrodial joint, that is formed by the articulation of the condyle of the mandible against the glenoid fossa and articular eminence of the temporal bone [36, 105]. The human TMJ disc has a biconcave geometry, rests between the mandibular condyle and the glenoid fossa and is peripherally attached to both the condyle and the temporal bone. The primary extracellular matrix components of the disc are collagen type I, some collagen type II, proteoglycans, and elastic fibers. Both the TMJ disc and the condylar cartilage are fibrocartilage. The mandibular condylar fibrocartilage is distinct from the TMJ disc in that the condylar fibrocartilage is considerably thinner than the TMJ disc [20, 22, 52, 53, 104, 114], lies adjacent to subchondral bone, and possesses a distinct zonal organization of condylar cartilage. Mastication and speech are two of the most important functions of the TMJ. The hinging and gliding (or rotation and translation) movement is guided by the shape of the bones, muscle, ligaments, and occlusion of the teeth [38, 64]. The TMJ is different from other joints anatomically, in organization and developmentally, so to use broad knowledge from other joints and hyaline cartilage to determine appropriate treatments for the TMJ is not justified, and so the further study of TMJ disease progression is required [141].

2.2 TEMPOROMANDIBULAR DISORDERS

A generic term used for any problem related to the jaw joint is temporomandibular disease/disorders (TMD) [64]. TMD can stem from injury to the jaw, TMJ or muscles of the head and neck [64]. TMDs can also be caused by grinding and/or clenching of teeth, dislocation of the TMJ disc, presence of osteoarthritis, stress, and aging [64]. TMDs can also arise from "traumatic injury, immune-mediated systemic disease, neoplastic growths, and incompletely understood neurobiologic mechanisms" [46]. The most common TMDs are pain dysfunction syndrome, internal derangement, arthritis, and traumas [64]. The most common signs and symptoms patients present with in a clinical setting are limitation of jaw opening or function, pain with jaw opening or function, and joint sounds [38]. Other "indications of TMD can include pain, clicking, locking, headaches, joint pain and tenderness, restricted range of motion, and painful mastication" [149]. However, pain is reported to be the most common reason for seeking treatment [48, 67, 143].

The clinical necessity for TMJ fibrocartilage regeneration is critical considering that up to 3-4% of the population seek treatment for TMD symptoms [48]. It has been observed that up to 70% of people with TMJ disorders suffer from displacement of the TMJ disc, or 'internal derangement' of the TMJ [42]. Among individuals with TMJ disorders, 11% have symptoms of TMJ-osteoarthrosis [86]. While the cause is unknown, these symptoms could be due to the decreased ability of articulating tissue to withstand normal conditions as a result of age, illness, or hormonal factors. Additionally, many different occurrences may lead to abnormal forces and joint loading such as trauma, parafunction as in clenching or grinding, displaced tissues and/or unstable occlusion [7, 8, 100, 116]. Considering the severity of these disorders, it is necessary to develop effective treatment methods. The risk factors and the causes that contribute to

individuals developing chronic TMD are not well understood, including a lack of scientifically established anatomical risk factors [46]. Chronicity of TMDs can be affected by physical and psychological factors including "oral habits, radiographic changes, secondary gain, coping skills, and higher levels of pain and disability on specific psychologic tests" [46]. Parafunctional jaw habits seem to propagate already established TMD symptoms, however do not seem to predispose a person to TMDs [46].

Current thinking on the etiology of TMD has shifted from disc position and shape to changes in the joint biochemistry occurring within the TMJ [38]. Pathologically, the process of joint degradation is "characterized by deterioration and abrasion of articular cartilage and local thickening and remodeling of the underlying bone" [166]. A vicious cycle can occur, for example with bruxism or constant overloading of the joint, where the overloading leads to biochemical changes in the synovial fluid and painful inflammation, which then causes adhesions and immobilization of the joint, leading to further alterations in the joint tissue responses [38]. Chronic clenching/bruxism can also lead to muscle inflammation and spasm which can exacerbate the TMJ problem [38]. Dysfunctional articular remodeling could be due to a decreased adaptive capacity of the articulating structures of the joint and/or excessive physical stress in the TMJ leading to degenerative changes in the joint [120]. TMJ degeneration can be caused by "a loss in equilibrium of anabolic and catabolic processes involving the chondrocyte proliferation, differentiation and matrix production, which is usually preceded or accompanied by increased levels of inflammatory mediators and often characterized by increased degradation of the components of the extracellular matrix" [141].

"Trauma, parafunction, unstable occlusion, functional overloading, and increased joint friction play a role" in TMD progression and may occur alone or be interrelated or co-existent

[120]. Unbalanced or excessive mechanical loading of the TMJ articulating tissues can also result in the progression of TMJ-osteoarthritis, as well as inducing internal derangement [120]. Problems with the mechanical loading affect the biochemistry in the TMJ leading to degenerative changes [120]. The onset of TMD symptoms may not be present unitl later stages in the disease, as the initial degeneration may be sub-clinical [141]. Altered mechanical loading, female hormones, and alterations in the extracellular matrix are three possible etiologies for TMD pathogenesis, and it is possible that an individual may be predisposed to TMJ degeneration with any one or multiple of these etiologies [141].

2.3 TMD DIAGNOSIS

"Patient history, physical evaluation and in most chronic cases behavioral or psychologic assessment" are the current gold standards for TMD diagnosis [46]. Patient "evaluation should include pain and jaw function history, as well as objective measurements of jaw function including inter-incisal opening, open pattern, and a range of eccentric jaw motions" [46]. During the patient evaluation, TMJ sounds should also be described and related to the joint functions [46]. However, it has been shown that the incisal distances alone are not enough information to understand the condylar movement in the joint space [97, 132].

The most common type of diagnostic procedure used to accompany physical examination and patient history is imaging, such as panoramic x-rays, CT scan, MRI, etc [38, 46, 47, 141]. These techniques are well established and are the current gold standard for diagnosis [47]. Electronic diagnostic devices can also be used as adjunctive diagnostic instruments for patients with orofacial pain [47]. These devices include jaw movement trackers, electromyography, and

joint sound recorders (sonography or vibratography) [47]. However, these electronic devices are more controversial as to whether they provide acceptable levels of technical and diagnostic validity to make important clinical decisions, and generally the scientific evidence backing up the value of these methods is lacking and inconsistent [47]. Research is also being completed to determine systemic and local biomarkers of TMJ disease, which could then be used as an option for early diagnosis and for evaluating efficacy of treatments [141]. Samples for biomarker analysis can come from synovial aspirates, tissue samples, serum or plasma, or urine [141]. However, there are still many inherent limitations including the invasive nature of sample gathering and unknown dilution effects, which can make it difficult to compare data, thus diminishing the utility of this approach for diagnosis of TMJ disease [141]. "Genetic factors may also play a role in which individuals are more prone to develop TMJ disorders or for predicting the severity of the disease progression," however there is much research still to be done before this can be used in the clinical setting [141]. Novel insights into the TMD process are beginning to come from computer and imaging technologies, which could be further developed into diagnostic and therapeutic strategies for use in the clinic [141].

2.4 TMD TREATMENT OPTIONS

TMD treatments range from physical therapy and other nonsurgical treatments, to minimally invasive surgical treatments, to invasive total joint replacements [64]. Treatments are directed towards first treating pain and dealing with the causes of joint pathology that lead to the joint inflammation and arthritis with non-surgical methods, resorting to invasive surgical techniques only when the non-surgical methods fail at improving the clinical situation [38, 64].

Conservative treatment can include soft food diets, physical therapy, dental splints, NSAID treatment, muscle relaxants, interocclusal splint, moist heat, ultrasound massage, and botox injections [38, 64]. Minimally invasive surgical procedures include arthrocentesis and arthroscopy [64]. More invasive surgical procedures include discectomy and total joint replacement [64]. Surgical options should be considered when the patient has severe TMJ pain and mandibular dysfunction, the cause of the pain and dysfunction is attributed to a diagnosis consistent with a significant intra-articular pathologic condition such as synovitis, osteoarthritis, or adhesions leading to disc displacement, and a full course of nonsurgical therapy has failed to improve the patient's symptoms [38, 46].

2.5 TMJ IMPLANTS

While most patients with TMD can be "successfully treated with non-invasive or minimally invasive procedures, there exists a small percentage of TMD patients (< 20%) who have severe pathology, pain, and dysfunction, which may require invasive surgical treatment" [87]. When the mandibular condyle is extensively damaged or degenerated, replacement with an alloplastic implant is an acceptable approach to achieve functional improvement [88-91]. Devices that have been used as surgical implants and replacements for the TMJ include "articular disc replacements, condylar replacements, fossa replacements, and total joint prostheses" [64]. In the past, the use of alloplastic materials for TMJ disc replacement had resulted in numerous failures including joint resorption, alteration of mandibular skeletal relationships, compromised motion, pain, and poor immune response. Unfortunately, these pitfalls have tainted the general outlook on TMJ reconstructive surgery.

The TMJ disc implants of the past caused major controversy. The silastic and Proplast alloplastic joint prosthetics "caused severe pain, malocclusion, foreign body giant cell reaction, severe osteoarthritis with bone destruction, erosion of the glenoid fossa causing a leakage of cerebrospinal fluid, as well as migration of particles via the lymphatic system to distant sites" [11, 12]. These inflammatory responses caused the need for more surgeries to remove the devices and repair the damage caused by the device [11, 12]. These problems led the Food and Drug Administration (FDA) to classify TMJ implants as class III devices, the highest risk category, in 1993 [12, 64]. Almost all of the TMJ devices were banned from the market in the early 1990s [12, 64]. The only device to remain on the market was the Christensen device [12, 64]. Studies showed a significant improvement of TMJ symptoms in 85% of patients with the Christensen device, and only a few needed additional surgical procedures [11]. In 1997, the Techmedica/TMJ Concepts device was approved by the FDA, after initially being removed from the market in the early 1990s [11, 64]. This device is custom made for each patient through CAD/CAM [11]. Including the TMJ concepts device only three companies have been approved to make four TMJ devices since December 30, 1998 [64]. The four approved TMJ implants are 1) Christensen/TMJ Implants, Inc., total joint implant, 2) Christensen/TMJ Implants, Inc., partial joint implant, 3) Techmedica/TMJ Concepts total joint implant, and 4) Walter Lorenz/Biomet Microfixation total joint implant [64].

Presently, there are three total joint replacement systems for the TMJ available on the market that are licensed by the FDA. The first device has been available since 1965. The Christensen total joint system consists of a vitallium fossa articulating against a chrome–cobalt condylar head. Screws are used to fix both the fossa and condylar prosthesis to the temporal bone and mandibular ramus, respectively [9]. TMJ Concepts offers a second device that "utilizes

a chromium–cobalt–molybdenum condylar head attached to a ramus framework made out of titanium alloy (6AL–4V) and a fossa component composed of ultra-high molecular weight polyethylene (UHMWPE) with a non-alloy titanium mesh backing" [9]. CAD-CAM technology is used to customize the components to each patient's anatomical defect. Multiple screws are used to attach the condyle and fossa to their respective skeletal components. The screws are placed in a nonlinear fashion to promote maximum stability. Biomet Microfixation offers the third available prosthetic total joint. "The fossa consists of a UHMWPE articular surface mounted on a metallic base which is used to secure the prosthesis with screws to the lateral margins of the glenoid fossa" [9]. The patient's anatomy requires preparation to conform to the prosthetic contours and any remaining space is filled with orthopaedic cement, because the Biomet device is a stock device available in only three sizes. While these devices have presented themselves as viable options for patients suffering from severe TMD symptoms, long term studies are crucial to establish the lifespan of these systems.

2.6 OTHER CRANIOFACIAL IMPLANTS

Craniofacial implants, such as plates and screws, are used in procedures such as osteotomies, bone graft stabilization during reconstructions, and for trauma reconstruction [133]. Previously, craniofacial bone plates and screws have been fabricated from stainless steel, vitallium, chromium-cobalt, copper and other metal alloys [92, 133]. The gold standard for fixation of craniofacial fractures is titanium plates and screws [14, 92, 133], due to the ability of titanium to osteointegrate [92]. However rigid fixation devices have disadvantages, which include "growth disturbance, plate migration, the need for subsequent removal, long term palpability, thermal

sensitivity, malunion, compatibility with future imaging needs, condylar displacement, and difficulty controlling postoperative occlusion" [14, 133]. It is estimated that 10-12% of craniofacial implants are removed due to infection, exposure, pain, and discomfort [92]. Resorbable polymer plates and screws are becoming more popular to use for craniofacial implants because they allow for fixation and stabilization but are not permanent [92]. Biodegradable polymers, such as poly-l-lactide, have been tested as materials for craniofacial implants, however they are biomechanically inferior to the metal counterparts, though they seem to react similarly in-vivo in an animal study [117]. Two shortcomings of the polymer plates and screws include the need for a heating device to provide malleability and the need to tap the bone prior to screw placement [14]. Biodegradable metals may provide a good alternative to the degradable polymer implants and the permanent titanium implants.

2.7 TMJ & CRANIOFACIAL IMPLANT DESIGN CHARACTERISTICS

The important design characteristics of TMJ and other craniofacial implants include "biocompatible materials, functionally compatible materials, low wear and fatigue, adaptability to anatomical structures, rigidly stabilized components, and corrosion resistant and non-toxic in nature" [64]. Device life expectancy is one of the more important characteristics and should be a minimum of 20 years, however most of the current devices are expected to last 10-15 years [64]. It has been suggested to increase the lifespan of the total joint replacement devices, that "the locking screws and locking compression plate for the condylar part of the prosthetic should be researched to improve stability of the implant and to avoid bone loss from revision surgeries" [64]. An ideal biodegradable fixation system would provide adequate strength and stability to

allow bone healing during joint function and then slowly decrease in strength and increase the physiological force transferred to the bone [133]. Major concerns for the craniofacial region include the strength of the material and the ability to withstand masticatory forces, and the amount of inflammation occurring as the material degrades, such that intense inflammation is avoided [133].

2.8 MAGNESIUM AS A BIOMATERIAL

Recently, magnesium alloys have been more closely studied as a potential biomaterial for degradable implants. Current investigations of magnesium alloys as scaffold material demonstrate great promise for the biological application of this metal to regenerate both hard and soft musculoskeletal tissues [21, 37, 39, 40, 50, 51, 61, 69, 73, 74, 78, 93, 127, 128, 137-140, 150-154, 156-159, 163, 167, 168]. It has been demonstrated that the degradation tendencies of magnesium alloys vary significantly in-vivo when compared to in-vitro investigations [152], and thus reiterating the importance of in-vivo studies. Studies of inflammatory response show that degrading magnesium scaffolds have good biocompatibility and react in-vivo with an appropriate inflammatory host response [21, 40, 78, 150, 153, 157, 159, 167, 168]. Furthermore, using a rabbit model, it was shown that degrading magnesium scaffolds promote bone formation [37, 39, 40, 50, 51, 69, 78, 93, 127, 128, 137, 138, 151, 152, 154, 156, 158, 159, 163, 167, 168]. While Mg has been studied extensively in the long bones [21, 37, 39, 40, 50, 51, 61, 69, 73, 74, 78, 93, 127, 128, 137-140, 150-154, 156-159, 163, 167, 168], it was currently unknown how Mg behaves in the craniofacial region.

2.9 TMD MODELS

Gaining a better understanding of the current experimental models used for TMD and the fibrocartilage degeneration process will allow for development of more appropriate models to better understand TMDs. Also, considering the severity of these disorders, it is necessary to develop effective treatment methods. The development of effective interventions for the treatment of TMD has been hindered by the fact that preclinical models of TMD inadequately reflect the pathology of the human state. Furthermore, while changes in feeding behavior and bite force have proven to be sensitive ways to detect the presence of inflammation in the TMJ, they may lack the sensitivity to detect more subtle changes of TMJ function.

To determine an appropriate TMJ degeneration model to use, a review was completed on the current most highly cited methods of inducing TMJ degeneration [5]. The types of methods used to induce TMJ degeneration include chemical injections such as complete Freund's adjuvant, mustard oil, formalin, and carrageenan; surgical interventions such as discectomy, disc displacement, and condylectomy; and mechanical perturbations such as splints, soft food diet, and tooth extraction [5]. Since a model that overloads the TMJ was of interest, surgical models and mechanical perturbations were considered to be the best options for TMD induction. However, surgical interventions have limitations including being invasive and penetrating the joint capsule, while mechanical models have the potential to be much less invasive and possibly reversible.

2.9.1 Dental Splints

Several methods of dental splinting have been used as mechanical injury models to change the occlusion or the way an animal chews. Dental splints do not penetrate the joint space, while mechanically affecting the occlusion or bite. Previously, splints have been attached to the incisors [28, 44, 80, 98, 107, 144, 145] and the molars [26, 82, 84, 103, 111-113], and the molar splints have been attached both unilaterally [26, 82, 111, 112] and bilaterally [84, 103, 113]. Dental splints have been made by attaching metal pieces and/or resin to the teeth. The model selected is a unilateral molar splint [26, 111, 112], which has the potential to provide differences between sides of the TMJ which is clinically relevant, due to the potential for TMDs to vary by side. The splints are also a reversible method, such that in future studies the splints can be removed at certain time points to determine if the joint heals or continues on the degenerative pathway.

2.9.2 Animal Models

Animal studies are beneficial for understanding the development of TMDs, as many types of TMDs can be modeled. By enabling both a mechanical intervention that may drive disease development and comprehensive, invasive tissue assessment, animal studies are uniquely suited for investigating the disease initiation and progression that cannot be completed and repeated in a patient study. A majority of the previous TMJ degeneration studies have been completed on mice and rats, with some being completed in rabbits, and a few in monkeys, pigs, and sheep [5]. A majority of these studies in the rats and mice only looked at histology, with a few behavioral tests in rats [5]. However, rat and mouse TMJs are too small for functional assessments such as

mechanical testing and joint kinematic analysis. In particular, the rabbit model was chosen due to the various TMJ injury and degeneration models already established in the literature [2, 5, 10, 26, 112, 129-131, 134]. Rabbits also exhibit a grinding mastication similar to that of humans [96].

2.10 BIOMECHANICS OF THE TMJ

Both static and dynamic loading occurs in the TMJ from mandibular motions, and the loading is a combination of compressive, tensile, and shear loading on the various articular surfaces [64]. Analysis of mandibular biomechanics can help with the understanding of TMJ form and function, the understanding of the mechanisms of TMDs such that methods can be developed to prevent, diagnose, and cure joint disorders, and improving of the design and behavior of TMJ prosthetic devices [64]. The reported measures from finite element modeling and direct measurement of TMJ loading vary throughout the literature due to limitations of the complex nature of the joint and limitations of the techniques and software packages used for modeling and analysis [64]. More comprehensive biomechanical analysis of the TMJ is needed to better understand the joint movements, applied forces, and resultant stresses in normal, diseased, reconstructed, and artificial joints [64].

3.0 TEMPOROMANDIBULAR JOINT FIBROCARTILAGE DEGENERATION FROM UNILATERAL DENTAL SPLINTS[1]

3.1 ABSTRACT

Objective: The objective of this study was to determine the extent to which altered loading in the temporomandibular joint (TMJ), as might be associated with a malocclusion, drives degeneration of articulating surfaces in the TMJ. We therefore sought to quantify the effects of altered occlusion on the mechanical properties and biochemical content and distribution of TMJ fibrocartilage in the rabbit.

Design: Altered occlusion was induced with a 1 mm splint placed unilaterally over the maxillary and mandibular molars for six weeks. At that time, TMJ fibrocartilage was assessed by compression testing, biochemical content (collagen, glycosaminoglycan (GAG), DNA) and distribution (histology), for both the TMJ disc and the condylar fibrocartilage.

Results: There were no changes in the TMJ disc for any of the parameters tested. The condylar fibrocartilage from the splinted animals was significantly stiffer and the DNA content was significantly lower than that in control animals. There was significant remodeling in the

[1] Submitted to Archives of Oral Biology as Henderson SE, Lowe JR, Tudares MA, Gold MS, Almarza AJ. "Temporomandibular Joint Fibrocartilage Degeneration from Unilateral Dental Splints" on April 7, 2014.

condylar fibrocartilage layers as manifested by a change in GAG and collagen II distribution and a loss of defined cell layers.

Conclusions: A connection between the compressive properties of TMJ condylar fibrocartilage after 6 weeks of splinting and the changes in histology was observed. These results suggest a change in occlusion, leads to condylar damage, which may contribute to pain associated with at least some forms of TMJ disease.

3.2 INTRODUCTION

The development of effective interventions for the treatment of temporomandibular joint (TMJ) disorders (TMD) has been hindered by the fact that preclinical models of TMD inadequately reflect the pathology of the human state. Patients who undergo surgery often have both pain and abnormal joint functional loading [38, 46]. In more severe cases, there is also degeneration of the articulating tissues, including the TMJ disc and the condylar fibrocartilage [120]. However, it is not clear whether abnormal loading leads to degeneration and then pain, or degeneration leads to abnormal loading and pain. In support of the latter, trauma, internal derangement, and parafunctional habits are all thought to be able to initiate the cascade of events that lead to TMD [64, 120]. The link between parafunctional habits and TMD would also support the suggestion that altered loading is the cause rather than the effect in the case of TMD where, in the case of bruxism (clenching), joint overloading would lead to biochemical changes in the synovial fluid and painful inflammation, which then causes adhesions and immobilization of the joint, leading to further alterations to the articulating surfaces [38]. In severe cases, the alteration could be a pathological process of joint degeneration, such as osteoarthritis, which is characterized by

deterioration and abrasion of the articulating fibrocartilage and local thickening and remodeling of the underlying bone [166].

Unfortunately, despite the development of several different preclinical models designed to drive TMD by changes in joint loading and occlusion [26, 28, 44, 80, 82, 84, 98, 103, 107, 111-113, 144, 145], there have been no detailed analyses of the articulating surfaces in the TMJ. Rather, changes to the articulating surfaces have only been suggested with results of histological analysis where differences in the distribution of extracellular matrix components in the condyle have been described [26, 82]. However, the mechanical properties and quantitative biochemical properties of the fibrocartilage are lacking, which can give more insight into the degeneration process.

Therefore, the objective of this study was to determine the effects of altered occlusion on the properties of TMJ fibrocartilage. TMJ fibrocartilage was assessed mechanically in compression and the biochemical content and distribution were determined. The hypothesis was that altered mechanical and biochemical properties and disorganized cellular presence in histology would serve as indicators for the presence of remodeling.

3.3 MATERIALS AND METHODS

3.3.1 Animal Model

The majority of previous TMD animal studies have been completed on small rodents [5]. However, these small rodent animal models do not lend themselves to mechanical analysis of the articulating joint tissue, while the TMJ's main function is mechanical support of jaw movement.

Consequently, the rabbit model was used in the present study, taking advantage of the facts that there is sufficient articulating joint tissue for mechanical analysis and TMJ injury and degeneration models already established in the literature [2, 5, 10, 26, 112, 129-131, 134]. A unilateral molar splint [26, 111, 112], was chosen for this study because it is associated with altered TMJ loading, in the absence of a direct manipulation of the joint, and most closely mirrors changes driven by a sudden change in malocclusion occurring from trauma or a radical dental procedure.

Skeletally mature, female, New Zealand White rabbits approximately 1 year in age and weighing between 5-7 kg were purchased from Myrtle's Rabbitry Inc. (Thompsons Station, TN), and Charles River Laboratories International, Inc. (Wilmington, MA). All rabbits were examined by a veterinarian prior to use in the study and were found to be in good health. All animal procedures were approved by the Institutional Animal Care and Use Committee at the University of Pittsburgh and in accordance with the National Institutes of Health guidelines for the use of laboratory animals.

All of the experimental group (splinted) rabbits were sedated with intramuscular ketamine (20 mg/kg) and xylazine (2 mg/kg) and maintained in a surgical plane of anesthesia with inhaled 2% isoflurane for two separate procedures: impressions and splint placement. During the first procedure, impressions were taken of the upper and lower right molars (Figure 1 A). Non-precious metal bite-raising splints were cast as crowns on molds made from the impressions (Figure 1 B). The thickness of each splint was approximately 1 mm. During the second procedure, the right molars were cleaned (with water and a cotton swab to remove food debris) and primed (with 34% Phosphoric Acid Tooth Conditioner Gel, Dentsply International Inc, Milford, DE), and the splints were attached with dental cement (GC FujiCEM 2, GC

Corporation, Tokyo Japan) (Figure 1 C). Splint placement was verified after 1 week of placement.

After 6 weeks, the rabbits were euthanized (100 mg/kg pentobarbital) and the TMJ tissues were harvested and processed for histology or were stored by wrapping in phosphate buffered saline (PBS) soaked gauze and freezing at -20 °C until future use for biomechanical and biochemical testing. Freeze thaw cycles have previously been shown not to affect the mechanical properties of the TMJ fibrocartilage [3].

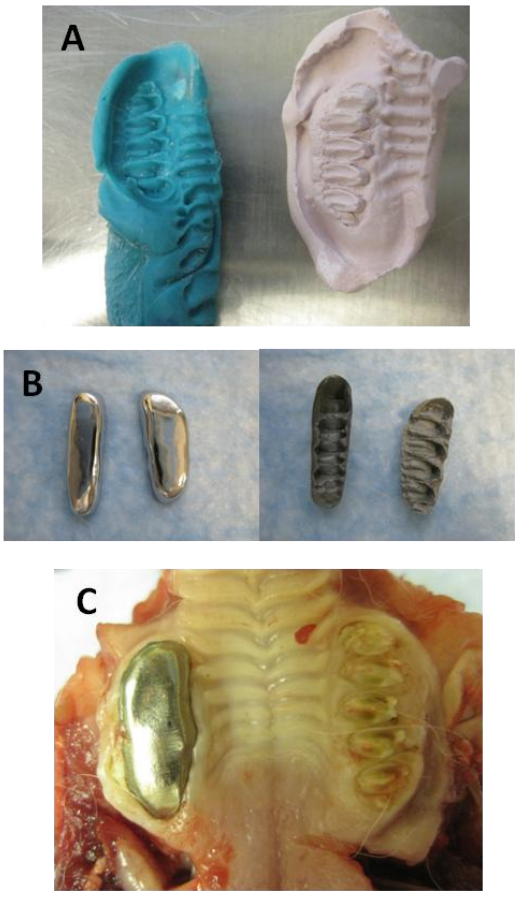

Figure 1. Unilateral molar bite raising splints. A) The splints were made by first taking an impression of the teeth, from which a plaster mold was made. B) The metal splints were cast as crowns, the superior and inferior views are shown. C) Upper splint in place after 6 weeks.

3.3.2 Unconfined Compression Testing – TMJ Disc

To characterize the compressive properties of the TMJ disc (n=8 per group), stress relaxation testing in unconfined compression was completed using an MTS Insight (Eden Prairie, MN) on cylindrical plugs (diameter = 2 mm) [49] (Figure 2 A, B). Samples were taken from the medial side of the intermediate zone of the discs, from both left and right discs of control and splinted animals. The samples were placed in a PBS water bath at a physiological temperature of 37 °C. First, the samples were exposed to a preload of 0.05 N to ensure contact with the surface, and determine the initial height of the sample. Ten cycles of preconditioning at a constant strain rate of 9% per minute to 10% strain was completed. Samples were then tested in stress relaxation to 10% strain and allowed to relax for 30 minutes [30, 49, 110]. The samples were then compressed in 5% increments to 30% strain, with 30 minutes of relaxation in between steps (Figure 2 C). The force and distance traveled were recorded throughout the test and were normalized to stress and strain, respectively. The peak stress was determined for each strain level, as well as the change in stress after the relaxation period resulting in the percent relaxation. The tangent modulus was calculated by finding the slope of the last 20% of the linear region of the loading curve for each strain step (Figure 2 D). A two-way ANOVA with Tukey's post hoc test ($p<0.05$) was used to determine if there were any significant differences between the variables at each strain step based on sample side (left/right) and experimental treatment (control/splinted).

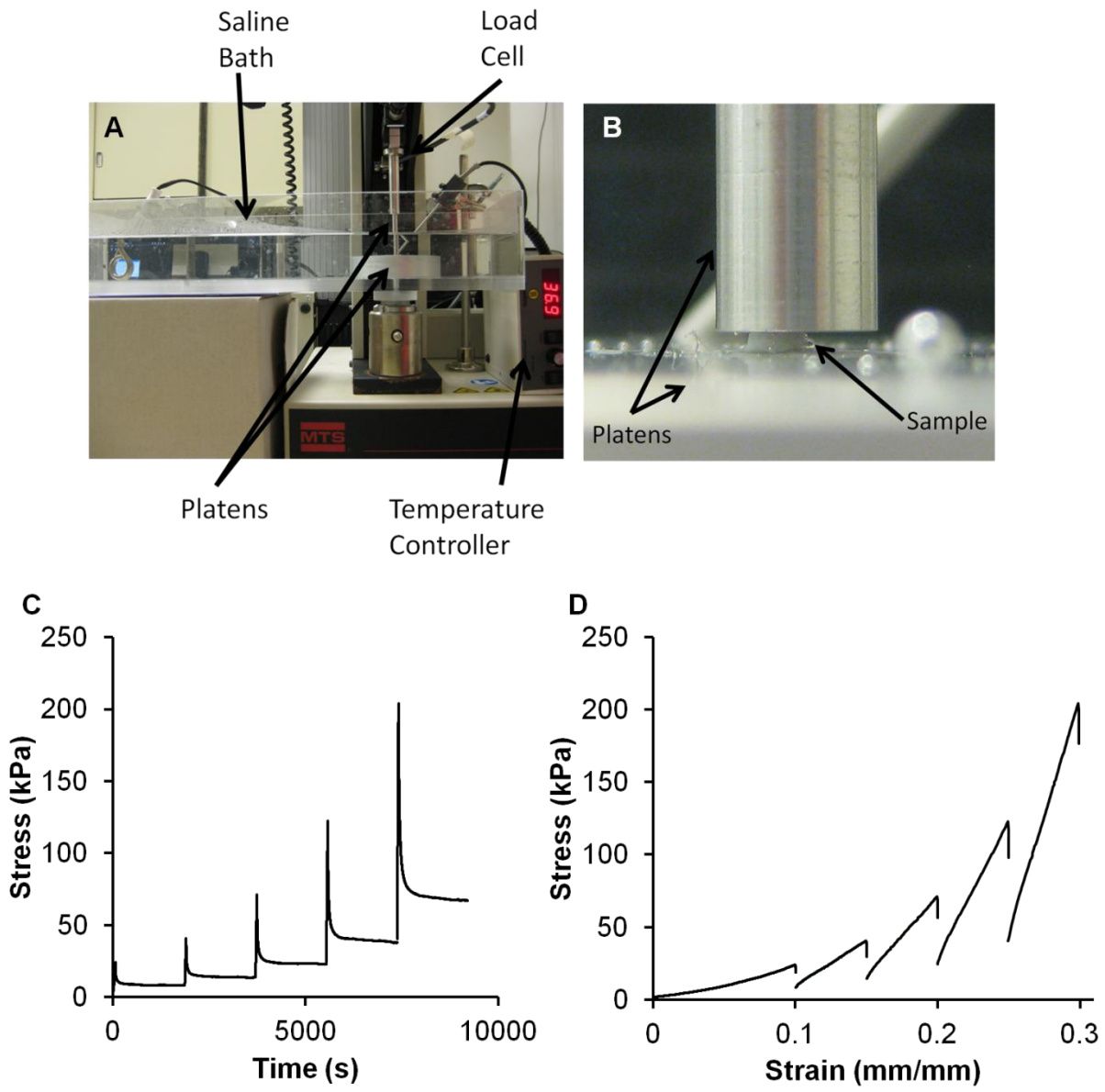

Figure 2. Unconfined compression of the TMJ disc. A) Unconfined compression testing set up. Samples were tested in a saline bath at 37 °C. B) Picture shows a representative TMJ disc sample and the platens. C) Stress of the TMJ disc sample over time. Each strain step is shown consecutively. Samples were compressed to the strain level (10%, 15%, 20%, 25%, 30%) and allowed to relax for 30 minutes. Representative curves are shown. D) Stress-strain loading curves for the TMJ disc. Representative curves are shown for each strain step 10%-30% with 5% increments.

3.3.3 Compression Testing to a Certain Force - Condylar Fibrocartilage

Compression testing to a certain force was used to test the condylar fibrocartilage because the fibrocartilage was too thin to remove from the bone consistently which was required for unconfined compression testing. The left and right condyles of splinted and control rabbits were tested in two regions: an anterior region and a posterior region (n=8). An indentor (Figure 3 A), 1 mm in diameter, was compressed into the fibrocartilage on bone at a constant rate of 0.1 mm/min until a force of 0.02 N (25.4 kPa) was reached, recording the force and the distance traveled (Figure 3 B). The thickness of the fibrocartilage was measured using a needle technique [118], in which a needle was inserted through the fibrocartilage and bone at a constant rate of 0.1 mm/min until a force of 0.2 N was reached (Figure 3 C), indicating full travel through the fibrocartilage and into the bone. The thickness of the fibrocartilage was determined to be the displacement when the slope of the loading curve was equal to 1 N/mm. The strain at 0.02 N was calculated by dividing the distance traveled by the indentor to 0.02 N by the thickness determined from the needle test. A two-way ANOVA was completed with Tukey's post hoc test ($p<0.05$) to determine by region if there were differences between left and right condyles and splinted and control rabbits, for strain and thickness.

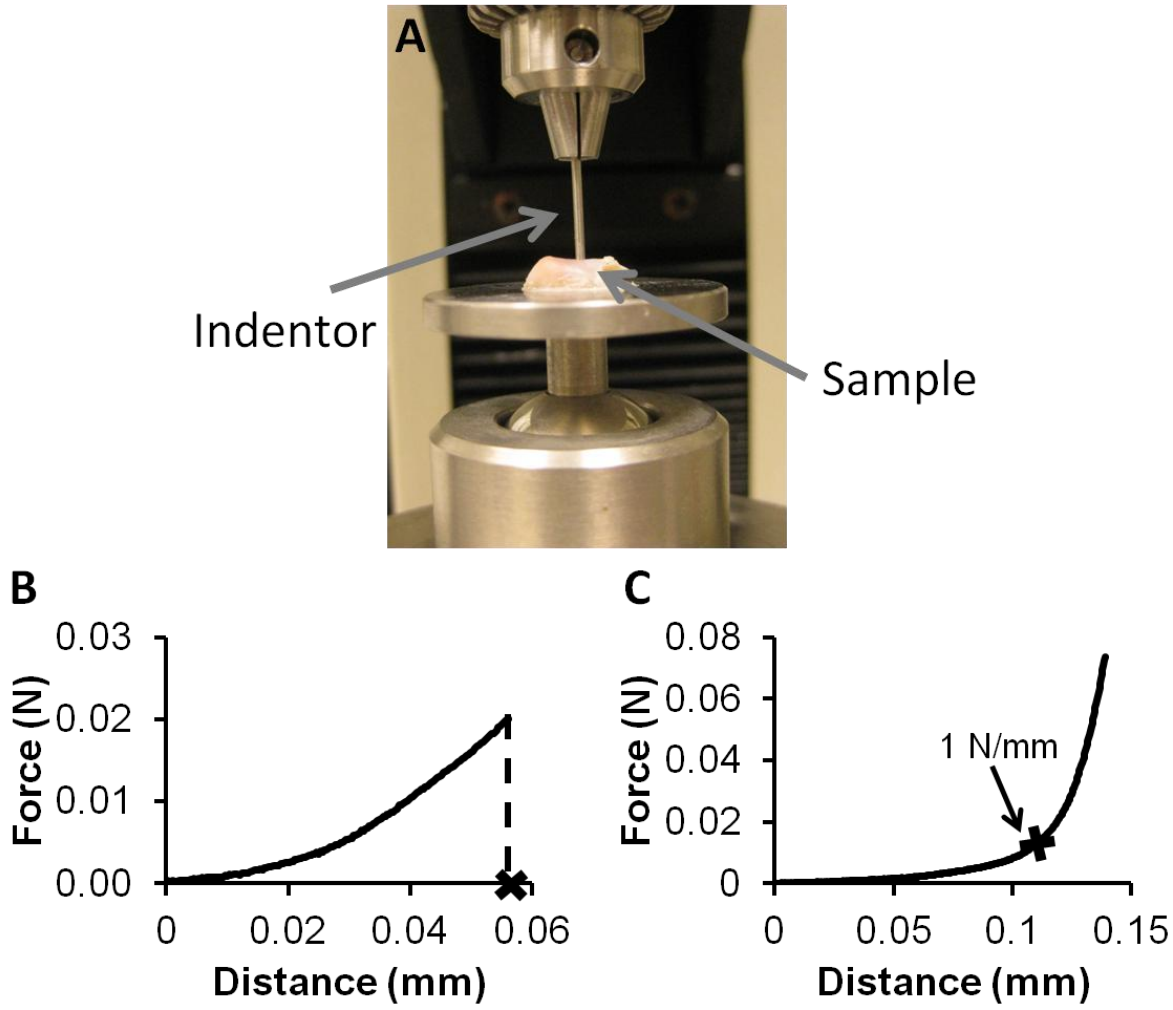

Figure 3. Compression testing to a particular force. A) Whole condyles were glued to a rotating stage allowing for multiple testing locations. The indentor was 1 mm in diameter. Samples were kept hydrated with PBS between testing steps. B&C) Condylar fibrocartilage loading curves. B) Representative loading curve to 0.02 N for compression testing of the condylar fibrocartilage, where the distance is used as displacement for strain. C) Representative loading curve for the thickness test of the condylar fibrocartilage. The thickness was the distance in the region where the slope rapidly changed, at the point where the slope was equal to 1 N/mm.

3.3.4 Biochemical and Histological Analysis of the TMJ Fibrocartilage

For biochemical analysis, TMJ disc and condylar fibrocartilage samples were prepared from the same samples used in compression testing, including the 2 mm punches of the disc and the fibrocartilage that was cut and scraped off of the condyles (n=8). Samples were prepared for digestion by first hydrating in PBS for at least one hour, and then the samples were placed in individual tubes and the wet weights were recorded. A speed vacuum was used to dry the samples over night, and then the dry weights of the samples were recorded. Samples were then digested in 1 mL of a 125 μg/mL papain solution over night at 60 °C [41]. All biochemical assays were performed on aliquots from the same digest. The total collagen content of the TMJ fibrocartilages was determined using a well-established hydroxyproline assay [4]. The content of glycosaminoglycan (GAG) was detected with the Sulfated Glycosaminoglycan Assay kit (Blyscan, Northern Ireland). The DNA content of the digest was measured using a PicoGreen dsDNA Kit (Molecular Probes, Inc., Eugene, Oregon). A two-way ANOVA was completed with Tukey's post hoc test ($p<0.05$) to determine for each biochemical assay, if there were differences between left and right sides and splinted and control rabbits for the TMJ disc and condylar fibrocartilage individually.

For histology, TMJ condyle samples from control and splinted rabbits (n=3) were fixed and decalcified in Formical (Decal Chemical Corp) to prepare for standard paraffin embedding and sectioning. Samples were embedded and sectioned by Alizeé Pathology (Thurmont, MD) at 6 μm. Slides from the condylar fibrocartilage were stained with Hematoxylin and Eosin (H&E) to visualize the cells, Safranin O (SafO) for GAG, and a for Collagen Type II (Col II) immunostain [35].

3.4 RESULTS

3.4.1 TMJ Disc

Under unconfined compression stress relaxation, there were no statistically significant differences between the left and right TMJ discs, nor between discs from splinted and control rabbits for any variable at any strain level (Figure 4 A, B, C). With all sample types the maximum stress and tangent modulus increased with each strain step (Figure 4 A, B). At 10% the average stress for all discs was 29±12 kPa, at 15% it was 51±20 kPa, at 20% it was 87±32 kPa, at 25% it was 144±48 kPa, and at 30% it was 225±67 kPa. The average tangent modulus for all samples was 440±235 kPa, 812±354 kPa, 1412±577 kPa, 2228±767 kPa, and 3332±931 kPa for each strain step 10-30%. The percent relaxation remained fairly constant across groups and strain points at approximately 65% (Figure 4 C).

There were also no statistically significant biochemical differences between left and right TMJ disc or discs from splinted and control rabbits. The overall average of the disc samples were approximately 67.3±4.4% water by weight (Figure 5 A). For the disc, the overall average of the total collagen content was approximately 70.1±8.6% dry weight (Figure 5 B). The overall average of the GAG content of the discs was approximately 1.78±0.55% dry weight (Figure 5 C). The overall average of the DNA content was approximately 0.11±0.02% dry weight (Figure 5 D). No histological differences were observed (data not shown).

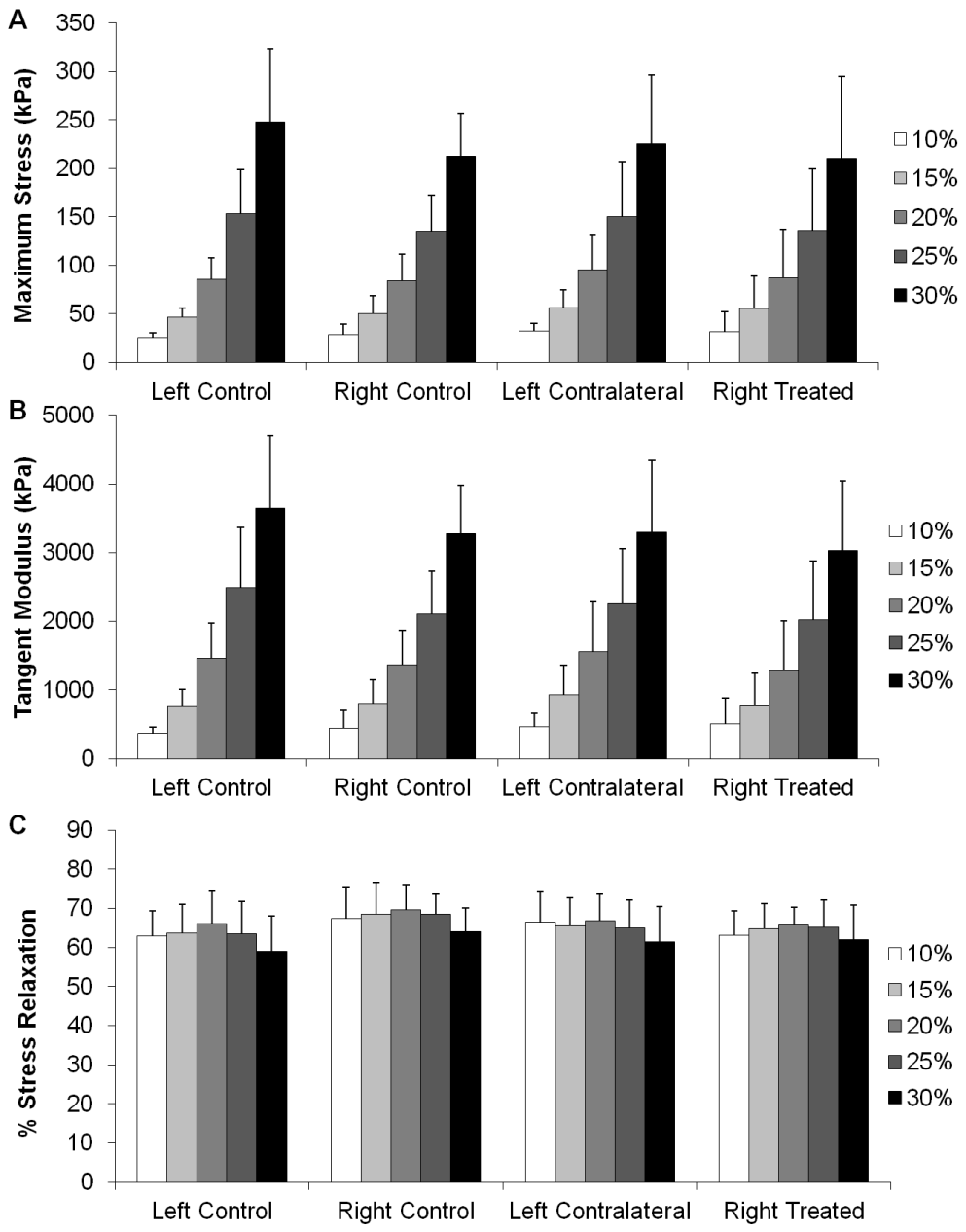

Figure 4. TMJ disc unconfined compression results. A) Maximum stress for each strain step of unconfined compression for each TMJ disc tested. No statistical differences were seen between groups at any strain level. B) Tangent modulus for each strain step in unconfined compression for each TMJ disc tested. No statistical differences were seen between groups at any strain level. C) Percent stress relaxation for each strain step in unconfined compression for each TMJ disc tested. No statistical differences were seen between groups at any strain level. Sample size of n=8 per group. All error bars are standard deviations.

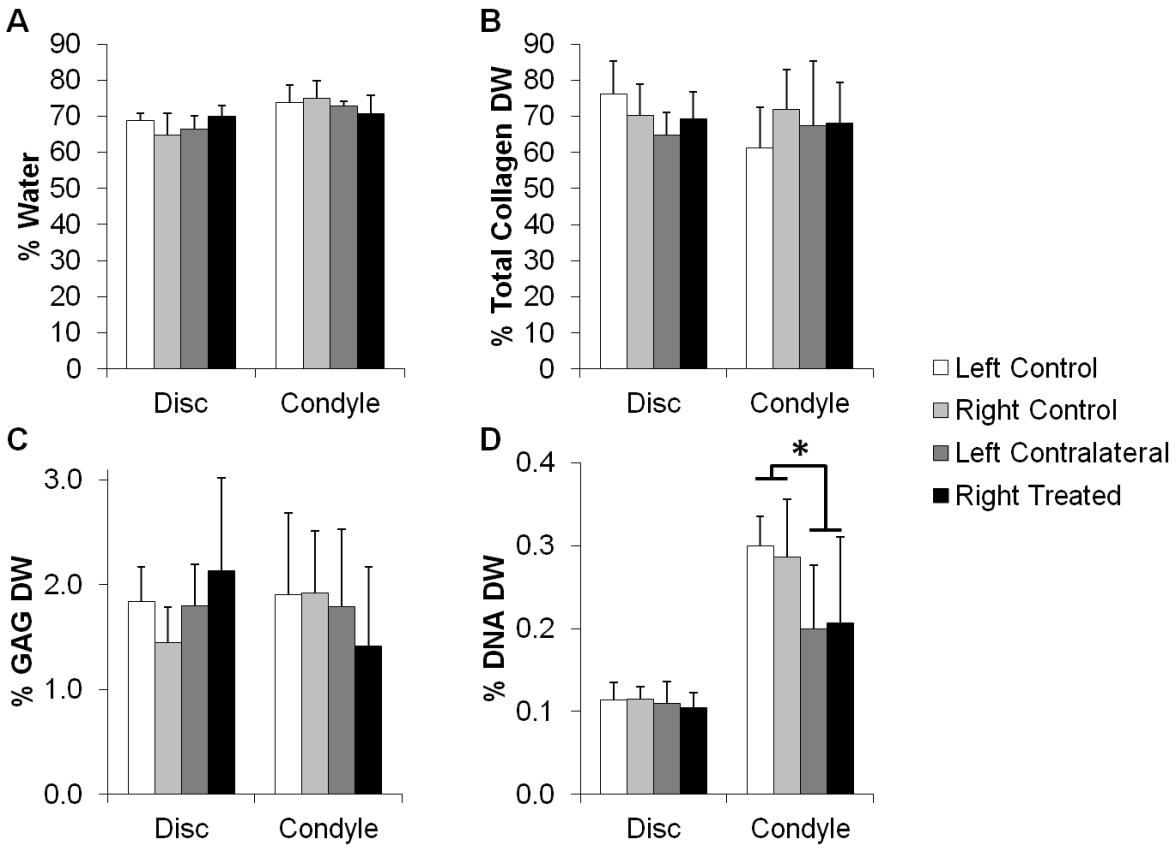

Figure 5. Biochemical composition for the TMJ disc and condylar fibrocartilage. A) Water content, B) Total collagen content per dry weight, C) GAG content per dry weight, D) DNA content per dry weight. The only statistical difference was in the condylar fibrocartilage DNA content with the average of the splinted condyles being less than the average of the control condyles ($p<0.05$). Sample size of n=8 per group. Data shown as average ± standard deviation.

3.4.2 Condylar Fibrocartilage

For the mechanical testing, there were no statistical differences between the left and right condyles, however the strain at 0.02 N of the posterior region of the normal condyles was significantly higher than the strain of the treated condyles (splinted 0.37±0.13 mm/mm, control 0.25±0.06 mm/mm, $p<0.05$, Figure 6 A). The overall average posterior thickness was 0.20±0.09 mm and the anterior thickness was 0.08±0.03 mm (Figure 6 B).

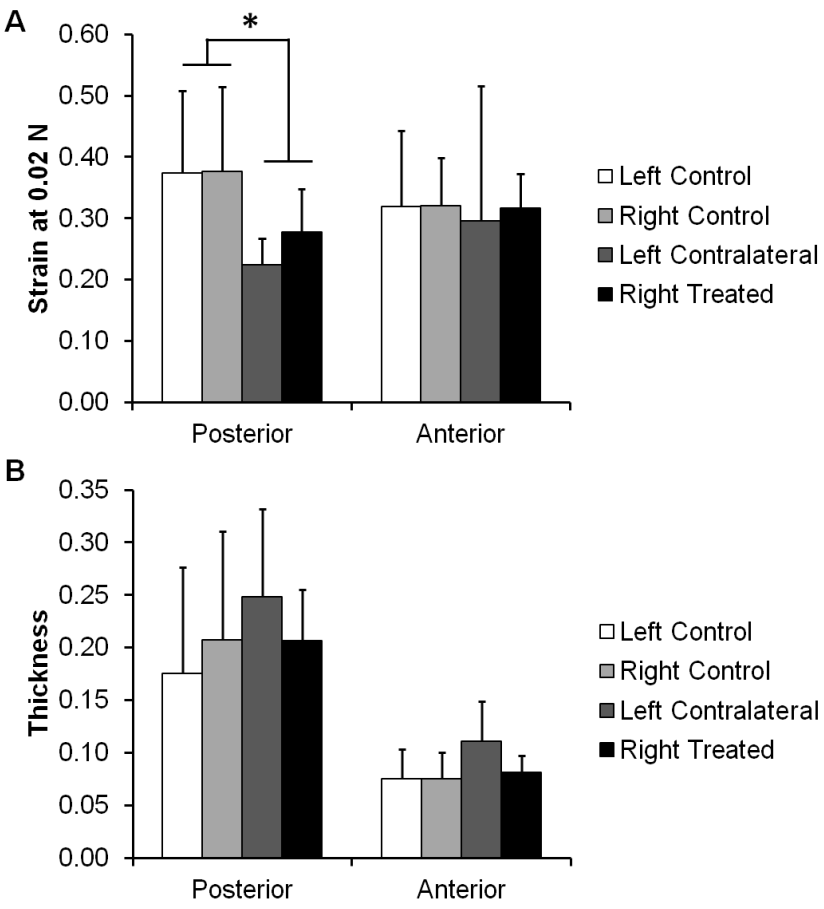

Figure 6. Condylar fibrocartilage compression results. A) Strain of the condylar fibrocartilage at 0.02 N of loading, as compression testing to a particular force was used on the TMJ condyles regionally. The posterior region of the splinted rabbit condyles was significantly stiffer than the control fibrocartilage. (*p>0.05) No other statistically significant differences were observed. B) Thickness of the TMJ condylar fibrocartilage. No statistically significant differences were observed. Sample size of n=8 per group. All error bars are standard deviations.

The biochemical results for the condylar fibrocartilage were fairly consistent between all samples left and right, as well as between splinted and control samples. The overall average of the condyle samples was approximately 73.2±4.4% water by weight (Figure 5 A). The overall average of total collagen content was approximately 67.1±12.7% dry weight for all samples (Figure 5 B), and the GAG content was approximately 1.78±0.70% dry weight for all of the condyles (Figure 5 C). The only statistically significant difference between the control and the

splinted condyles was for DNA content (Figure 5 D). The control condyles were 0.29±0.05% dry weight DNA while the splinted condyles were 0.20±0.09% dry weight DNA ($p<0.05$).

Histological analysis revealed an almost complete loss of the subchondral layer of the fibrocartilage, in the posterior regions of the contralateral splinted rabbit condyles. This loss was accompanied by a loss of defined cell layers, and only a fibrous layer remaining to cover the bone. This change is illustrated with whole condyles stained with H&E, SafO, and Col II immunostain (Figure 7, 4X magnification), where differences in anterior (Figure 8, 10X magnification) and posterior (Figure 9, 10X magnification) regions of the condyles, respectively, can be seen for all stain types. On the H&E stained slides, the lacunae appear to be losing their shape and columnar nature and the subchondral region of the fibrocartilage were seen to shrink in both of the splinted condyles (Figure 7, Figure 8, Figure 9; parts C, D) compared to the control condyles (Figure 7, Figure 8, Figure 9; parts A, B). GAG staining revealed a change in distribution between the controls (Figure 7, Figure 8, Figure 9; parts E, F) and the splinted condyles (Figure 7, Figure 8, Figure 9; parts G, H). GAG staining was seen throughout the length of the treated condyle and the normal condyles. However, GAG stained regions seem to be thinner in the contralateral splinted condyles compared to the normal condyles. A similar pattern of changes as the GAG was seen in the Col II staining for the splinted condyles (Figure 7, Figure 8, Figure 9; parts K, L) as compared to the control (Figure 7, Figure 8, Figure 9; parts I, J) condyles. A difference was also noted between the treated and contralateral sides of the splinted rabbits. For both the GAG and Col II staining in the contralateral condyle, the GAG and Col II layer ended approximately midway through the anterior-posterior length of the condyle. The GAG and Col II staining was in the anterior regions (Figure 8 G, K) but not the posterior regions (Figure 9 G, K).

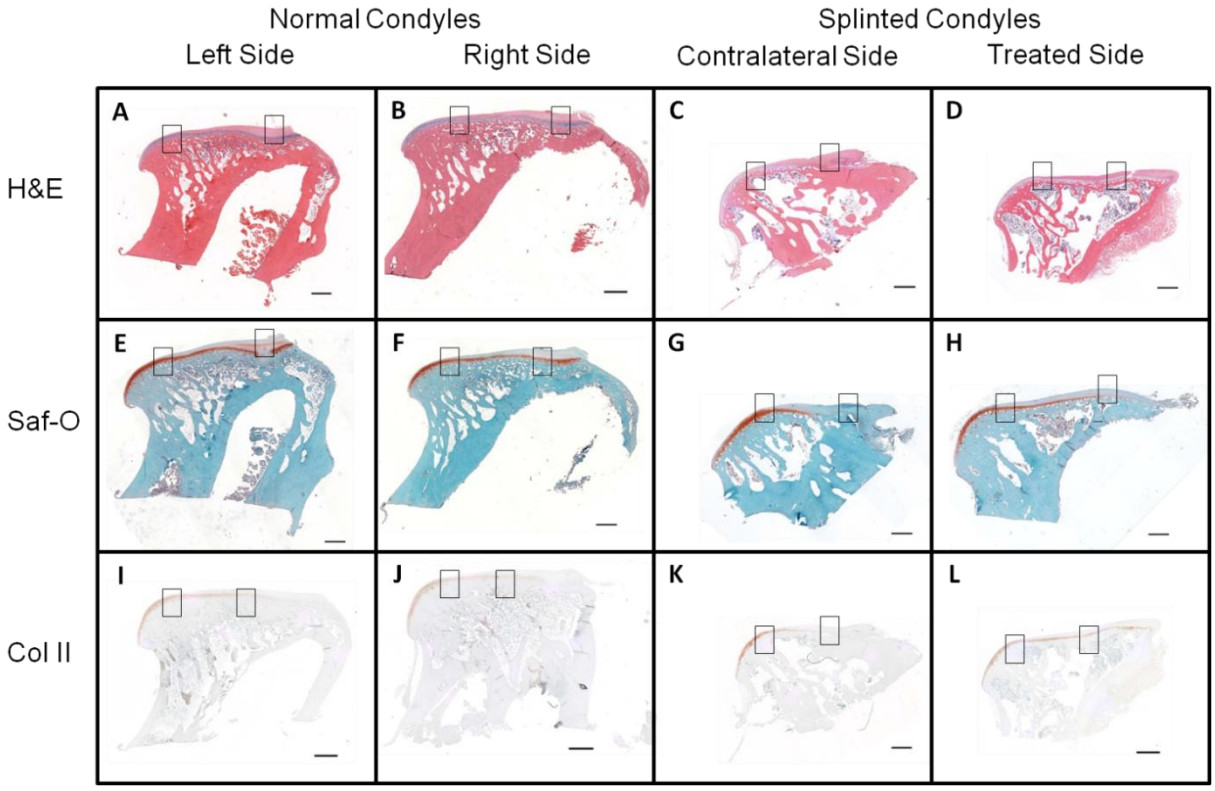

Figure 7. Histology showing the entire TMJ condyles at 4X magnification (scale bars = 1 mm). Boxes indicate the areas shown in Figure 8 and Figure 9 at 10X magnification. Figure 8 shows the anterior regions (boxes on the left of the images). Figure 9 shows the posterior regions (boxes on the right of the images). Staining used for comparison included H&E, Saf-O for GAG staining, and Collagen Type 2 immunostain. The right and left condyles of control animals were compared to the left (contralateral) and right (treated) condyles of splinted animals. Representative pictures shown from at least n=3.

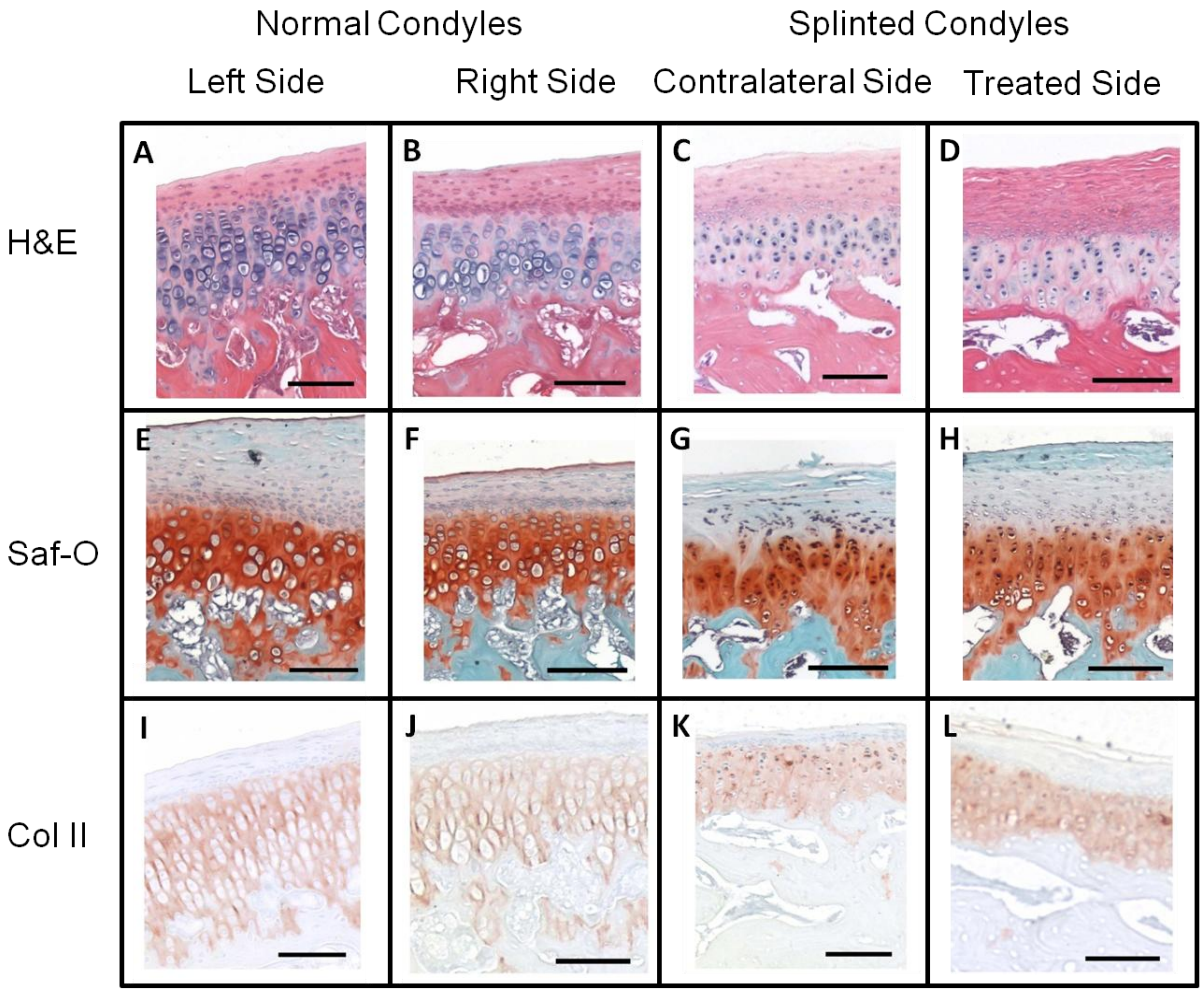

Figure 8. Histology showing the anterior regions of the TMJ condyles at 10X magnification (scale bars = 100 µm). Boxes showing the location of each image were in Figure 7 on the left of each figure. Staining used for comparison included H&E, Saf-O for GAG staining, and Collagen Type 2 immunostain. The right and left condyles of control animals were compared to the left (contralateral) and right (treated) condyles of splinted animals. Representative pictures shown from at least n=3.

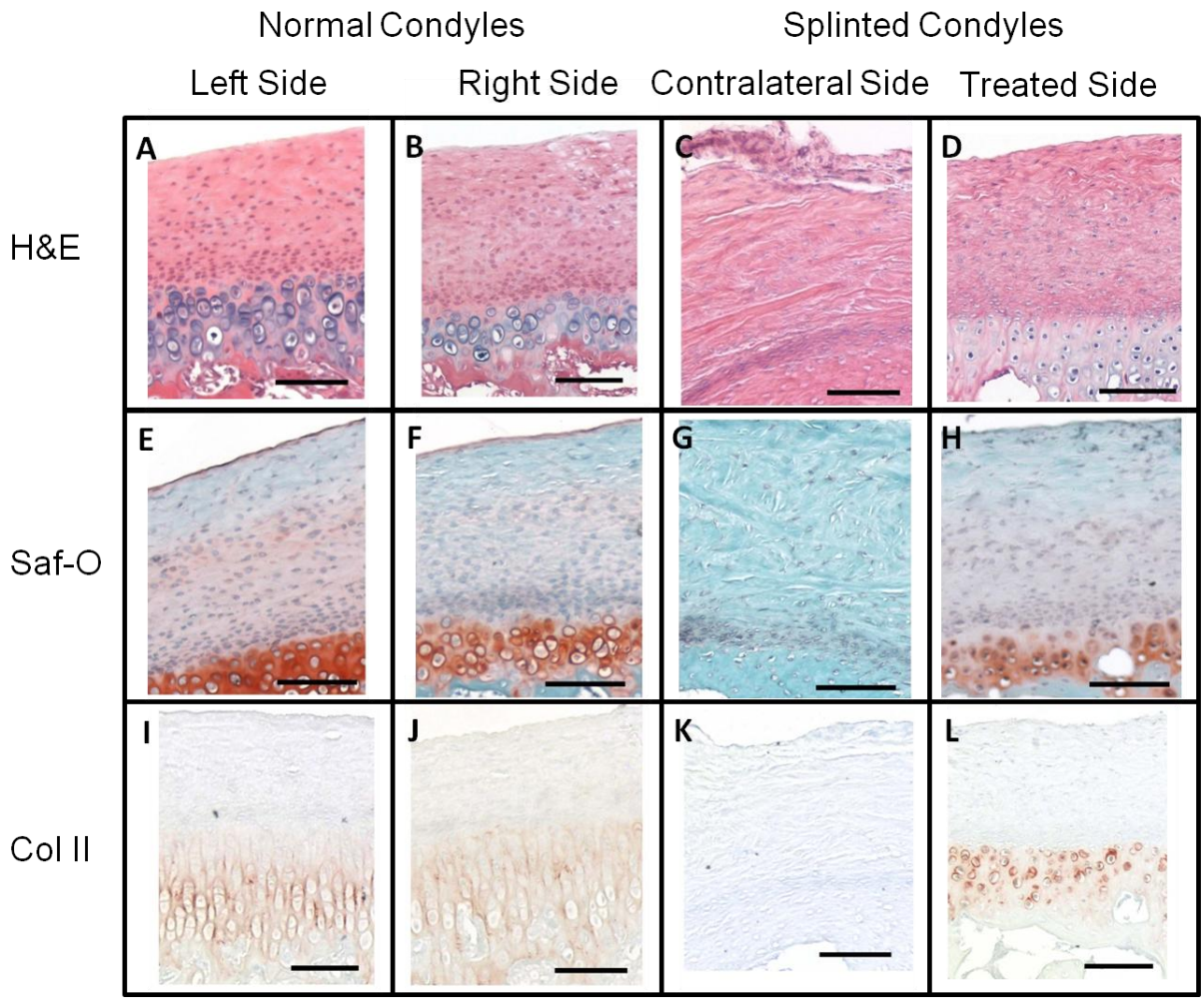

Figure 9. Histology showing the posterior regions of the TMJ condyles at 10X magnification (scale bars = 100 µm). Boxes showing the location of each image were in Figure 7 on the right of each image. Staining used for comparison included H&E, Saf-O for GAG staining, and Collagen Type 2 immunostain. The right and left condyles of control animals were compared to the left (contralateral) and right (treated) condyles of splinted animals. Representative pictures shown from at least n=3.

3.5 DISCUSSION

The primary observation from this study was that unilateral splint placement can drive uneven condylar fibrocartilage degeneration, as measured mechanically, biochemically, and as seen in histology. The uneven effect of the splint, between the treated and contralateral sides, was more pronounced in the posterior region of the condyle. Overall, splint placement resulted in the degeneration of the subchondral collagen type II/GAG rich layer of the contralateral condylar fibrocartilage, while having little effect on the TMJ disc. Furthermore, it was shown that condylar fibrocartilage degeneration can occur with the TMJ disc in its correct anatomical location (no displacement). No changes were found in the mechanical properties of the TMJ disc, which agreed with the lack of changes in the biochemistry and histology of the disc. The TMJ disc properties generally agreed with previous studies of the normal TMJ disc in both the mechanical behavior and the biochemical composition [49, 70]. These results support a shift in focus from the TMJ disc to the condylar fibrocartilage in terms of the initial sources of TMJ pain and degeneration.

In terms of the condyle, the rabbit unilateral splint model seemed to affect the deep subchondral cartilage layer more than the surface fibrous layer. The histology agreed with a previous rabbit molar splint study where the splinting seemed to affect the deep cartilage layer [26]. A connection between the compressive properties of TMJ fibrocartilage after 6 weeks of splinting and the changes in histology was observed. The condylar fibrocartilage compressive data suggested that abnormal loading causes changes in the extracellular matrix distribution of TMJ fibrocartilage leading to stiffer fibrocartilage. The posterior region of the splinted condyles was stiffer than the control tissue, for at the same force/stress there was less displacement. The changes were not yet apparent in the biochemistry of the condylar fibrocartilage except in the

DNA content, which could correspond to the changes with the loss of the cell layers of the cartilage layer seen in histology. Lack of change measured in GAG content could be attributed to isolation of the thin fibrocartilage for digestion. A regional isolation, anterior and posterior, was not possible, which would likely show a decrease in GAG content in the posterior of the contralateral condylar fibrocartilage. One possible way to capture more of the GAG content regionally would be to digest the fibrocartilage on the bone, to prevent leaving a layer of the fibrocartilage on the bone after scraping the fibrocartilage off of the bone for the digest.

The unilateral splint model was advantageous because the joint capsule was not penetrated. This particular splint model will allow future studies to focus on removing the splints at various time points to gain a better understanding of how/when degeneration becomes an irreversible condition. This rabbit model will also allow for a multidisciplinary approach to understanding TMDs by allowing other analyses such as pain and kinematic assessments to be incorporated. This TMD animal model also had limitations. While the rabbit is larger than many TMD animal models, it still only provided a limited amount of soft tissue for testing. The rabbit mouth was also small and was difficult to access for dental procedures. This model also did not drive changes to the TMJ disc at 6 weeks.

We do believe this rabbit splint model is worth pursuing because it provides a mechanical mechanism for degeneration of the TMJ articulating tissues [120]. We have shown that abnormal loading leads to stiffer condylar fibrocartilage. Other mechanical properties can also be affected, such as shear [122, 123] and friction [120, 121]. The increased friction could displace the disc, leading to further degeneration. As such, more modes of mechanical testing are needed, and at longer time points, to test these hypothesizes, that only larger animal models allow.

The results of this study suggest a possible explanation as to why some patients have TMJ pain, but no TMJ disc problems. With this particular model, the TMJ condyle was undergoing changes, while no changes were observed in the TMJ disc. Thus, it is possible that there is condylar fibrocartilage degeneration in some TMD patients which cannot be detected with current imaging techniques. Importantly, degeneration of the condylar fibrocartilage may be the source of mediators responsible for their pain. This research raises the question whether disc derangement is necessary for TMJ osteoarthritis to occur, or whether mild osteoarthritis is enough to cause pain. Longer time points are necessary to determine if disc degeneration would start to occur. While more studies are needed to understand the link between TMJ degeneration and the development of TMJ pain, if degeneration of the fibrocartilage is the trigger for pain, it will be essential to determine whether these changes are reversible following normalization of occlusion, as it is conceivable that in chronic TMD patients, the degeneration has reached a point at which it is no longer reversible.

3.6 CONTRIBUTIONS

I assisted with the rabbit dental procedures, completed tissue harvest, mechanical and biochemical data collection, data analysis, and prepared and edited the manuscript. Mr. Lowe prepared the samples for histology and completed the staining and imaging of the sections and helped with manuscript editing. Ms. Desai assisted with mechanical testing. Dr. Hagandora assisted with the mechanical testing development. Mr. Tudares performed the dental procedures and helped with manuscript editing. Dr. Gold helped with the project design and manuscript editing. Dr. Almarza helped with project design, data analysis, and manuscript editing.

4.0 ANALYSIS OF PAIN IN THE RABBIT TEMPOROMANDIBULAR JOINT AFTER UNILATERAL SPLINT PLACEMENT[2]

4.1 ABSTRACT

Aims: The aims of the study were to determine the effects of altered temporomandibular joint (TMJ) loading in the rabbit on endpoints of nociception used in small rodents and look for possible correlation between nociception and remodeling of the condylar fibrocartilage.

Methods: Unilateral molar dental splints were used to alter TMJ loading. Changes in nociceptive threshold were assessed with a mechanical probing of the TMJ region on 9 splinted and 3 control rabbits. C-Fos in the nucleus caudalis was assessed with standard anatomical immunohistochemical techniques from 3 splinted and 6 control animals. Retrogradely labeled TMJ afferents were studied with patch clamp electrophysiological techniques from 3 splinted and 3 control animals. Remodeling of TMJ condyles was assessed by histology on 3 splinted and 3 control animals. A student's t-test or a Mann-Whitney U test was used with significance set at $p<0.05$ to compare splinted to control samples.

Results: While variable, there was an increase in mechanical sensitivity in splinted rabbits. The increase in c-Fos+ cells in splinted rabbits was also significant (86±8 cells/section

[2] Submitted to Journal of Oral and Facial Pain and Headache as Henderson SE, Tudares MA, Gold MS, Almarza AJ. "Analysis of Pain in the Rabbit Temporomandibular Joint after Unilateral Splint Placement" on March 27, 2014. First revision submitted May 28, 2014. Second revision submitted July 14, 2014.

vs. 64±15 cells/section, $p<0.05$). The rheobase (364±80 pA) and action potential threshold (−31.2±2.0 mV) were higher in TMJ afferents from splinted rabbits compared to control (99±22 pA and −38.0±2.0 mV, $p<0.05$). There was significant remodeling in the condylar fibrocartilage layers as manifested by a change in glycosaminoglycan distribution and a loss of defined cell layers.

Conclusion: Behavioral and anatomical results were consistent with an increase in nociceptive signaling in concert with condylar remodeling driven by altered TMJ loading. Changes in excitability and action potential waveform were consistent with possible compensatory changes of TMJ afferents for an overall increase in afferent drive associated with joint degeneration. These compensatory changes may reflect pain adaption processes that many patients with TMJ disorders experience.

4.2 INTRODUCTION

Pain is reported to be the most common reason for seeking treatment for temporomandibular disorders (TMD) [48, 67, 143], and up to 4% of the population seek treatment for TMD [48]. One of the mechanisms that can underlie TMD progression is unbalanced or excessive mechanical loading of the temporomandibular joint (TMJ), which can drive changes in the biochemistry and dysfunctional remodeling of the joint fibrocartilage leading to joint degeneration [120]. The development of effective interventions for the treatment of TMD has been hindered by the dearth of data linking the changes observed in preclinical models to the development and manifestation of the pathology of the human state. While it is clear that a subpopulation of TMD patients suffer from degeneration of the joint [120], previous histological

analyses have provided little insight into the nature and extent of the degeneration [26, 82]. Furthermore, no study has elucidated whether there is a point in which the degeneration becomes irreversible, or whether there is a relationship between the extent of degeneration and the manifestation of pain.

A number of TMD models have been developed in small rodents such as rats and mice where a variety of behavioral [106], anatomical [169], and physiological [43] endpoints have been used as evidence of pain and/or changes in pain in these models. However, there has been considerably less progress in translating and applying these approaches to larger animal models, such as the rabbit, which may enable the use of analyses not feasible in smaller species. For example, while the main function of the TMJ is mechanical support of jaw movement, it is difficult to determine the mechanical properties of joint tissue from small rodents. Similarly, while parafunctional habits have been linked to the development of TMD, the link between the altered TMJ loading associated with these habits and the manifestation of pain has yet to be determined. To begin to address these issues, we have developed a reversible method for inducing TMD in the rabbit using altered TMJ loading that enables control over the timing between the onset and resolution of the altered loading. As a first step in the characterization of this model, the objective of this study was to determine whether behavioral, anatomical, and physiological endpoints widely used to infer the presence of pain in rodent models of TMD were applicable to the rabbit model of TMD associated with altered loading.

4.3 METHODS

4.3.1 Animal Model

Skeletally mature, female, New Zealand White rabbits approximately 1 year in age weighing between 5-7 kg were purchased from Myrtle's Rabbitry Inc. (Thompsons Station, TN), Covance Research Products Inc. (Princeton, NJ), and Charles River Laboratories International, Inc. (Wilmington, MA). All rabbits were examined by a veterinarian prior to use in the study and were found to be in good health. All animal procedures were approved by the Institutional Animal Care and Use Committee at the University of Pittsburgh and in accordance with the National Institutes of Health guidelines for the use of laboratory animals.

Altered TMJ loading was achieved through the placement of splints, unilaterally over the opposing maxillary and mandibular molar arch of the right side [26, 111, 112]. Unilateral splints were used as a way to impart sudden abnormal unbalanced occlusion, which could occur in patients that suffered trauma or a dramatic change in occlusion from a dental procedure such as orthognathic surgery. Splints were custom made from impressions taken from each rabbit (Figure 10 A) which were cast as crowns (of non-precious metal) on molds made from the impressions (Figure 10 B). The thickness of each splint was approximately 1 mm, which was approximately one third of the height of the molars (approximately 3 mm). The 1 mm thickness was chosen because thinner splints could not be manufactured easily, and much thicker splints did not allow for the rabbit to close its mouth. Splints were subsequently attached to the appropriate arch with dental cement (GC FujiCEM 2, GC Corporation, Tokyo Japan) following cleaning (with water and a cotton swab to remove food debris) and priming teeth (with 34% Phosphoric Acid Tooth Conditioner Gel, Dentsply International Inc, Milford, DE). The retention

of the splints was checked at one week post splint placement. Both the collection of impressions and the placement of splints were performed with intramuscular ketamine (20 mg/kg) and xylazine (2 mg/kg) used for sedation and inhaled 2% isoflurane used to establish and maintain a surgical plane of anesthesia. After 6 weeks, the rabbits were euthanized (100 mg/kg pentobarbital) and the brainstems and trigeminal ganglia were harvested and processed for immunohistochemistry and whole cell patch clamp, respectively. TMJ condyles were also harvested for histology.

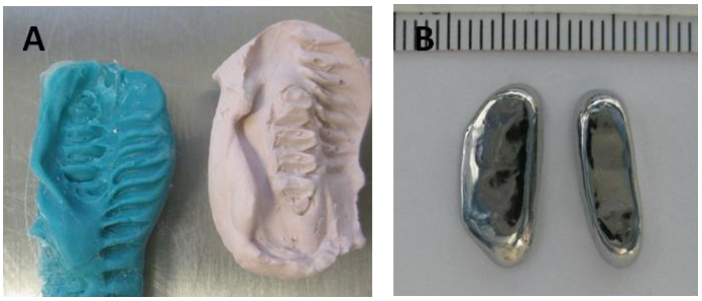

Figure 10. Unilateral molar bite raising splints. A) The splints were made by first taking an impression of the teeth, from which a plaster mold was made. B) The metal splints were cast as crowns, the superior view is shown.

4.3.2 Behavioral Nociceptive Testing

Previously, joint degeneration has been correlated to pain in small rodent models, such as rats and mice, by using behavioral approaches. Calibrated von Frey hairs (VFH) has been one approach applied in rodent models of TMD pain that assesses the presence of hyperalgesia and allodynia in the skin overlying the TMJ [106]. Mechanical nociceptive threshold was assessed with an electronic VFH device (IITC Life Science Inc, Woodland Hills, CA) using a protocol

similar to that developed for assessing TMJ sensitivity in the rat [106]. Briefly, the rabbits were habituated to handling for at least 3 days prior to baseline nociceptive testing, and were unrestrained for testing. The skin over the TMJ was shaved at least 1 day prior to nociceptive testing. The electronic VFH device fitted with a blunt tip (5 mm dia.) was applied to the skin over the TMJ. The stimulus was applied 3 times, with a stimulus interval of several seconds. A positive response was noted when the rabbit flinched or pulled its head away from the application of the stimulus. Withdrawal frequency data was compared over time and between rabbits. Testing was performed bilaterally on nine splinted rabbits. Baseline data were collected for at least three days prior to taking impressions, and then measurements were collected twice during the first week after the splinting procedure, and once a week thereafter for a total of 6 weeks. Data were also collected on three control rabbits without splints over the course of 6 weeks to determine if there was any change over time for healthy rabbits. Behavioral observations were collected by an investigator unblinded to whether rabbits were from control or experimental groups.

4.3.3 Anatomical c-Fos Immunoreactivity

There is considerable evidence to support the suggestion that the number of neurons demonstrating Fos-like immunoreactivity (Fos-LI) in the superficial spinal [29] and trigeminal [169] dorsal horn can be used as a measure of nociceptive activity, and therefore nociception. Fos has been used previously to monitor ongoing/inflammation hypersensitivity both in somatic joints and the TMJ [16, 81, 169]. As a complimentary endpoint to changes in mechanical sensitivity, the presence of the immediate early gene, c-Fos, was assessed in the brainstem. The brain-stem and cervical spinal cord (C1-C2) of splinted and control rabbits were harvested and

post-fixed in 4% paraformalydehyde and cryoprotected in 30% sucrose. Sections (50 μm) were taken from the region of brainstem tissues 3 mm rostral to 6 mm caudal to the obex. Floating sections were processed for immunohistochemistry as previously described [25, 169]. Briefly, the sections were first blocked with normal horse serum (Vector Laboratories, Burlingame, CA), then a goat anti-Fos antibody (c-Fos (4): sc-52-G, Santa Cruz Biotechnology, Dallas, TX) was applied, followed by a biotinylated horse anti-goat antibody (Vector Laboratories). The sections were processed with avidin-biotinperoxidase complex (ABC) (Vector Laboratories), and a nickel-cobalt diaminobenzidine (DAB) reaction (Vector Laboratories) so that Fos positive (Fos+) neurons could be identified with black staining of the nuclei. Negative controls for the immunohistochemistry were generated by not using any primary antibody; only the secondary antibody was applied (Figure 11 D). At least three random sections per rabbit were analyzed and the number of c-Fos positive cells were counted in two standardized regions on the left and right sides of the brainstem in ImageJ software (Figure 11 A, B, C). The two regions were totaled for each slide and the cell counts from each rabbit averaged. The experimenter counting Fos+ cells was blinded to the group. Brainstems from three splinted rabbits were compared to six control rabbits. Data were checked for normality with the Anderson-Darling Test for Normality, and a Student's *t*-test was used with significance set at $p<0.05$ to compare the average number of c-Fos+ cells in splinted rabbits compared to control rabbits.

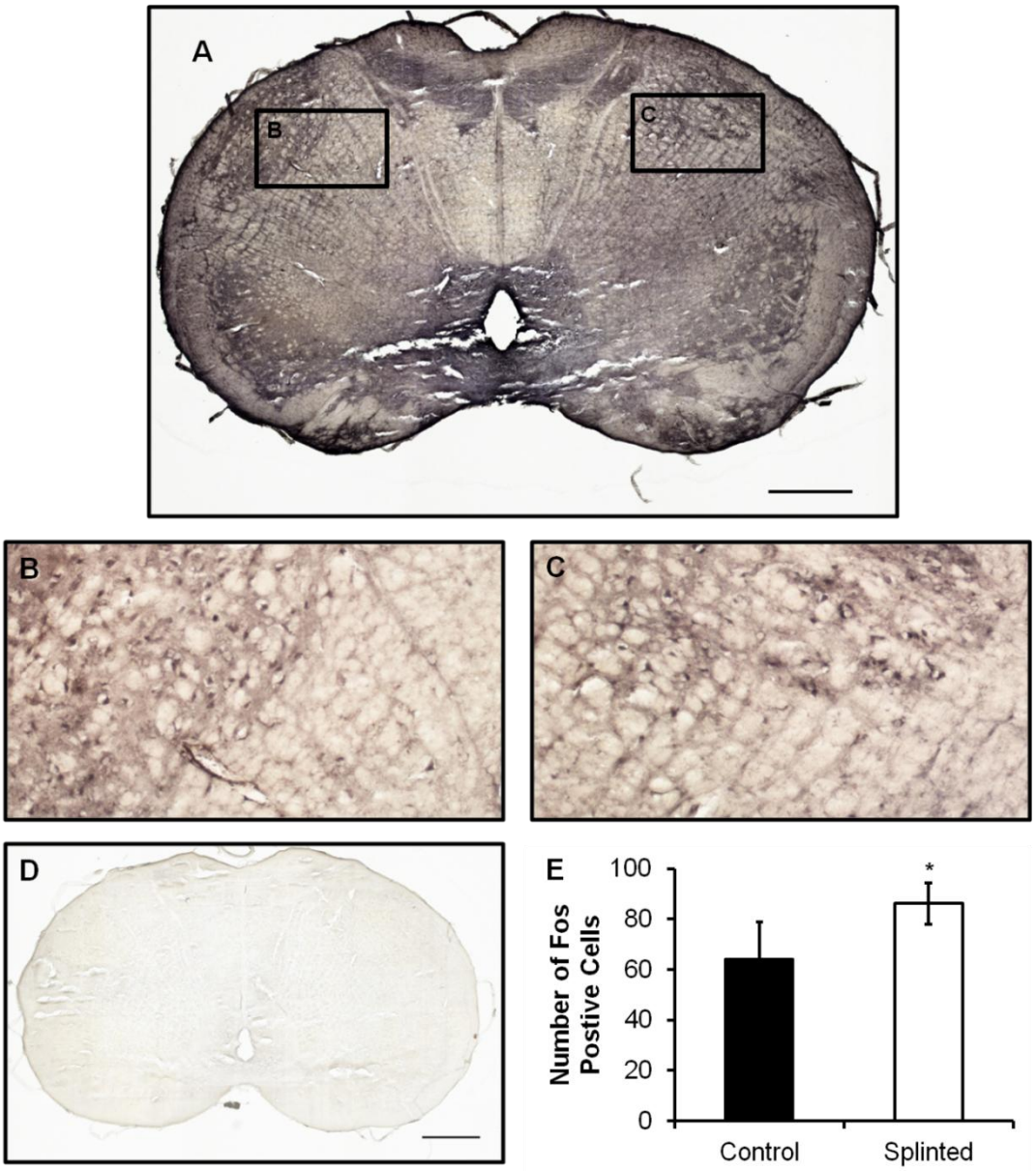

Figure 11. Anatomical c-Fos immunoreactivity. A) c-Fos immunohistochemical staining on a whole brainstem (Scale bar = 1 mm). Regions counted were boxed off. B) and C) Regions in which the c-Fos+ cells were counted totaled and averaged for comparison between splinted rabbits and control rabbits. D) Negative control showing no staining (Scale bar = 1mm). E) Average number of c-Fos+ cells in were totaled from both regions of splinted and control rabbit brainstems and compared ($p<0.05$). Data shown as average ± standard deviation. Samples were collected from 3 splinted rabbits and 6 control rabbits.

4.3.4 Electrophysiology

Electrophysiology has been used previously in rodents to monitor changes in the excitability of afferent neurons innervating the TMJ, under the assumption that sensitization and/or spontaneous activity in putative nociceptive afferents will be associated with ongoing pain and TMJ hypersensitivity [43]. Whole cell patch clamp electrophysiological analysis of acutely dissociated retrogradely labeled TMJ afferents was used as a third measure of altered nociception in the splinted rabbits. Moving the jaw excites many neurons, not only the TMJ nociceptors, however while DiI selection is not overly specific to nociceptors, the putative nociceptors were analyzed. Trigeminal ganglia from three control and three splinted rabbits, six weeks after splint placement, were harvested and dissociated immediately after the animals were euthanized for study in-vitro with protocols developed for rats and mice that were adapted to the rabbit [43, 55]. Prior to splint placement on the experimental animals, at the time of impressions while the rabbits were anesthetized, 10 μl of a 17 mg/mL retrograde tracer DiI (1,1′-dioctadecyl-3,3′,3′-tetramethyl indocarbocyanine perchlorate, Molecular Probes, Eugene, OR) suspension in a saline solution was injected into both the left and right sides of the TMJ [15, 43]. The joint capsule was located through palpation, while opening and closing the mouth. The location of the DiI was confirmed at the time of tissue harvest via direct visualization of the joint capsule. A similar procedure was completed on the control rabbits. The assumption was that the ongoing stimulus from the splint should override any affect from the needle. Importantly, however, both control and splinted animals received injections and comparisons were made between these two groups. Following dissociation of trigeminal ganglia, DiI labeled TMJ neurons were readily identifiable under epifluorescence illumination (Figure 12 A). Whole cell patch clamp recording was used to assess the excitability of these neurons. A standardized series of protocols was employed to

assess the cell capacitance, action potential threshold, properties of the action potential waveform (overshoot, duration, after hyperpolarization magnitude, and rate of decay of the after hyperpolarization), rheobase, and the response to suprathreshold current injection [43]. Briefly, a single action potential was first evoked with a depolarizing current injection via a 4 ms square pulse to analyze the properties of the waveform. The rheobase, the amount of current injection needed to evoke an action potential, was determined by slowly increasing the current amperage until the pulse evoked an action potential. Then, to assess excitability, a square 750 ms pulse was injected at 1X, 2X, and 3X rheobase, and the number of action potentials evoked at each level was recorded. The slope of the stimulus-response function was compared between control and splinted rabbits. The control data was pooled as differences between sides was not expected. The experimental data was pooled after no differences were found between the left and right sides. Putative nociceptive afferents were collected from 3 splinted rabbits with a total of 20 cells analyzed, and from 3 control rabbits with a total of 14 cells analyzed. Data were checked for normality with the Anderson-Darling Test for Normality, and a Student's *t*-test or a Mann-Whitney *U* test were used with significance set at $p<0.05$ to compare the variable values in splinted rabbits compared to control rabbits.

4.3.5 Condylar Histology

TMJ condyles from control and splinted rabbits (n=3) were fixed and decalcified in Formical (Decal Chemical Corp, Suffern, NY) to prepare for standard paraffin embedding and sectioning. Samples were embedded and sectioned by Alizeé Pathology (Thurmont, MD) at 6 μm. Slides were stained with Safranin O/Fast Green to visualize the glycosaminoglycans (GAG) and to visualize the shape and distribution of cells in the fibrocartilage.

4.4 RESULTS

4.4.1 Behavioral Pain Assessments

The behavioral reactions of the splinted rabbits were varied (Table 1). A positive response was noted when the rabbit flinched or pulled its head away from the application of the stimulus. In the splinted group, three rabbits never responded, one rabbit responded for a time then stopped responding, three rabbits responded after a few weeks and continued to respond through the remainder of the testing period, and two rabbits responded intermittently. The contralateral side appeared to be more affected than the splinted right side with more rabbits reacting to the stimulus: of the nine splinted rabbits, four rabbits responded to stimuli applied to the contralateral side and two responded to the ipsilateral/treated side at six weeks. The total number of splinted rabbits responding to the applied stimulus increased with time, with two rabbits reacting at one week and four rabbits reacting at six weeks. Over the course of six weeks, six of the nine splinted rabbits reacted to the stimulus at least once. None of the splinted rabbits responded during the first week after splinting. None of the control rabbits reacted to the applied stimulus at baseline or over the course of 6 weeks.

Table 1. Summary of the behavioral von Frey hair test results. Table shows the total number of rabbits that responded at a particular time point, and the number of rabbits that responded on the left and on the right. Note that adding left and right might not equal the total because some rabbits reacted on both sides. A total of 9 splinted rabbits and 3 control rabbits were tested.

Time Point	Control - Total Number of Rabbits Responding	Splinted - Total Number of Rabbits Responding	Splinted - Number of Rabbits Responding on Left Side	Splinted - Number of Rabbits Responding on Right Side
Baseline	0	0	0	0
Week 1	0	2	1	2
Week 2	0	3	2	1
Week 3	0	3	3	1
Week 4	0	3	3	0
Week 5	0	4	4	3
Week 6	0	4	4	2

4.4.2 Anatomical Analysis

The c-Fos staining was largely restricted to the nucleus of neurons in the dorsal medulla. There were, on average 64±15 Fos+ cells/section in control rabbits and 86±8 Fos+ cells/section in splinted rabbits. This difference was statistically significant, $p<0.05$ (Figure 11 E). One control brainstem was removed as an outlier from the results because the average number of cells per slide was over three standard deviations away from the average without the data point. There were no differences between the left and right sides of the brain stems for the splinted or control rabbits, so only the total values per section were reported.

4.4.3 Electrophysiological Analysis

For the patch clamp experiments, the greatest difference between groups was in rheobase or the amount of current required to evoke an action potential. The rheobase (364±80 pA) and action potential threshold (−31.2±2.0 mV) were higher in rabbits with splints compared to rheobase (99±22 pA) and action potential threshold (−38.0±2.0 mV) in the control rabbits ($p<0.05$) (Figure 12 B). However, there was a trend toward an increase in the number of action potentials evoked in response to suprathreshold stimuli in neurons from splinted rabbits (Figure 12 D, E). The action potential duration decreased significantly from 11.5±1.7 ms to 6.1±0.9 ms and the after hyperpolarization decay time constant also decreased significantly from 16.7±1.5 to 13.4±1.2 ms in neurons from splinted animals ($p<0.05$) (Table 2). The action potential waveforms are shown in Figure 12 C and the passive and active electrophysiological properties of the TMJ neurons are summarized in Table 2.

Table 2. Passive and active electrophysiological properties of TMJ nociceptive afferents from control and splinted animals. Putative nociceptive afferents were collected from 3 treated rabbits with a total of 20 cells analyzed and from 3 control rabbits with a total of 14 cells analyzed. Results presented as average ± standard error of the mean. Statistical significance was set at *p<0.05.

	Capacitance (pF)	Resting Membrane Potential (mV)	Amplitude (mV)	Action Potential Duration (ms)	After-hyperpolarization Amplitude (mV)	After-hyperpolarization Decay Time Constant (ms)
Control	50.0 ± 3.7	-60.8 ± 1.6	45.4 ± 2.6	11.5 ± 1.7	16.7 ± 1.5	166.4 ± 29.4
Splinted	51.2 ± 5.1	-57.8 ± 1.4	42.6 ± 2.8	6.1 ± 0.9*	13.4 ± 1.2	68.5 ± 7.3*

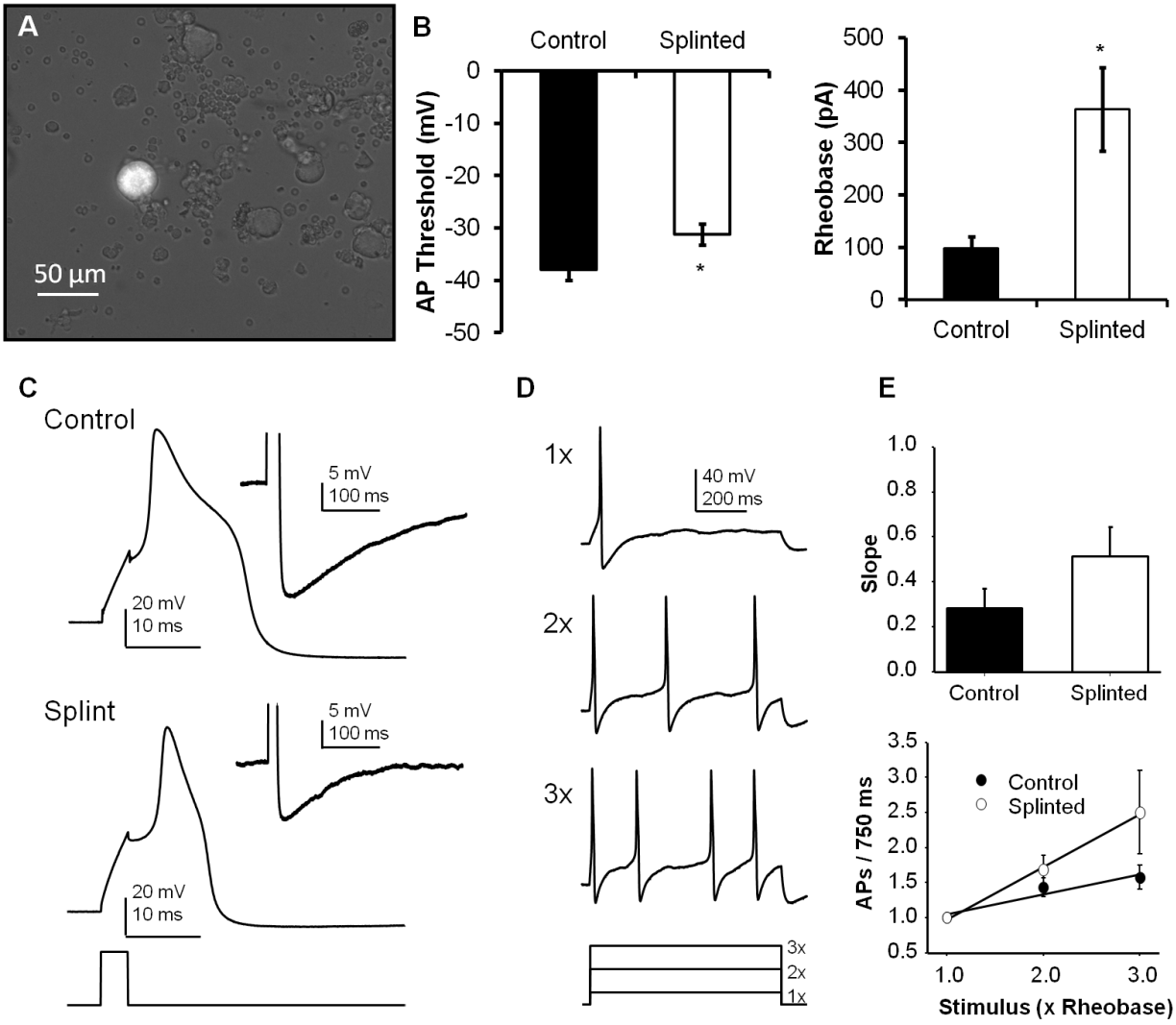

Figure 12. Electrophysiological results. A) Retrogradely DiI labeled TMJ afferent. The DiI labeled neurons were tested with whole cell patch clamp (scale bar = 50 µm). B) Action potential threshold and rheobase of the TMJ afferent nerves. The action potential threshold was higher after 6 weeks of splinting. (*p<0.05). The rheobase or the amount of current required to evoke an action potential, was higher after 6 weeks of splinting (*p<0.05). Data presented as average ± standard error of the mean. C,D,&E) Action potential behavior in afferent neurons from control and splinted rabbits. C) Action potentials from a control neuron and a splinted neuron in response to a 4 ms current injection. D) Action potential response to suprathreshold current. 1x, 2x, and 3x rheobase current was injected for 750 ms, and the number of action potentials in response were counted. E) Plot of the number of action potentials with respect to the stimulus. There was a trend for more action potentials with increasing stimulus for splinted rabbits, however the slope difference was not statistically significant (p<0.05). Putative nociceptive afferents were collected from 3 treated rabbits with a total of 20 cells analyzed and from 3 control rabbits with a total of 14 cells analyzed.

4.4.4 Condylar Histology

A change of the GAG distribution in the subchondral layer of the fibrocartilage was observed between the splinted and the control animals (Figure 13). GAG staining was seen throughout the length of the control condyles and the treated side of the splinted rabbits. In the contralateral condyles of the splinted rabbits, the GAG staining ended midway through the anterior-posterior length of the condyle, leaving behind a fibrous layer (Figure 13 C). The subchondral layer lost definition of the columnar lacunae in both the treated and contralateral condyles from splinted rabbits.

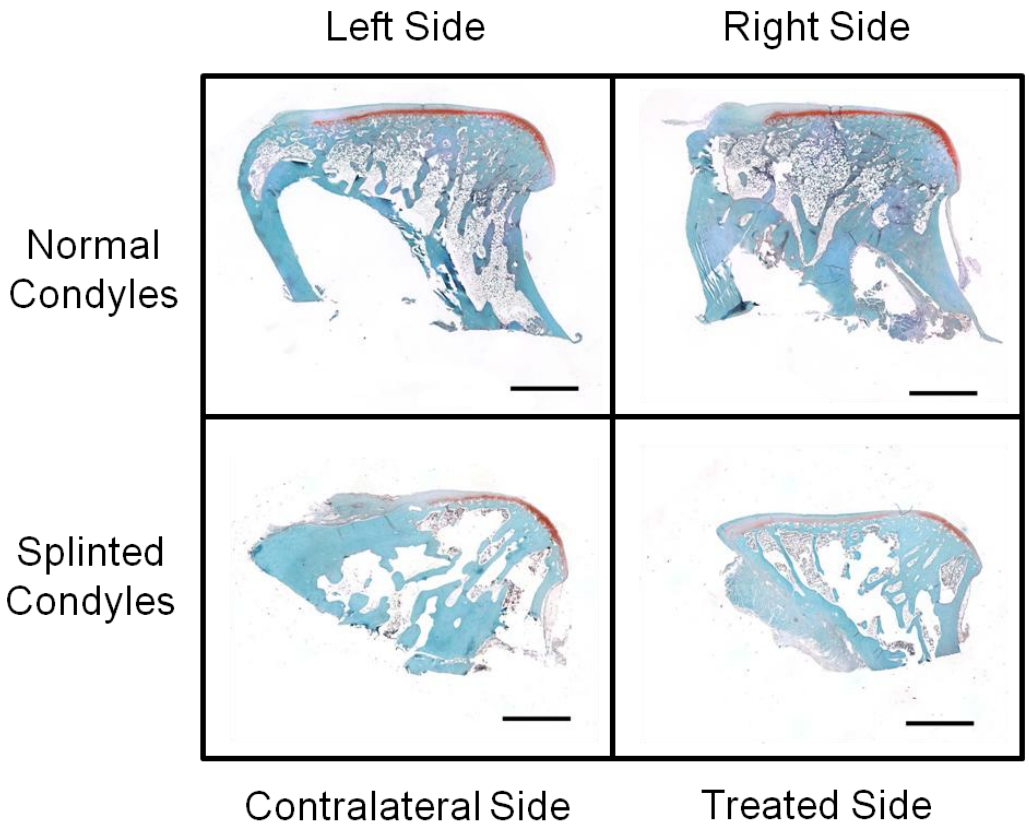

Figure 13. Histology of the TMJ condylar fibrocartilage, showing staining for GAG. A) The left and B) right condyles from normal rabbits and C) the contralateral/left and D) treated/right condyles of the splinted rabbits (Scale bar = 2 mm). Images shown are representative samples from n=3.

4.5 DISCUSSION

The objective of this study was to determine whether endpoints widely used to infer the presence of pain in rodent models of TMD were applicable to a rabbit model of TMD associated with altered joint loading. These endpoints included mechanical probing of the tissue over the TMJ, increases in Fos-like immunoreactivity in the trigeminal nucleus caudalis, and an increase in the excitability of TMJ afferents. Changes in these endpoints were correlated with changes in joint histology, which agreed with previous studies [26, 82]. Six weeks after unilateral splint placement, marked changes in the condylar fibrocartilage were present. These changes were associated with an increase in the response to mechanical probing over the TMJ and Fos-LI. In contrast, a decrease in the excitability of putative TMJ nociceptive afferents was observed in splinted animals.

The behavioral changes observed in the rabbit were consistent with results from previous rat studies that showed an increase in behavioral nociceptive response from an inflammatory agent being injected into to the joint space [106]. However, differences with previous studies were also observed. There was a limited sensitivity in the rabbit TMJ. The rabbits presented with an all or nothing response, and the response was dramatic when one was observed. This suggests that an alternative behavioral approach may be useful and needed for the rabbit, an approach that lends itself to more graded changes for measuring pain response. The variability may be an important feature of the model that not only increases its relevance to the clinical picture, but is a feature that may be exploited to help identify mechanisms underlying the variability in the manifestation of pain in the clinical population of TMD patients.

The c-Fos data also followed the same trends as found in previous studies of TMJ pain in rats [16, 169], where c-Fos+ cell counts were higher in the experimental animals than the

controls. The overall c-Fos+ cell counts in the control rabbits in this study were higher than the control animals in previous small rodent orofacial pain studies However, it should be noted that c-Fos+ cell counts comparable to those reported here have been reported in studies involving other species, such as cat and guinea pig [32, 60]. Nevertheless, the high level of Fos staining in control rabbits suggests non-nociceptive input drives Fos in the rabbit trigeminal nucleus caudalis, and thus a more specific endpoint may be useful in the rabbit model. And while the splint-induced increase in c-Fos+ cells we observed was significant, there are several likely explanations for the relatively modest increase observed. Differences in the quality and the intensity of the applied stimulus can affect the number of Fos+ cells observed [56], and most studies in rodents employ relatively intense stimuli with relatively short intervals between induction of inflammation and analysis of c-Fos staining [16, 63, 169]. Along these lines, while joint degeneration was clearly evident in our model, the sensitivity to evoked stimuli is particularly problematic in the clinical population and nothing was done to drive additional oromotor activity in the present study prior to tissue harvest. If compensatory changes suggested by the decrease in afferent excitability discussed below were also manifest in the brainstem and/or higher central nervous system centers, the relatively modest increase in c-Fos staining may reflect the efficacy of these processes. Additional experiments will be needed to address these possibilities. In the future, it will also be important to look at a detailed time-course of the c-Fos changes associated with the splint model. The differences that arise between the c-Fos expression and the von Frey test may be due to the variability in the von Frey test, which appeared to lack the sensitivity one would hope for in a nociceptive test.

Electrophysiological results were not only opposite to those expected, but also to those previously reported in rodent models in which an increase in TMJ afferent excitability was

observed in association with TMJ inflammation [43]. We suggest that there are at least three likely explanations for these discrepant results, and these hypotheses will need to be tested in future experiments. The first may simply be due to experimental differences, where increases in excitability were observed after a relatively short period (a few days to a week) of inflammation, where a frank inflammatory stimulus was used to drive the changes [43, 55]. A very different approach was used in the present study where the neurons were studied after a considerably longer period of time post injury, giving the neurons time to compensate for the stimulus. Second, these differences may reflect species differences where the increase in nociceptive input in the rabbit TMJ model is due to changes in transduction and/or transmitter release for example, rather than an increase in excitability per se. Even in the rodent literature, there is an ongoing debate about whether the increased mechanical sensitivity observed in models of acute and persistent inflammation are due to an increase in afferent excitability, where despite robust changes in the response to thermal stimuli, no changes in the response to mechanical stimuli are generally reported in studies involving the skin-nerve preparation [68, 72, 76, 94]. Third, the changes in excitability and action potential waveform observed are consistent with compensatory changes in TMJ afferents for an overall increase in afferent drive associated with joint degeneration. Given how critical normal TMJ function is to survival, the presence of compensatory inhibitory mechanisms make intuitive sense. This latter possibility suggests an alternative basis for the manifestation of TMD pain, or at least why joint pathology may not be the best predictor of pain and loss of function, where the failure to engage such compensatory mechanisms may contribute to greater pain and disability observed in a subpopulations of TMD patients. Future studies will be needed to determine what is occurring through time to the neurons as they change and compensate for the ongoing pain stimulus.

The changes observed in electrophysiology are all consistent with an increase in potassium ion (K+) current in TMJ afferents, which include decreased excitability, membrane hyperpolarization, decreased action potential duration, and an increase in after hyperpolarization amplitude. Currently, treatments for pain are being developed with drugs such as retigabine, that increase K+ channel activity as a means to reduce the nerve activity [119]. In this regard, our results were particularly striking given that, decreases in K+ channel activity have often been identified as mechanisms accounting for the increases in excitability seen in many studies [119]. Our particular animal model is one of the first to show evidence of an increase in K+ current in response to a pain-inducing challenge.

The study was sufficient to establish significant changes in joint properties, nociception, c-Fos and electrophysiological properties. While the behavioral changes were variable, suggesting the need for more sensitive assays, the changes with this endpoint were also significant. While the rabbit model may be very useful for a number of endpoints, it will be necessary to develop more sensitive nociceptive assays for this species. The potential importance of timing and the ability to recover from the changes in the joint in the absence of another form of intervention, both suggest that detailed analysis of both onset and recovery is important, but beyond the scope of the initial characterization of the model. Establishing a timeline for all endpoints to enable a correlation analysis would be important for a future study that asks the question of whether there is a point at which the changes that develop in the joint are irreversible and a chronic pain state will have been established.

TMD is a multifactorial and very complex disease process. This study focused on a very particular type of joint degeneration, and on discrete parts of the process: altered loading leading to local tissue stress, inflammation, and pain. This study is one step in the process for gaining a

better understanding of TMDs. Taken together, our data indicate that abnormal TMJ loading can lead to condylar fibrocartilage remodeling. Loss of the subchondral cartilage layer may lead to abnormal fibrocartilage mechanical properties, which if unchecked could lead to further degeneration of the joint. This could be a possible mechanism for the transition from acute to chronic pain in TMD patients. In the acute phase, this fibrocartilage degeneration could also be sensed by nerves in the synovium or subchondral bone. These findings could help explain why patients in the clinic present with pain but with no apparent damage to their TMJ, as MRI or panoramic x-ray could not detect the changes to the condylar fibrocartilage as observed in the histology of this study. Further development of this rabbit model could lead to a better understanding of TMJ pain and degeneration.

4.6 CONTRIBUTIONS

I assisted with the rabbit dental procedures, helped to collect the behavioral data, harvested the appropriate tissues, completed the analysis on the behavioral data and the anatomical data, prepared and edited the manuscript. Mr. Tudares performed the rabbit dental procedures, collected the behavioral data, completed the c-Fos staining and imaging, and helped with manuscript editing. Mr. Lowe assisted with the condylar histology. Dr. Gold and his post-doc Dr. Lee collected and analyzed the electrophysiological data and helped with the project design, data analysis, and manuscript editing. Dr. Almarza helped with project design, data analysis, and manuscript editing.

5.0 FUNCTIONAL ANALYSIS OF THE RABBIT TEMPOROMANDIBULAR JOINT USING DYNAMIC BIPLANE IMAGING[3]

5.1 ABSTRACT

The dynamic function of the rabbit temporomandibular joint (TMJ) was analyzed through non-invasive three-dimensional skeletal kinematics, providing essential knowledge for understanding normal joint motion. The objective of this study was to evaluate and determine repeatable measurements of rabbit TMJ kinematics. Maximal distances, as well as paths, were traced and analyzed for the incisors and for the condyle-fossa relationship. From one rabbit to another, the rotations and translations of both the incisors and the condyle relative to the fossa contained multiple clear, repeatable patterns. The slope of the superior/inferior incisor distance with respect to the rotation about the transverse axis was repeatable to 0.14 mm/degree and the right/left incisor distance with respect to the rotation about the vertical axis was repeatable to 0.03 mm/degree. The slope of the superior/inferior condylar translation with respect to the rotational movement about the transverse axis showed a consistent relationship to within 0.05 mm/degree. The maximal translations of the incisors and condyles were also consistent within

[3] Published as Henderson SE, Desai R, Tashman S, Almarza AJ. 2014, "Functional Analysis of the Rabbit Temporomandibular Joint Using Dynamic Biplane Imaging" Journal of Biomechanics, April 11, 2014, 47(6): 1360–1367. Epub 2014 Feb 18. DOI: 10.1016/j.jbiomech.2014.01.051, PMID: 24594064

and between rabbits. With an understanding of the normal mechanics of the TMJ, kinematics can be used to compare and understand TMJ injury and degeneration models.

5.2 INTRODUCTION

Some estimates suggest that over ten million Americans are affected by temporomandibular joint (TMJ) disorders (TMDs) [99]. Clinical symptoms of TMDs include jaw locking, clicking, headaches, joint pain and tenderness, restricted range of motion, painful mastication, and deterioration of the disc and the articulating surfaces of the TMJ [149]. Clinical exams often used to diagnose TMDs only test the end positions of the teeth and do not focus on the travel path of the joint. It is important to understand the kinematics of the joint to determine if early changes in the function of the joint may suggest oncoming TMDs.

Knowledge of dynamic TMJ function through three-dimensional (3D) skeletal kinematics is essential for understanding normal joint behavior and investigating the effects of injury or disease in the TMJ. Many factors contribute to joint motion including muscular forces, passive structures constricting movement, and dynamic physical forces such as contact, gravity and inertia [83, 108]. However, little is known on how these factors combine for everyday movement, making replication of kinematics difficult [124]. 3D visualization and measurement techniques are necessary to measure skeletal kinematics with high precision and accuracy.

Various kinematic studies have been performed on humans, many looking at the effects of partial and total joint replacement and other invasive treatments on joint motions [13, 45, 71, 77, 79, 101, 136, 164]. While incisal movement alone is not enough to understand the movement of the mandibular condyles [97, 132], 3D jaw tracking systems have provided more

insight into condylar motion [13, 45, 71, 77, 79, 101, 136]. In-depth TMD patient studies have not been performed with these systems because it is hard to identify patients at early stages of dysfunction. The current 3D systems are beneficial for human patient studies, but cannot be implemented in non-compliant animal models.

Animal studies are uniquely suited for investigating the disease initiation and progression that cannot be completed and repeated in a patient study, by enabling both mechanical interventions that may drive disease development and comprehensive, invasive tissue assessment. In particular, the rabbit model was chosen due to the various TMJ injury and degeneration models already established in the literature [2, 5, 10, 26, 112, 129-131, 134]. Rabbits also exhibit a grinding mastication similar to that of humans [96]. Several studies have previously collected normal rabbit kinematics; however, most were done invasively and only focused on incisal movement [62, 65, 66, 75, 95, 109, 131, 146-148, 160-162], instead of also understanding condylar movement [96].

Non-invasive 3D x-ray imaging systems have been developed to combine x-ray videos with 3D morphology from bone scans and have been extensively validated in human and animal joints [17, 18, 23, 124, 126], including one study of normal minipig mastication [23]. Our study investigated the dynamic nature of the TMJ condyle with respect to the fossa, as well as the incisor relationship in rabbits. The objective of this study was to determine and evaluate repeatable measurements of rabbit TMJ kinematics. The relative motion of the condyle with respect to the fossa was tracked. Maximal distances, as well as path, were traced and analyzed for the incisors and for the condyle-fossa relationship. By establishing kinematics for control animals, future kinematic assessments can be used to help understand the progression of specific TMDs.

5.3 METHODS

5.3.1 Animal Model

Three skeletally mature female New Zealand White rabbits, approximately 1 year in age, and weighing approximately 5kg, were purchased from Myrtle's Rabbitry Incorporated (Thompsons Station, TN). All rabbits were examined by a veterinarian and were found to be in good health. All animal procedures were approved by the Institutional Animal Care and Use Committee at the University of Pittsburgh, in accordance with the National Institutes of Health guidelines for the use of laboratory animals.

5.3.2 Measurement of TMJ Kinematics: High-Speed Biplane Radiography

TMJ kinematics were assessed using a unique high-speed stereo-radiographic system, consisting of two sets of 110kW pulsed x-ray generators (CPX 3100CV; EMD Technologies, Quebec, Canada), 40cm image intensifiers (Thales, Neuilly-sur-Seine, France) using a 20cm field of view, and high-speed 4 Megapixel digital video cameras (Phantom v10, Vision Research, Wayne, New Jersey, USA). The system configuration is shown in Figure 14. Data was collected at a frame rate of at least 170 frames/s for 1s with 4 megapixel image resolution. Short-duration (1ms) exposures were performed to acquire images free of motion blur.

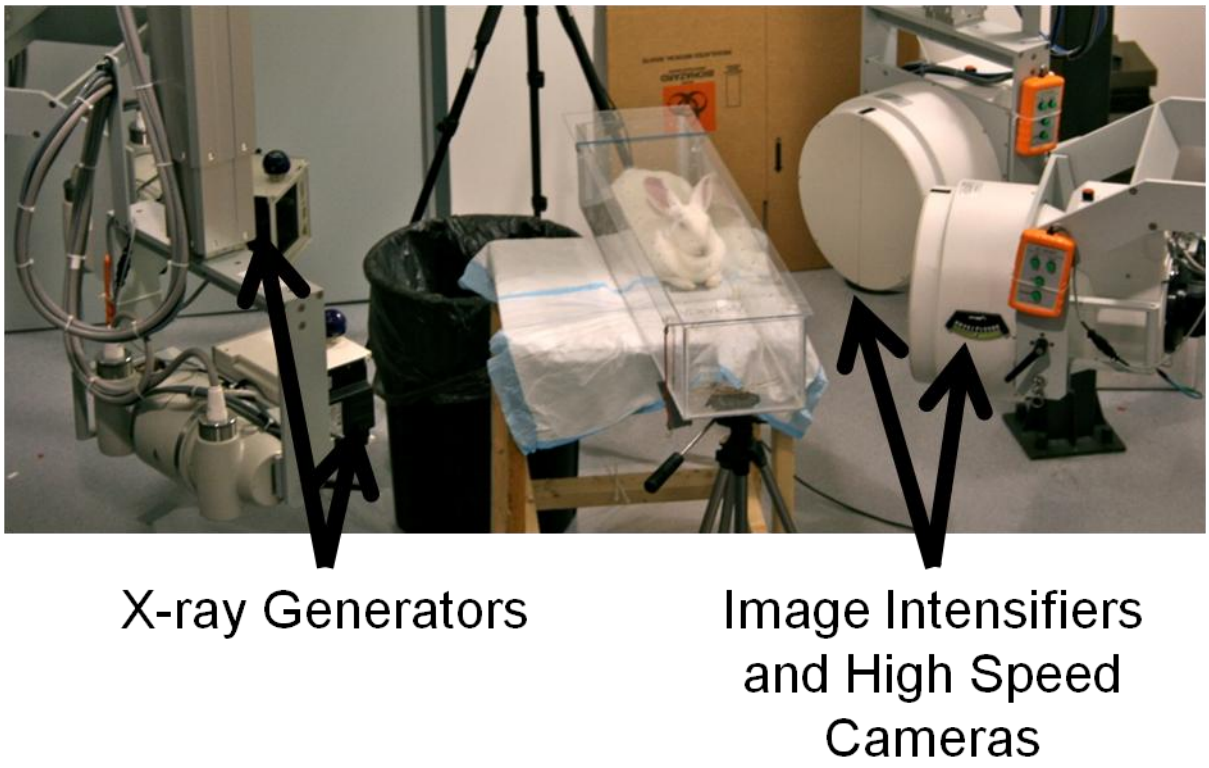

Figure 14. High-speed biplane radiography was used for image collection. Rabbits were placed in a radiolucent box between two sets of x-ray generators and image intensifiers with high speed cameras.

This system has been used extensively for studies of joint motion in humans and animals, with accuracy in the range of 0.07-0.3 mm for a 40 cm field of view [31, 124, 126]. For these rabbit studies, a 20 cm field of view was used, reducing image pixel size by a factor of two with a concomitant increase in accuracy.

The rabbits were placed in a ventilated radiolucent cage (Figure 14). Small pieces of dried fruit were placed in the rabbit's mouth and radiographic images (Figure 15 A) were acquired for a 1 second period. The process was repeated to collect at least three acquisitions per rabbit.

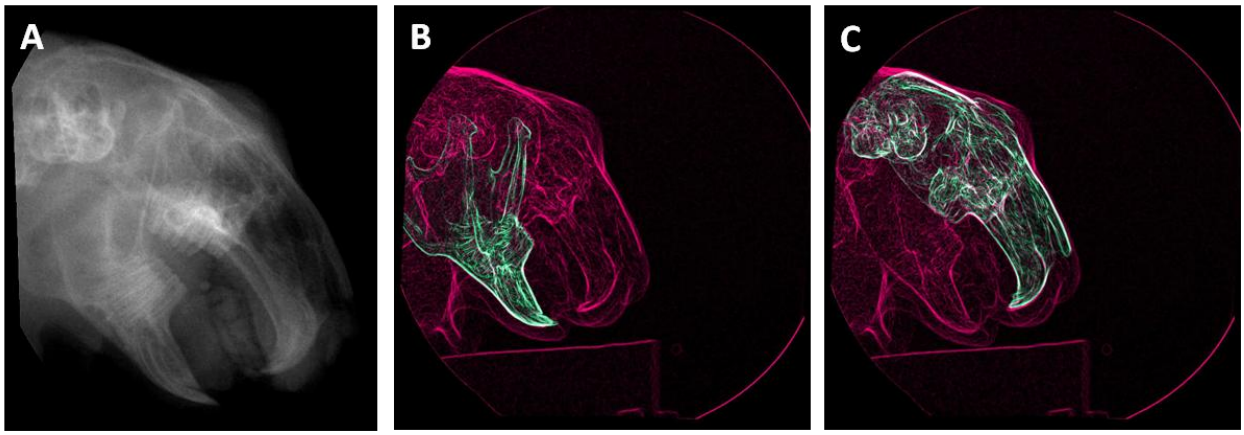

Figure 15. Sample images from x-rays and 2D to 3D registration. A) Sample x-ray image from the high resolution cameras at one frame in time. B and C) For 2D to 3D registration, the collected x-ray images (pink) are matched frame by frame with the virtual x-ray images (green) from the CT scan. One of the two combined images is shown for each the mandible (B) and the skull (C).

The model-based technique for determining 3D kinematics of skeletal structures from biplane radiographic views has been extensively described and validated. We have performed multiple in-vivo and in-situ validations of our measurement methods for the knee, shoulder and cervical spine, by implanting beads on the bones (which can be tracked with high accuracy using well-established radio-stereometric techniques), and comparing this “gold standard" marker/bead tracking to the markerless tracking method employed for this study [6, 18, 54, 124, 165]. Typical 3D measurement precision for these studies is in the order of 0.1-0.2 mm during dynamic testing (and substantially better than 0.1 mm for static imaging). Dynamic accuracy for joint kinematics (relative motion between two bones) was measured directly, and was typically around ±0.5 mm for translations and ±0.7 degrees for rotations. These are direct assessments of accuracy for clinically relevant measurements acquired at functionally relevant movement speeds that account for propagation of all sources of error.

In actuality, the accuracy for this rabbit TMJ study was substantially better. Under similar bone sizes and imaging conditions, TMJ tracking accuracy would equal or exceed that for the knee/shoulder, because there are more features and image details in the skull and mandible than there are for the knee or shoulder. The knee and shoulder validation studies were done with radiographic imaging resolution of approximately 0.5 mm/pixel and CT slice spacing of 0.6 or 1.2 mm (within-slice resolution of approximately 0.5 mm). The rabbit jaw is much smaller, so a smaller field of view was employed; the images used for tracking had a pixel size of approximately 0.125 mm. Head/jaw CT scans were obtained using a micro-CT system with isotropic, 0.1 mm voxels. While we have not specifically assessed accuracy under these conditions, it is certain that better imaging resolution will improve tracking accuracy. We are conservatively estimating that this 400% improvement in radiographic image resolution, combined with a 500% (or better) improvement in CT scan resolution (along with the greater bone details inherent in the skull and mandible images), will result in a error reduction (relative to the shoulder/knee studies) of at least a factor of 2. Thus, we estimate that the accuracy for TMJ kinematics is approximately ±0.2 mm in translation and ±0.4 degrees in rotation. For the incisors, this 0.2 mm error relates to 5% error in the differences in superior-inferior translations measured between rabbits. For the condyles, an error of 0.2 mm results in a 15% error in the differences in superior-inferior translations measured between rabbits.

Briefly, a 3D model of each bone to be tracked was derived from a computed tomography (CT) scan (as described below). A virtual model of the biplane x-ray system was created for generating a pair of digitally reconstructed radiographs (DRR's) via ray-traced projection through the CT bone model. The bone model was automatically repositioned within the virtual model until a best match was achieved between the simulated DRR's and the actual radiographic

image pair (Figure 15 B, C). This technique determined the 3D positions and orientations of the mandible and the skull for each motion frame.

5.3.3 Bone Models from Micro-Computed Tomography

Accurate, animal-specific bone models were required for both model-based tracking and kinematic analysis. After euthanasia, the entire head, including the mandible and skull, was scanned at high resolution (102.5 μm isotropic voxels) using a micro-computed tomography system (Inveon micro-CT system by Siemens at the Rangos Research Center Animal Imaging Core, Children's Hospital of Pittsburgh of UPMC). The mandible and skull bones (with teeth) were segmented from each other and from soft tissue and reconstructed into both surface and volumetric models using Mimics software (Materialise, Inc).

5.3.4 Coordinate Systems

Anatomical coordinate systems were set up similar to the systems used by Brainerd *et al.* [23]. The transverse axis was aligned through the center of the condyles (or fossas for the skull), the longitudinal axis was parallel to the occlusal plane (where the molars meet) running posterior to anterior, and the vertical axis was the cross product of the transverse and longitudinal axes (Figure 16). The coordinate systems were centered between the condyles and fossas for the mandible and skull, respectively. The orientations of the anatomical coordinate systems were determined using standard rigid body transformations, and translations and rotations were determined. The joint rotations were calculated in the order of rotation about the transverse axis, rotation about the vertical axis, and rotation about the longitudinal axis.

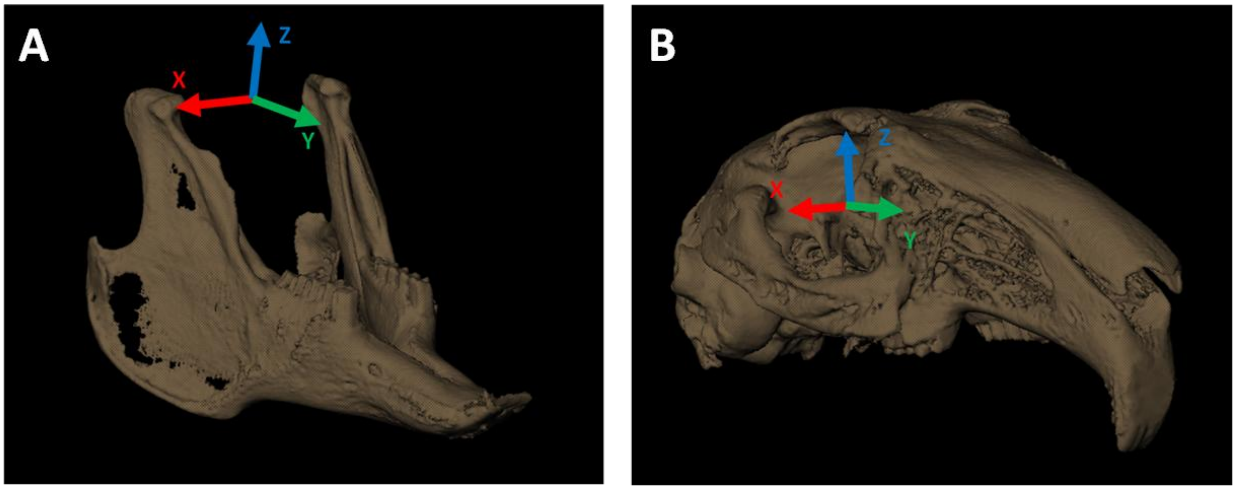

Figure 16. The anatomical coordinate systems. A) For the mandible the system was set up with the transverse axis (x-red) aligned through the center of the condyles, the longitudinal axis (y-green) was parallel to a plane through the occlusal plane (where the teeth meet), and the vertical axis (z-blue) was the cross product of the transverse and longitudinal axes. B) The skull coordinate system was set up in a similar manner. The coordinate systems were centered between the condyles and fossas, for the mandible and skull respectively.

5.3.5 Analysis of Biodynamics

Our analysis focused on the dynamic behavior of the TMJ rather than only the end of range displacement of the jaw. The center points on the incisors were tracked in all three planes (Figure 17 A, B). The relative motion of the condyle in relation to the fossa was tracked by placing points at the most superior point of the condyle and in the concave region of the fossa (Figure 17 D, E). The relative motion of the centers of the two points was determined in all three anatomic planes. These points were rigidly fixed and the position measured in each frame. A future study will need to determine the reliability of determining the coordinate planes.

For each animal, kinematics from at least three representative chewing cycles were analyzed from each of a minimum of three different acquisitions. Three acquisitions per rabbit

were chosen based on the observation of three distinctive complete chewing cycles; one chewing cycle is equal to a full opening and closing of the mandible. One full chew cycle was determined on a time graph to be the distance or rotation from one peak to the next peak (Figure 18). Analyses were performed to determine the maximal translations and travel paths for both the incisors and the condyles.

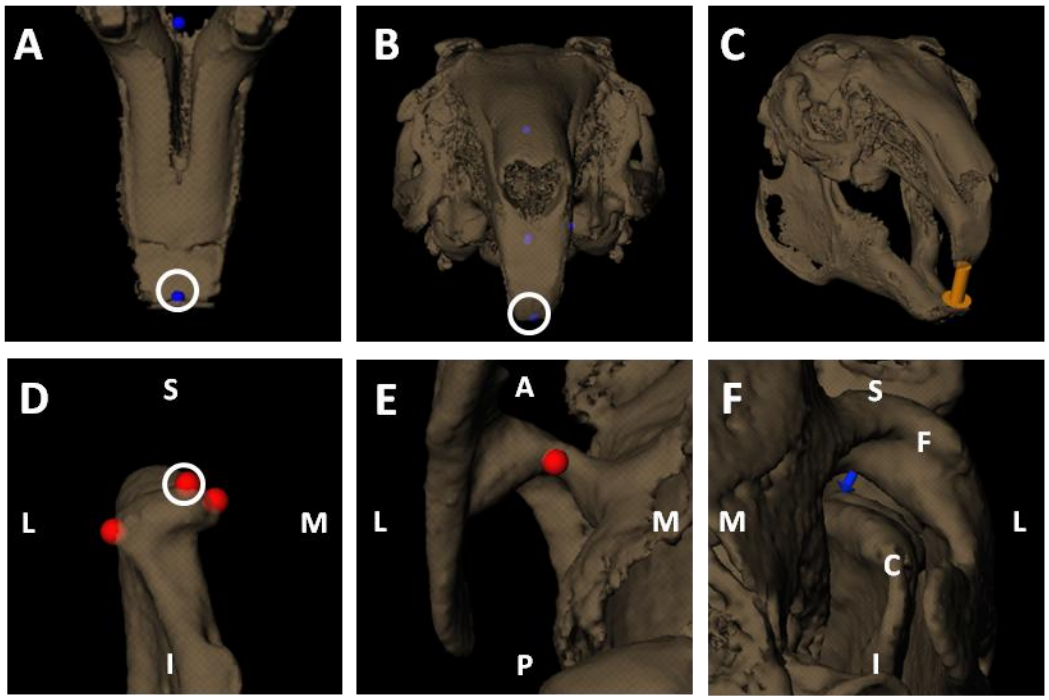

Figure 17. Points placed for measurements. A) Mandible incisor point, superior view. B) Skull incisor point, anterior view. C) Vector demonstrating the distance between the incisor points. D) Condylar point, anterior view. E) Fossa point, inferior view. F) Vector indicating the distance between the condylar point and the fossa point (condyle is labeled with C and the fossa with F). Figures are labeled by directions: A-anterior, P-posterior, M-medial, L-lateral, S-superior, I-inferior.

5.3.5.1 Incisors- Maximal Translations

Motion of the incisors was described by quantification of their total displacement right/left, superior/inferior, and anterior/posterior during a chew cycle from peak displacements in each direction during each chew cycle (Figure 18 A). Thus, three parameters of the contact point on the incisors were compared: 1) Maximal change in superior/inferior translation; 2) Maximum left/right translation; 3) Maximum anterior/posterior translation.

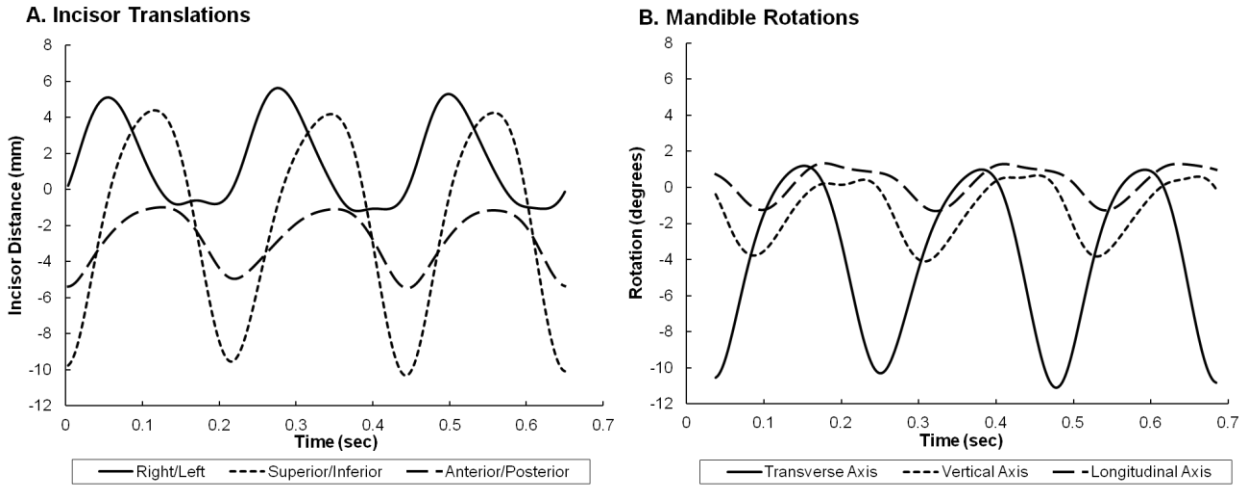

Figure 18. Incisor translations and mandible rotations. A) The change in distance of the mandible incisors from the skull incisors with relation to time. B) The change in the rotation of the mandible around the vertical, transverse and longitudinal axes with relation to time. One chew cycle is considered to be from one peak to the adjacent peak. Representative data shown.

5.3.5.2 Incisors- Path

To describe path, each mandible rotation in the coordinate plane (Figure 18 B) was compared to each incisor translation to identify any relationships that existed. The translation-rotation relationships analyzed were chosen when a repeatable linear pattern was observed, which allowed for the slope to be compared between different acquisitions. If no repeatable and/or

linear pattern was observed, the slope was not calculated. The following slopes were chosen for analysis: 4) Slope of the superior/inferior translation of the incisors with respect to mandible rotation about the transverse axis (Figure 19 A); 5) Slope of the left/right translation of the incisors with respect to the mandible rotation about the vertical axis (Figure 19 B).

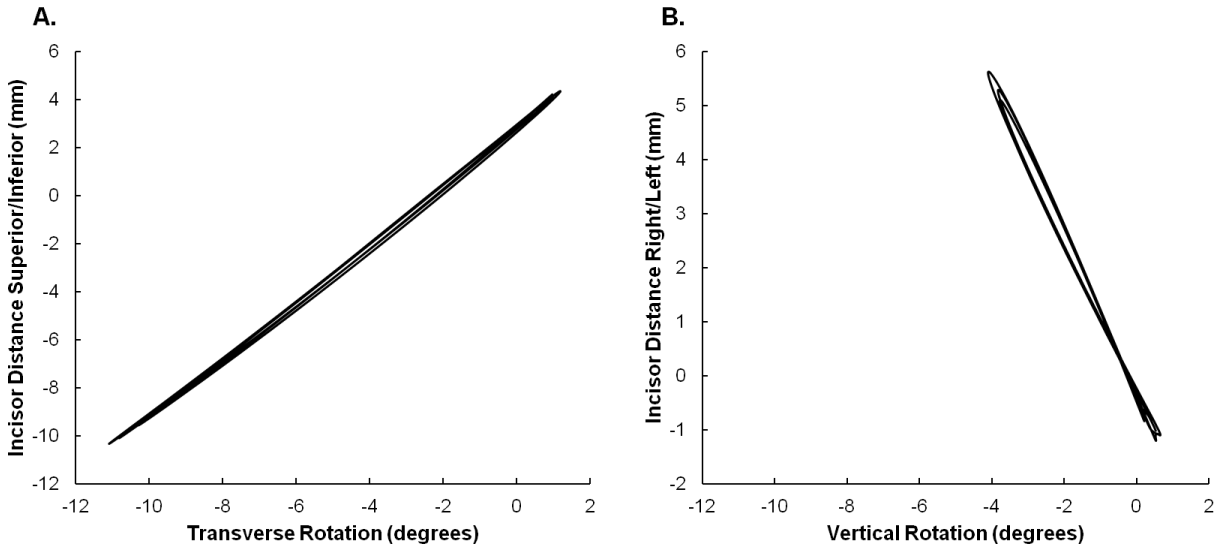

Figure 19. Comparison of the distance of the mandible incisors from the skull incisors with respect to the rotation of the mandible. A) The distance traveled superior/inferior with respect to the rotation of the mandible around the transverse axis. B) The distance traveled right/left with respect to the rotation of the mandible around vertical axis. Representative data shown.

5.3.5.3 Condyle- Maximal Translations

The movement of the mandible was somewhat elliptical in the coronal plane and always started to the same side during an acquisition. As established in the literature, the side in which the mandible first moves is the working side, while the other is called the balancing side [96]. The total displacement for both the working side and balancing side condyles was measured. Total superior/inferior displacement was found by subtracting the maximal opening from the maximal

closing of the mandible relative to the fossa during a chew cycle. Additionally, the total displacement anterior/posterior was calculated. The left to right condyalr displacement was minimal. The following parameters were described: 6) Maximum working condyle superior/inferior translation relative to the fossa; 7) Maximum balancing condyle superior/inferior translation relative to the fossa; 8) Maximum working condyle anterior/posterior translation relative to the fossa; 9) Maximum balancing condyle anterior/posterior translation relative to the fossa.

5.3.5.4 Condyles- Path

The translations of the condyles were plotted with respect to the mandible rotations, and the relationships to be analyzed were chosen when a repeatable linear pattern was observed, which allowed for the slope to be compared between different acquisitions. If no repeatable and/or linear pattern was observed, that specific evaluation was not used. The analysis of the superior/inferior movement of the condyle relative to the fossa with respect to the rotation of the mandible about the transverse axis was performed according to the direction of chewing. Analysis depended on the side of mastication as well as the opening and closing of the mouth. The only repeatable behavior was seen in the superior/inferior translation of the condyles with respect to the transverse axis rotation of the mandible (Figure 20 A, B). For this measure, a linear pattern was observed when analyzing the slope of only the first fifty percent of the closing cycle. Comparisons were made amongst the slopes calculated from the closing condyle cycle of the working and balancing sides of the mandible: 10) Slope of the working side superior/inferior translation of the condyle relative to the fossa with respect to the mandible rotation about the transverse axis; 11) Slope of the balancing side superior/inferior translation of the condyle relative to the fossa with respect to the mandible rotation about the transverse axis.

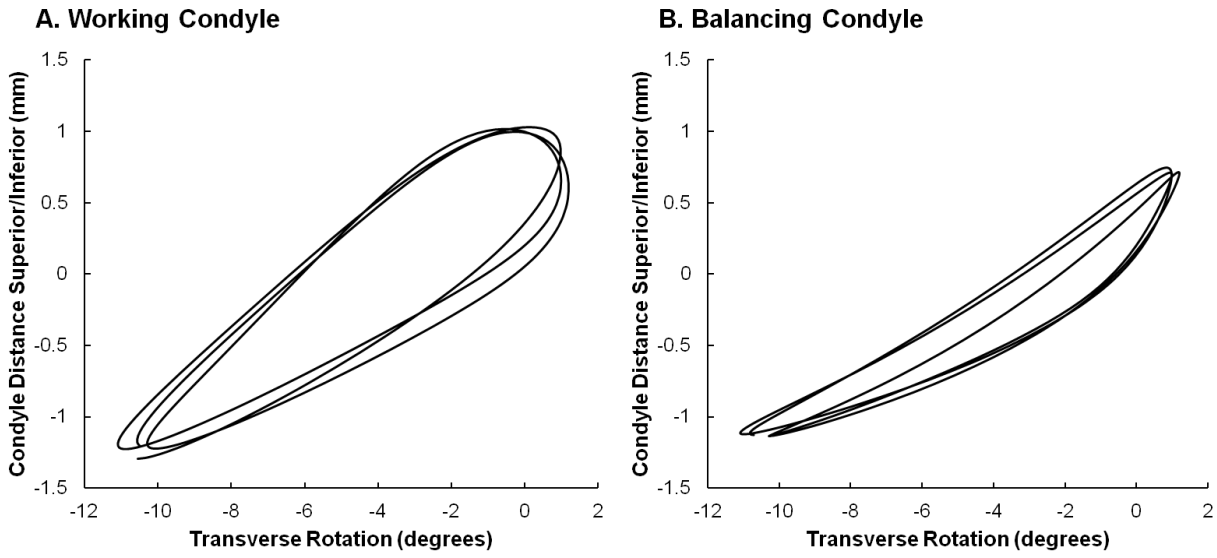

Figure 20. Comparison of the distance of the condyle relative to the fossa with respect to the rotation of the mandible. The distance traveled superior/inferior with respect to the rotation of the mandible around the transverse axis of the A) working side condyle and the B) balancing condyle. At an angle of 0° the mouth is considered to be closed. The opening of the mouth translations are represented by the bottom line of the ellipse and the closing of the mouth translations are represented by the top line. Representative data shown.

5.3.6 Statistical Analysis

In summary, first, to determine differences amongst chewing stage (opening and closing) for all biodynamics parameters for multiple chewing cycles a student t-test was performed. The data was found to have a normal distribution using the Anderson-Darling Test for Normality. Then, a one-way ANOVA (Minitab 16, State College, Pennsylvania, USA) with Tukey's post hoc testing was then used to assess differences for all biodynamics parameters amongst chewing cycles within individual acquisitions, amongst acquisitions within each rabbits, and amongst rabbits from at least three acquisitions. The data used for the ANOVAs was found to have a normal

distribution using the Anderson-Darling Test for Normality. A statistically significant difference was established as $p<0.05$. All data was reported as an average ± standard deviation of the mean.

In more detail, statistical analyses for all reported biodynamic variables were performed in four stages. Firstly, chewing stage (opening, closing) within a chewing cycle, for all chewing cycles, acquisitions, and rabbits were assumed to be different; however, no statistically significant differences were found and therefore the values for opening and closing for each chew cycle were averaged into one opening/closing value per cycle. Then secondly, all chewing cycles (at least three) within an acquisition, for all acquisitions and rabbits were assumed to be different; however, no statistical significance was found for the opening/closing value between chew cycles and hence the values of chew cycles for each acquisition were averaged into one chew cycle value per acquisition. Thirdly, acquisitions (at least three) for each rabbit, from all rabbits were assumed to be different; again, no statistically significant differences were observed. Thus, all biodynamic parameters are averaged into one acquisition value per rabbit. Fourthly, acquisitions between rabbits were assumed to be different; and in this case one rabbit was different than the other two, which did not allow for the data to be averaged for all rabbits.

5.4 RESULTS

Evaluation of the movement of the upper and lower incisors from opening to closing revealed a periodic pattern in all three directions and all three rotations (Figure 18). In the superior/inferior direction, the total incisor displacement was 9.03±1.55 mm for Rabbit 2, which was statistically different from the other two rabbits with an average displacement of 14.55±3.71 mm ($p<0.05$, for details see Table 3). The total displacement, between the upper and lower incisors in the right/left direction was statistically different for Rabbit 2 with a distance of 3.70±1.11 mm compared to the average of the other two rabbits at 6.58±1.09 mm ($p<0.05$, Table 3). In the anterior/posterior direction, the maximum displacement was significantly different between Rabbits 1 (4.99±1.13 mm) and 2 (1.82±0.43 mm), but neither were different from Rabbit 3 (3.20±0.86 mm) ($p<0.05$, Table 3).

Repeatable measurable relationships (Figure 19) were found by determining the slopes of the incisor displacement in the superior/inferior direction with respect to the rotation of the mandible about the transverse axis curves. Rabbit 2 (1.33±0.04 mm/degree) was statistically different from Rabbits 1 and 3 (1.19±0.03 mm/degree) for the slope of the superior/inferior displacement with respect to rotation about the transverse axis ($p<0.05$). The slopes of the incisor displacement right/left with respect to the rotation of the mandible about the vertical axis curves were also repeatable with an average of −1.38±0.06 mm/degree with no statistical differences between rabbits ($p<0.05$, Table 3).

Comparison of the distance of the condyles of the mandible from the fossas in the superior/inferior, right/left, and anterior/posterior directions with respect to the rotation around the transverse axis, longitudinal axis, and vertical axis showed various discernible patterns. The superior/inferior displacement of the working condyle showed that Rabbit 2 and 3 had an

average displacement of 1.59±0.25 mm whereas Rabbit 1 had a statistically different total displacement of 2.42±0.18 mm (Table 3). Similarly, an analysis for displacement superior/inferior of the balancing condyle showed that Rabbit 2 and 3 had an average displacement of 1.43±0.09 mm whereas Rabbit 1 had a significantly different displacement of 1.95±0.18 mm (Table 3). Between rabbits, the average working condyle displacement anterior/posterior was 4.57±1.24 mm and the average balancing condyle displacement anterior/posterior was 4.07±0.48 mm (Table 3). Neither parameter showed statistically significant differences amongst the rabbits. The right/left condylar displacement was generally less than 0.5 mm and did not follow a consistent pattern and was not compared.

The relationship between the distance superior/inferior with respect to the rotation around the transverse axis of the condyle relative to the fossa created a repeatable pattern for both the chewing and balancing condyle (Figure 20). All other relationships showed neither a linear nor consistent repeatable pattern. Within rabbits, the slope of the closing cycle of the working condyle averaged was 0.21±0.04 mm/degree with no statistical differences between rabbits (Table 3). The closing cycle of the balancing condyle slope was 0.14±0.01 mm/degree for Rabbit 2, which was statistically different from the other two rabbits with a value of 0.09±0.02 mm/degree ($p<0.05$). The slope of the condyle on the working side as the mouth closed was roughly two times larger than the slope of the condyle on the balancing side ($p<0.05$).

Table 3. Kinematic data sorted by consistent and variable measurements across rabbits including: total incisor displacements, slopes of incisor displacement with respect to rotations, total condyle displacement and slope of condyle displacements with respect to rotations for the working and balancing condyles. The average and standard deviation values are presented. Values are significant when p<0.05.

	Rabbit 1	Rabbit 2	Rabbit 3
Consistent Measurements			
Slope of Incisor Distance Right/Left vs. Vertical Rotation	-1.39 ±0.07	-1.42 ±0.08	-1.39 ±0.01
Total Working Condyle Displacement Anterior/Posterior	5.24 ±0.73	3.20 ±1.63	4.94 ±0.36
Total Balancing Condyle Displacement Anterior/Posterior	4.35 ±0.49	3.50 ±0.05	4.18 ±0.18
Slope of Working Condyle Distance Superior/Inferior vs. Transverse Rotation	0.23 ±0.04	0.21 ±0.02	0.18 ±0.01
Variable Measurements			
Total Incisor Displacement Superior/Inferior	16.52 ±2.12	9.03 ±1.55*	12.59 ±4.28
Total Incisor Displacement Right/Left	7.03 ±0.70	3.70 ±1.11*	5.90 ±1.51
Total Incisor Displacement Anterior/Posterior	4.99 ±1.13^	1.82 ±0.43^	3.20 ±0.86
Slope of Incisor Distance Superior/Inferior vs. Transverse Rotation	1.18 ±0.03	1.33 ±0.04*	1.21 ±0.01
Total Working Condyle Displacement Superior/Inferior	2.42 ±0.18*	1.46 ±0.16	1.72 ±0.31
Total Balancing Condyle Displacement Superior/Inferior	1.95 ±0.18*	1.50 ±0.05	1.36 ±0.01
Slope of Balancing Condyle Distance Superior/Inferior vs. Transverse Rotation	0.10 ±0.01	0.14 ±0.01*	0.07 ±0.01
	* p<0.05 when different from other two rabbits ^p<0.05 between rabbits with ^ but not with the third rabbit		

5.5 DISCUSSION

The characterization of the kinematic masticatory patterns of the rabbit is important in understanding the normal movement of the TMJ. The normal mechanics of the TMJ can be used to compare and distinguish kinematics of injured/degenerated joints, as well as healing joints. Our results demonstrate that from one rabbit to another the rotation and translation of both the incisors and the condyle movement relative to the fossa contain many clear, repeatable patterns. Specifically, for the incisors, the slope of the superior/inferior distance with respect to the rotation about transverse axis was repeatable to 0.14 mm/degree and the right/left distance with respect to the rotation about the vertical axis was repeatable to 0.03 mm/degree. For the condyles the slope of the superior/inferior translation with respect to the rotational movement about the transverse axis showed a consistent relationship within trials of each rabbits and between all of the rabbits to within 0.05 mm/degree. Furthermore, the maximal translations of the incisors and condyles were also consistent within rabbits and between rabbits. Some differences between the individual rabbits were expected, due to the natural variations between rabbits.

Previous studies have used various methods of recording rabbit jaw kinematics including magnetic sensing systems, photoelectric sensing systems, cineradiographic systems and video recording systems [62, 65, 66, 75, 95, 96, 109, 131, 146-148, 160-162]. These studies were all invasive with the placement of bone markers, sensors, magnets, and screws. Comparing our results to previous rabbit kinematic studies showed that our study yielded similar findings. In several studies, the chewing patterns were studied by affixing a magnet to the mandible and a magnetic sensor to the skull and the voltage differences were measured [65, 75, 96, 131, 160-162]. The general paths and patterns of the incisors in the vertical and horizontal directions were

similar to what we observed (Figure 21), but numerical comparison was not possible, due to the measurement techniques. Similar chewing patterns were also seen with the photoelectric sensing systems [66, 95, 109]. The cineradiographic studies allowed for comparisons of the rotations about the transverse axis; similar rotations were found generally ranging from approximately 10-14° [146-148]. Another study found similar results for the incisal movement as rabbit study using 3D video analysis with skin markers during mastication of food and water [62]. The superior/inferior displacement with food was roughly 13.1±3.0 mm compared to our average between the three rabbits being 12.7±3.7 mm. However, unlike our results the right/left movement recorded was larger with a mean of 17.6±3.0mm as opposed to our mean of 5.54±1.70 mm, which was closer to their mean for the water stimulus (3.6±0.5 mm) [62]. The difference may arise from the variability that arises from the use of skin markers and the type of food stimulus.

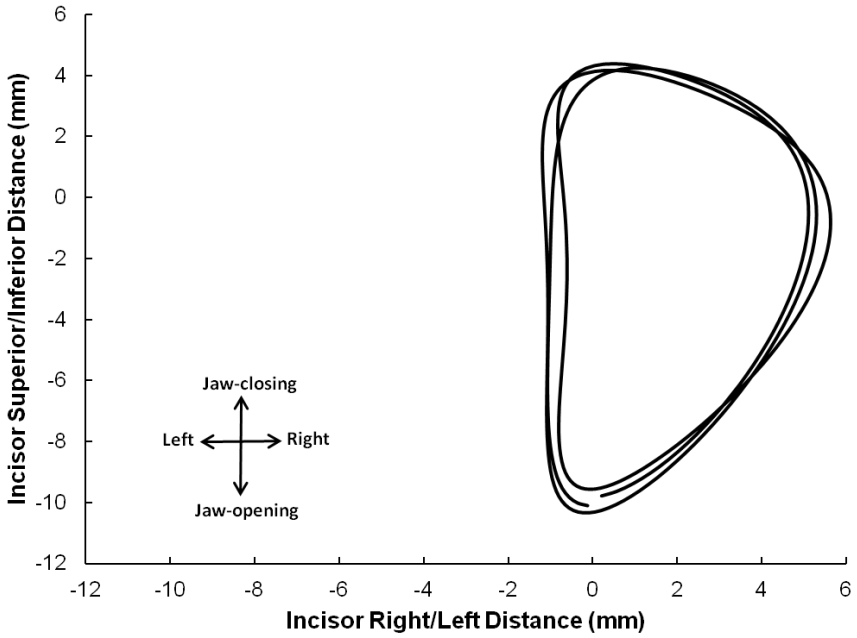

Figure 21. Translation of the mandible incisors from the skull incisors in the coronal plane. The total movement superior/inferior with respect to right/left for three chewing cycles within one acquisition of one rabbit. Representative data shown.

One rabbit research study measured the mandibular condylar movement during mastication [96]. The measurements were invasively done by removing the zygomatic arch and recording the motion of the condyles with a video camera on anaesthetized rabbits. Similar working side and balancing side path patterns for the motion of the condyles to our paths (Figure 22) were found. The incisor paths were also similar and recorded by magnetic sensors.

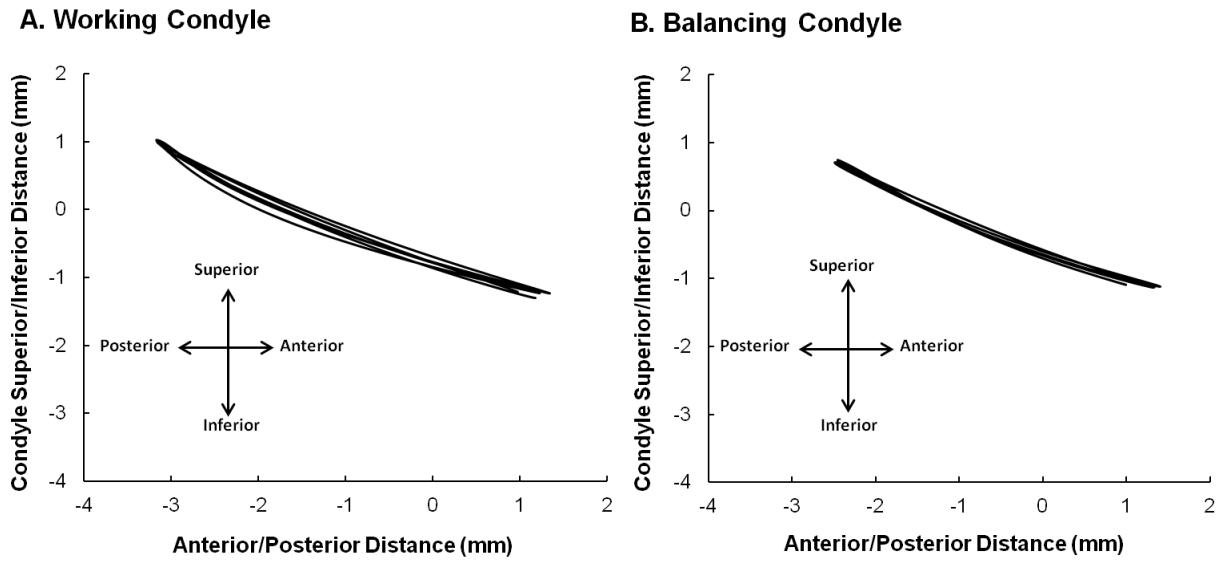

Figure 22. Condyle Distance - Translation of the condyle relative to the fossas in the sagittal plane. A) Total movement of the working side condyle superior/inferior with respect to right/left and B) total movement of the balancing side condyle superior/inferior with respect to right/left. The translations shown are for three continuous chewing cycles within one acquisition of one rabbit. Representative data shown.

The dynamic biplane x-ray imaging system we used was beneficial because it allowed for non-invasive measurement of normal rabbit chewing, both at the incisors and within the joint space. In the future, our system can be used to determine kinematic differences and changes over time in chewing patterns between healthy and degenerated joints in animal models. Gaining a better understanding of the current models used for TMD and the fibrocartilage degeneration process will allow for development of more appropriate models to better understand TMDs. Based on evidence that TMJ degeneration and pain results in alterations in oral-motor patterns, we hypothesize that kinematic analysis will identify a specific pattern of use-dependent changes in joint function that constitute a signature for the presence of permanent degeneration and pain. This will be studied in the future through the use of a mechanical induction of TMJ degeneration using unilateral dental splints.

5.6 CONTRIBUTIONS

I assisted with data collection and analysis, completed the microCT analysis and data processing, and prepared and edited the manuscript. Ms. Desai worked on the data analysis and helped with preparing and editing the manuscript. Ms. McCarty helped with some of the data processing. Dr. Tobita assisted with the microCT collection. Dr. Tashman collected the kinematic data and helped with project design and manuscript editing. Dr. Almarza helped with project design, data analysis, and manuscript editing.

6.0 KINEMATIC ANALYSIS OF THE RABBIT TEMPOROMANDIBULAR JOINT AFTER UNILATERAL SPLINTS[4]

6.1 ABSTRACT

Analysis of mandibular biomechanics may help with understanding the mechanisms of temporomandibular joint (TMJ) disorders (TMDs) by investigating the effects of injury or disease on TMJ movement. Altered loading from trauma, functional overloading, joint friction, and unstable occlusion can contribute to the development and progression of TMDs. The objective of this study was to determine the effects of altered occlusion on TMJ kinematics. Altered occlusion of the TMJ was mechanically induced in rabbits via a unilateral molar dental splint (n=3). TMJ motion was assessed through three-dimensional skeletal kinematics twice, once before and once after 6 weeks of splint placement with the splints removed allowing three days of recovery. The relative motion of the condyle to the fossa was tracked, as well as the distance between the incisors. The condyles were separated by side, where the direction the mandible first moves is called the working side, while the other is the balancing side. An overall decrease in the range of joint movement was observed at the incisors and in the joint space between the condyle and fossa. The incisor movement decreased from 7.0±0.5 mm to 6.2±0.5

[4] Submitted to Journal of Biomechanics as Henderson SE, Tudares MA, Tashman S, Almarza AJ. "Kinematic Analysis of the Rabbit Temporomandibular Joint after Unilateral Splints" on July 18, 2014.

mm right-left, from 5.5±2.2 mm to 4.6±0.8 mm anterior-posterior, and from 13.3±1.8 mm to 11.6±1.4 mm superior-inferior ($p<0.05$). The total magnitude of the maximum distance between the points on the condyle and fossa decreased from 3.6±0.8 mm to 3.1±0.6 mm for the working condyle and from 2.8±0.4 mm to 2.5±0.4 mm for the balancing condyle ($p<0.05$). The largest decreases were seen in the anterior-posterior direction for both condyles. It has been shown previously, that the incisal path alone does not provide enough details to thoroughly characterize the motion of the TMJ; consequently, determining the changes in condylar movement may lead to a better understanding of early predictors in the development of TMDs, and determining when symptoms become a chronic, irreversible problem.

6.2 INTRODUCTION

Trauma, parafunction, unstable occlusion, functional overloading, and increased joint friction can contribute to the progression of temporomandibular joint (TMJ) diseases (TMDs) [120]. The clinical necessity for gaining more knowledge about TMJ degeneration is critical considering that up to 3-4% of the population seek treatment for symptoms of TMDs [48]. Computer and imaging technologies are being developed and are beginning to provide novel insights into the progression of TMDs and could possibly be developed into rational diagnostic and therapeutic strategies [141]. In one type of TMD, unbalanced or excessive mechanical loading of the TMJ articulating tissues can result in the progression of TMJ osteoarthritis [120]. Analysis of mandibular biomechanics should improve the understanding of TMJ form and function, as well as improve the understanding of the mechanisms of TMDs [64].

One of the main functions of the TMJ is to allow for repeatable movement of the jaw. However, non-invasive quantification of these joint movements (kinematics) has been technically challenging. Non-invasive 3D x-ray imaging systems have been developed to combine x-ray videos with 3D morphology from bone scans to allow for measurements of distances and velocities within the joint space [17, 18, 23, 57, 124, 126]. Previously, incisal range of motion in the vertical and horizontal directions have been shown to decrease with induction of a particular TMD in rabbits with displaced TMJ discs [131]; however, the condylar movement paths were not studied. Condylar movement paths may provide additional information on changes occurring from the injury, as it has been shown that the incisal path alone does not give enough details to thoroughly understand the movement of the TMJ [97, 132]. Our previous study determined repeatable measurements for non-invasive assessments of normal rabbit chewing, both at the incisors and within the joint space [57]. The repeatable measurements of rabbit TMJ kinematics included maximal distances and movement paths for both the incisors and the condyle-fossa relationship [57]. Knowledge of dynamic TMJ function through three-dimensional (3D) skeletal kinematics is essential for investigating the effects of injury or disease in the TMJ.

The objective of this study was to determine the effects of altered occlusion on the TMJ kinematics. Altered occlusion of the TMJ was mechanically induced in rabbits via unilateral molar dental splints placed for six weeks. It was hypothesized that kinematic analysis would identify an overall decrease in joint motion after six weeks of splinting.

6.3 METHODS

6.3.1 Animal Model

Skeletally mature, female, New Zealand White rabbits approximately 1 year in age weighing between 5-7 kg were purchased from Charles River Laboratories International, Inc. (Wilmington, MA). All rabbits were examined by a veterinarian prior to use in the study and were found to be in good health. All animal procedures were approved by the Institutional Animal Care and Use Committee at the University of Pittsburgh and in accordance with the National Institutes of Health guidelines for the use of laboratory animals.

Unilateral dental splints were chosen as the method for altering the occlusion because the splints could be removed at a later point in time and the joint space was not penetrated [26, 111, 112]. For three separate procedures, impressions, splint placement, and splint removal, all rabbits were sedated with ketamine and xylazine, and a surgical plane of anesthesia was maintained with isoflurane. Impressions were taken of the upper and lower right molars of the rabbits to create a unique mold for casting the splints as crowns made from non-precious metals (Figure 23). The thickness of each casted splint was approximately 1 mm. During a second procedure, the right maxillary and mandibular molar arches were cleaned and primed, and then the splints were attached to the respective molars with dental cement. Splint placement was verified after 1 week. Splints were removed at 6 weeks, three days prior to the final kinematic data collection. Kinematic data was collected twice, once before impressions and splint placement and once 6 weeks after splint placement, with the splints removed for three days on three rabbits (n=3). After the second kinematic data collection, the rabbits were euthanized and the whole head was frozen and saved for micro-computed tomography (CT).

Figure 23. Unilateral molar bite raising splints. A) The splints were made by first taking an impression of the molars. B) A plaster mold was made from the impressions. C) The metal splints were cast as crowns on the molds, and the superior and inferior views are shown.

6.3.2 Kinematics

As per our published methods [57], TMJ kinematics were assessed using a unique high-speed stereo-radiographic system consisting of two sets of 110 kW pulsed X-ray generators (CPX 3100CV; EMD Technologies, Quebec, Canada), 40 cm image intensifiers (Thales, Neuilly-sur-Seine, France) using a 20 cm field of view, and high-speed 4 Megapixel digital video cameras (Phantom v10, Vision Research, Wayne, New Jersey, USA). The rabbits were placed in a radiolucent ventilated cage (Figure 24 A) and fed small pieces of dried fruit. Radiographic images were collected at 170 frames/s for 1 s with 1 ms exposures at 4 Megapixel image resolution (Figure 24 B). At least three data acquisitions per rabbit were collected. Three rabbits were tested before splint placement and after 6 weeks of splint placement with the splints removed three days prior to the second data collection.

The markerless, model-based technique used for determining 3D kinematics has been extensively described, validated, and tested [19, 31, 57, 124-126], including testing of the rabbit TMJ [57]. Briefly, a 3D model of each bone to be tracked was derived from a CT scan (as described below) (Figure 24 C). A virtual model of the biplane x-ray system was created for

generating a pair of digitally reconstructed radiographs (DRR's) via ray-traced projection through the CT bone model. The bone model was automatically repositioned within the virtual model until a best match was achieved between the simulated DRR's and the actual radiographic image pair (Figure 24 D). This technique determined the 3D positions and orientations of the mandible and the skull for each motion frame. After euthanasia, the entire head, including the mandible and skull, was scanned at high resolution (105 μm isotropic voxels) using a micro-computed tomography system (Inveon micro-CT system by Siemens located at the Rangos Research Center Animal Imaging Core, Children's Hospital of Pittsburgh of UPMC). The mandible and skull bones (with teeth) were segmented from each other and from soft tissue and reconstructed into both surface and volumetric models using Mimics software (Materialise, Inc. Leuven, Belgium) (Figure 24 C).

Anatomical coordinate systems were set up similar to the systems used by Brainerd et al. [23] and in our previous study [57] to determine the joint translations and rotations. The transverse (x) axis was aligned through the center of the condyles, the longitudinal (y) axis was parallel to a plane through the occlusal plane, and the vertical (z) axis was the cross product of x and y (Figure 25 A).

The relative motion of each condyle with respect to the fossa was tracked (Figure 25 B, C). The distance between a fixed point on the condyle and a fixed point on the fossa was measured throughout the chewing cycles (Figure 24 Ei). Points were placed at the superior most point of the condyle and in the convex region of the fossa. The relative motions of the centers of the two points were determined in all 3 anatomic planes. The measurement points were placed in the same location on the condyle and fossa for pre and post splint data collection for each rabbit. The pre and post splint motions were analyzed in each direction, as well as in the total

magnitude of the vector (Figure 24 Eii). The movement of the mandible was somewhat elliptical in the coronal plane and always started to the same side during an acquisition. As established in the literature, the side in which the mandible first moves is the working side, while the other is called the balancing side [96]. The condyles were analyzed by working and balancing condyles as previously established in the literature [57, 96]. Of the three rabbits, one rabbit consistently had the left condyle as the working condyle, one rabbit had the right condyle consistently as the working condyle, and the third rabbit the working condyle switched from the right condyle pre splint to left condyle post splint. Again, the splint was placed on the right molars.

The relative motion near the incisors was measured as well. Since, the incisor teeth were observed to grow and change shape from the treatment they were not directly included in the analysis. To be consistent with the changing incisors from pre and post splint, the incisor markers were instead placed on the skull and mandible at the center of the incisors at the interface where the teeth met the bone on the posterior side (Figure 25 D).

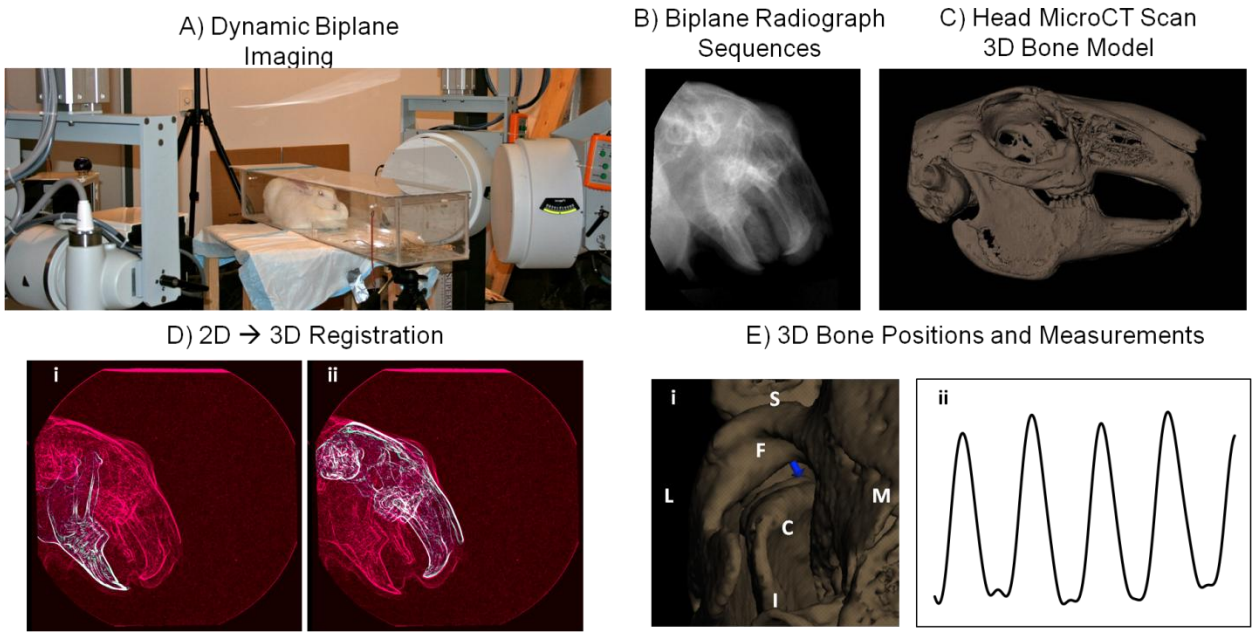

Figure 24. Overview of methods for kinematic data collection. A) High-speed biplane radiography was used for image collection. Rabbits were placed in a radiolucent box between two sets of x-ray generators and image intensifiers with high speed cameras. B) Sample x-ray image from the high resolution cameras at one frame in time. C) 3D bone model created from a microCT scan of the rabbit head. D) For 2D to 3D registration, the collected x-ray images (pink) are matched frame by frame with the virtual x-ray images (green) from the CT scan. One of the two combined images is shown for each the mandible (i) and the skull (ii). E) 3D distances can be measured. (i) Vector indicating the distance between the condylar point and the fossa point (the condyle is labeled with C and the fossa with F). (ii) Sample displacement curve. The picture in E is labeled by directions: A-anterior, P-posterior, M-medial, L-lateral, S-superior, I-inferior.

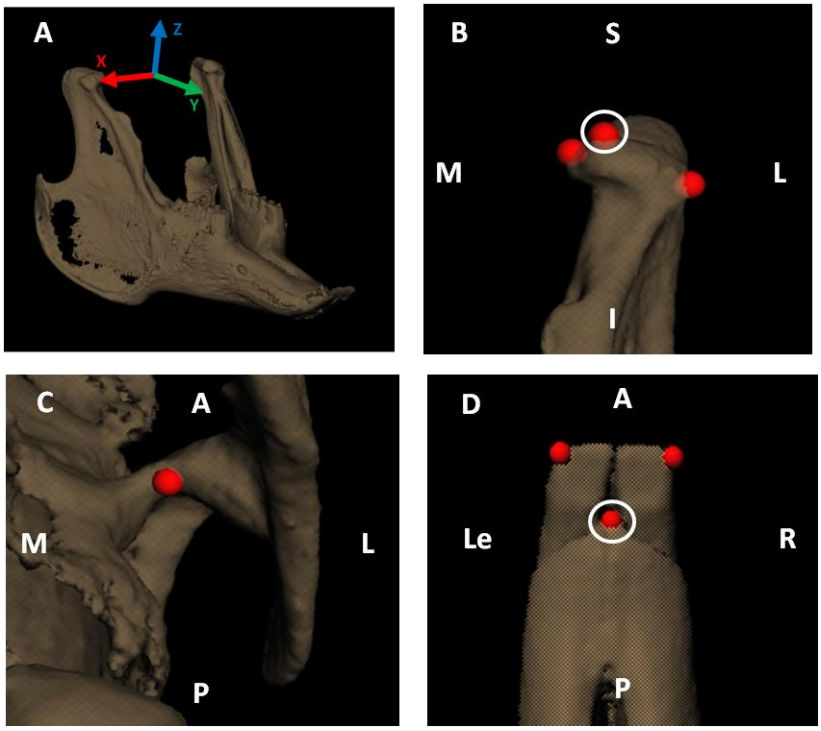

Figure 25. Kinematic analysis tools were used to set up the measurements. A) The anatomical coordinate system for the mandible was set up with the transverse axis (x-red) aligned through the center of the condyles, the longitudinal axis (y-green) parallel to a plane through the occlusal plane (where the teeth meet), and the vertical axis (z-blue) was the cross product of the transverse and longitudinal axes. The skull coordinate system was set up in a similar manner (not shown). B) Condylar measurement point, anterior view of left condyle. C) Fossa measurement point, inferior view of left fossa. D) Mandible incisor measurement point, superior view. Pictures are labeled by directions: A-anterior, P-posterior, M-medial, L-lateral, Le-left, R-right, S-superior, I-inferior.

Based on our previous study [57], some of the rotation-translation relationships were shown to be linear and repeatable, so the slopes of these relationships were also compared. The slope of the movement of the condyles in the superior-inferior direction with respect to the transverse rotation during the first 50% of closing was determined for both the working and balancing condyles. The slopes of the paths from the incisal point in the superior-inferior direction with respect to the transverse rotation and the incisal point in the anterior-posterior direction with respect to the vertical rotation were also determined. Only one acquisition was

analyzed for each rabbit pre and post splint, if the acquisition had at least three complete chewing cycles. All kinematic data was reported as an average ± standard deviation. Data was tested for normality with an Anderson Darling Test for Normality and found to be normal. A repeated measures ANOVA with Tukey's post hoc test ($p<0.05$) was used to assess the differences for all kinematics values before and after splinting.

6.4 RESULTS

Overall, the altered occlusion from the splint caused the range of motion of the condyles and the teeth to decrease. The distances the condyles traveled on both the working and balancing sides significantly decreased after splinting (Table 4). The total magnitude of the maximum distance between the points on the condyle and fossa decreased by 15.0% for the working condyle and by 8.9% for the balancing condyle ($p<0.05$). Figure 26 A and B shows the total magnitude of the condyle-fossa distance over time and the decrease in distance traveled from the splint. Breaking the movement into the vector components, both the anterior-posterior displacement and the superior-inferior displacement significantly decreased ($p<0.05$). The anterior-posterior displacement decreased by 20.5% and the superior-inferior by 8.9% for the working condyle and for the balancing condyle the displacements decreased by 14.9% and 13.6%, respectively (Table 4). Figure 26 C and D show the superior-inferior motion with respect to the anterior-posterior motion, for the working and balancing condyles, pre and post splint. The right-left movement of the condyles was minimal and thus, not reported.

The paths of the condyles were analyzed by determining slope of the superior-inferior distance with respect to the transverse rotation during the first 50% of the closing cycle. The

slopes for the working condyle significantly increased by 13.7% after splinting ($p<0.05$) (Table 4). The shapes of the curves are shown in Figure 26 E and F for the working and balancing condyles, respectively.

The distances the incisors traveled also significantly decreased after splinting ($p<0.05$) (Table 4). The right-left movement decreased by 11.2%. The anterior-posterior movement decreased by 16.1%. The superior-inferior movement decreased by 13.0%. The shapes of the curves are shown in Figure 27 A and B. Figure 27 C shows the change in movement from pre to post splint in the coronal plane.

Table 4. Kinematics results for rabbits before and after splinting for 6 weeks, with the splint removed three days prior to testing. The data was separated into the working and balancing condyle and the incisors. AP: anterior-posterior movement. SI: superior-inferior movement. RL: right-left movement. The average and standard deviation values are presented. *Differences were significant when $p<0.05$.

Measurement	Pre-Splint	Post - Splint
Working Condyle AP (mm)	4.9 ± 0.8	3.9 ± 0.4*
Working Condyle SI (mm)	2.2 ± 0.5	2.0 ± 0.2*
Working Condyle Magnitude (mm)	3.6 ± 0.8	3.1 ± 0.6*
Working Condyle SI vs Transverse Rotation (mm/°)	0.21 ± 0.02	0.24 ± 0.04*
Balancing Condyle AP (mm)	4.3 ± 0.8	3.6 ± 0.2*
Balancing Condyle SI (mm)	1.8 ± 0.3	1.6 ± 0.14*
Balancing Condyle Magnitude (mm)	2.8 ± 0.4	2.5 ± 0.4*
Balancing Condyle SI vs Transverse Rotation (mm/°)	0.07 ± 0.02	0.08 ± 0.04
Incisors AP (mm)	5.5 ± 2.2	4.6 ± 0.8*
Incisors SI (mm)	13.3 ± 1.8	11.6 ± 1.4*
Incisors RL (mm)	7.0 ± 0.5	6.2 ± 0.5*
Incisors RL vs Vertical Rotation (mm/°)	-1.38 ± 0.06	-1.36 ± 0.09
Incisors SI vs Transverse Rotation (mm/°)	1.12 ± 0.08	1.14 ± 0.08*

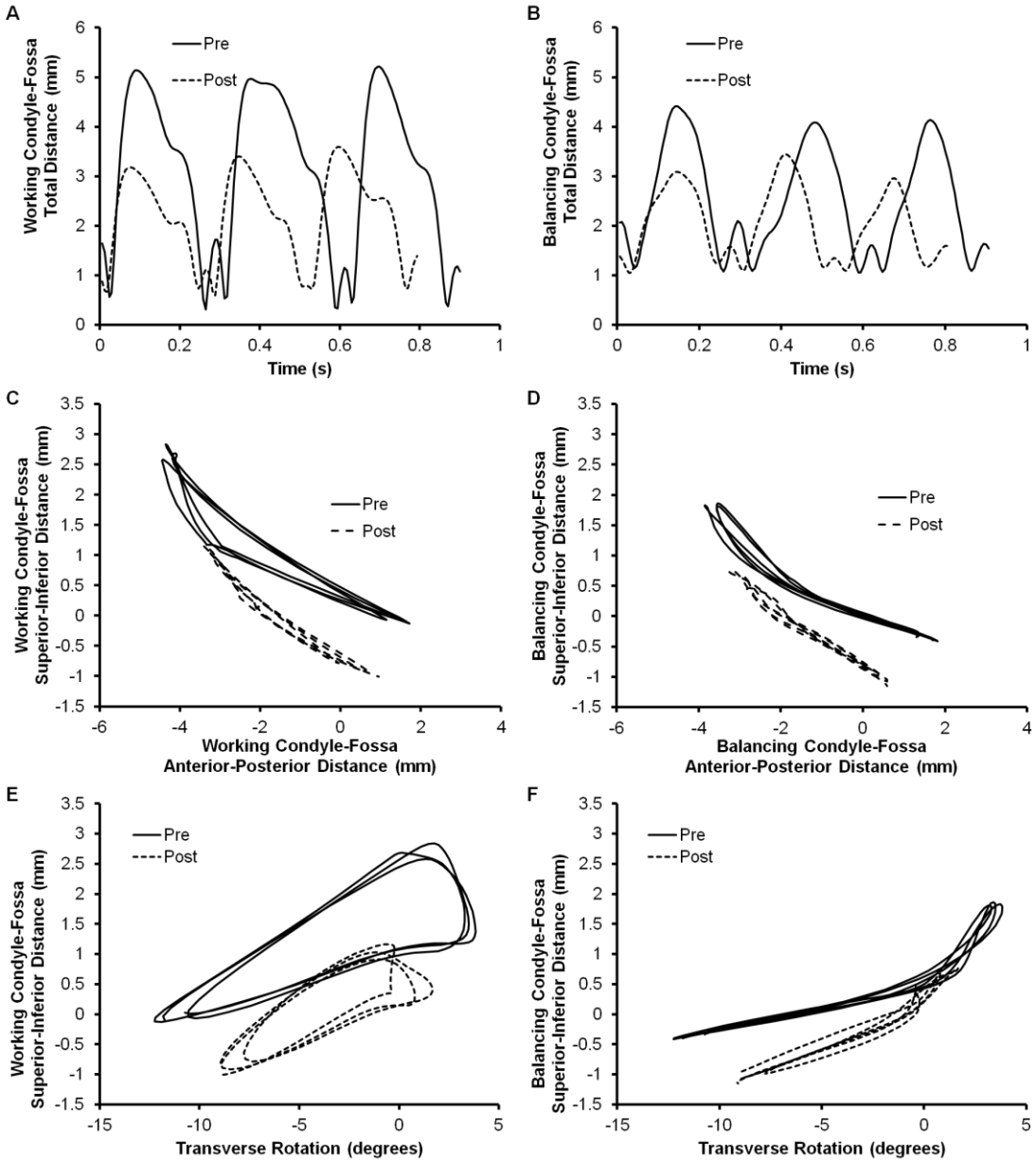

Figure 26. Condyle-fossa relationships pre and post splint. A) Working and B) Balancing side condylar kinematics showing the total condyle-fossa distance with respect to time, pre and post splinting. C) Working and D) Balancing side condylar kinematics showing the superior-inferior condyle-fossa distance with respect to the anterior-posterior condyle-fossa distance, pre and post splinting. E) Working and F) Balancing side condylar kinematics showing the superior-inferior condyle-fossa distance with respect to the transverse rotation, pre and post splinting. Representative curves from one rabbit shown.

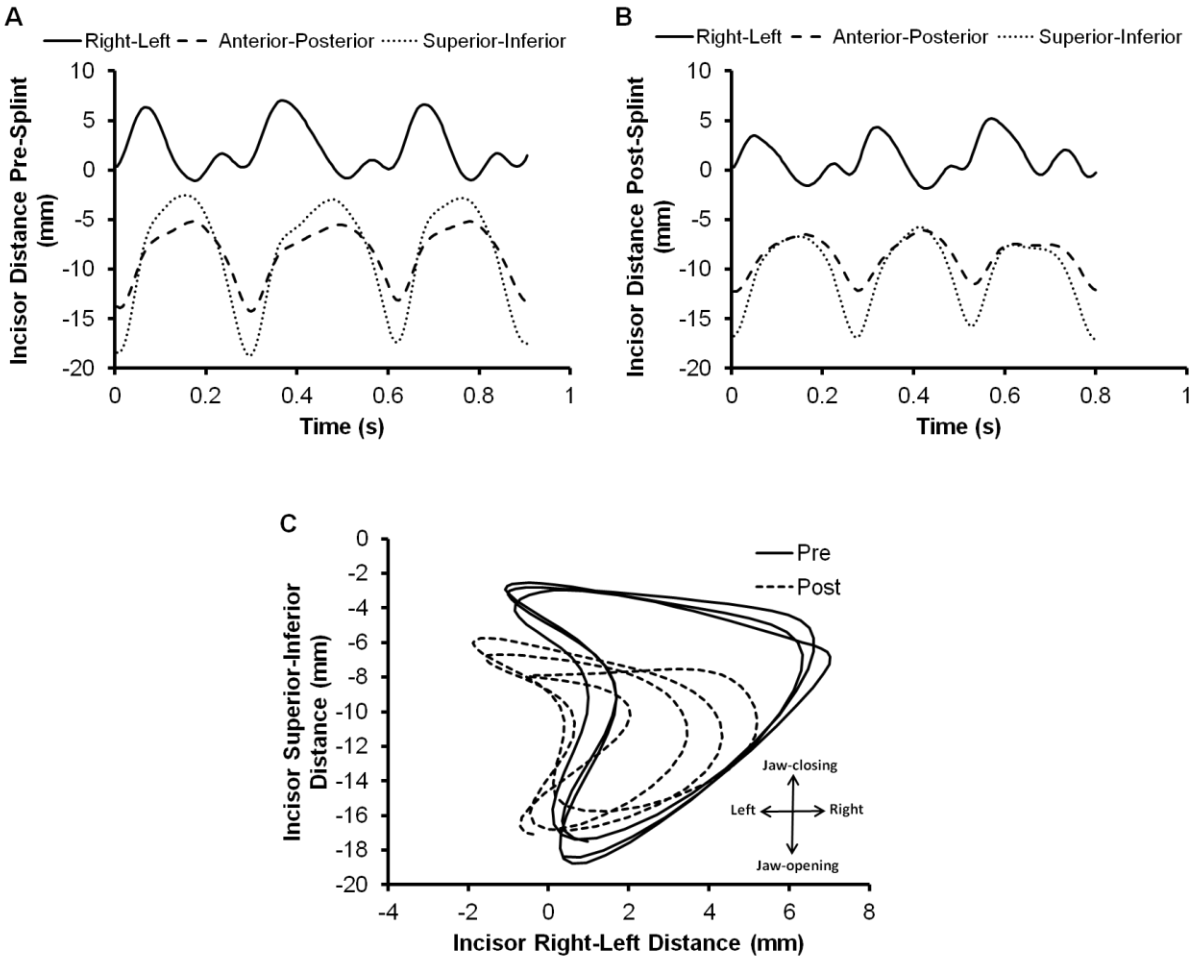

Figure 27. Patterns of incisor movement pre and post splint. A) The change in distance of the mandible incisors from the skull incisors with relation to time pre splint and B) post splint. C) Relationship of the mandible incisors to the skull incisors in the coronal plane pre and post splint. Three chewing cycles are shown in each graph. Representative curves from one rabbit shown.

6.5 DISCUSSION

An overall decrease in the range of joint movement at both the condyles and the incisors was observed after placement of dental splints for six weeks. The persistent change in kinematics is likely due to abnormal occlusion and the degeneration of the condylar fibrocartilage observed in a previous study [58]. The kinematics of the rabbit TMJ at the condyles and the incisors were easily measured with our non-invasive system before and after splint placement to determine changes in the joint movement. The decreased range in incisal movement post splint was comparable to a previous TMJ disc injury study [131]; however, the specific values could not be compared due to different measurement techniques. The pre splint control incisal data was also consistent with our previous study and with other normal rabbit kinematic studies [57, 62, 96, 131].

Determining the changes in condylar movement may lead to a better understanding of early movement predictors in the development of TMDs. This knowledge of dynamic TMJ function through 3D skeletal kinematics is essential for investigating the effects of injury or disease in the TMJ. The altered occlusion model used in this study has been shown to produce condylar fibrocartilage degeneration that would likely not be detected by conventional MRI scans [58]. Understanding the changes in joint movement that occur from various types of TMDS could allow for earlier diagnosis and treatment, for example, if a certain signature of changes in movement are observed earlier before onset of severe joint degeneration. As such, our study suggests that decreases in 20% anterior-posterior displacement of the working condyle might be indicative of condylar degeneration.

A limitation of this study was that only one microCT scan could be obtained per rabbit head after the final time point. Ideally a microCT scan would be collected for each time point

that kinematic data was collected. However, due to the size limitations of the scanner, the heads could only be scanned after euthanasia and decapitation. We had to assume that the bony structures of the joints were not affected by the treatment. Another assumption of this study was that the bony structure of the skull and mandible were rigid. However, it has been shown that the mandible can deform during joint motion [1, 27], which led to some minor errors in the DDR matching process. There were a few frames in each chew cycle where the mandible and fossa were barely touching along the edges of both of the condyles. Rabbits' teeth are also constantly erupting, so in future studies with longer time points the teeth may need to be filed down to their original height. Even with these limitations, we feel this study provided an important understanding of what can change in the TMJ motion from inducing joint remodeling from altered occlusion.

In this study, once the splints were removed it was observed that the joint motion did not immediately return to baseline, and that the range of motion had decreased. During preliminary data collection, kinematic data was collected on one rabbit that still had the splint. Scans were taken once before splinting and one day after the splint was placed. From this preliminary dataset the anterior-posterior motion of the working condyle decreased by approximately 50% after splinting. After six weeks of splinting with the splints removed for three days, the anterior-posterior motion of the working condyle was still 20% less than the baseline measurement. While the magnitude of decrease in motion after splint removal might not at first seem high, when compared to maximum decrease in motion that an object on the molars can cause, the overall change indeed might be high.

The splint model used in this study was advantageous because it allowed for removal of the splints, and the joint space was not penetrated. Future work will need to look at various

lengths of time between splint placement and removal and allow time for recovery to understand if and when the change in joint movement has the potential to correct itself and the joint to heal or when the change becomes chronic and permanent. The potential exists with this type of TMD animal model to combine the kinematic analysis with other assessments such as pain measurements and mechanical assessments of the TMJ tissues, which will allow for multidisciplinary studies of various types of TMDs. The combination of assessment methods will allow for a fuller understanding of the TMJ disease progression in animal models.

6.6 CONTRIBUTIONS

I assisted with the rabbit dental procedures and kinematic data collection, I completed the microCT scans, data processing, and data analysis, and prepared and edited the manuscript. Mr. Tudares performed the rabbit dental procedures and trained the rabbits, and assisted with data collection. Mr. Mortimer assisted with some of the data processing. Dr. Tashman collected the kinematic data, and helped with project design and manuscript editing. Dr. Almarza helped with project design, data analysis, and manuscript editing.

7.0 MAGNESIUM ALLOYS AS A BIOMATERIAL FOR DEGRADABLE CRANIOFACIAL SCREWS[5]

7.1 ABSTRACT

Recently, magnesium (Mg) alloys have received significant attention as a potential biomaterial for degradable implants, and this study was directed at evaluating the suitability of Mg for craniofacial bone screws. The objective was to implant screws fabricated from commercially available Mg-alloys (pure Mg and AZ31) in-vivo in a rabbit mandible. First, Mg-alloy screws were compared to stainless steel screws in an in-vitro pull-out test and determined to have a similar holding strength (~40N). A finite element model of the screw was created using the pull-out test data, and the model can be used for future Mg-alloy screw design. Then, Mg-alloy screws were implanted for 4, 8, and 12 weeks, with two controls of an osteotomy site (hole) with no implant and a stainless steel screw implanted for 12 weeks. MicroCT (computed tomography) was used to assess bone remodeling and Mg-alloy degradation, both visually and qualitatively through volume fraction measurements for all time points. Histologic analysis was also completed for the Mg-alloys at 12 weeks. The results showed that craniofacial bone remodeling occurred around both Mg-alloy screw types. Pure Mg had a different degradation

[5] Published as Henderson SE, Verdelis K, Maiti S, Pal S, Chung WL, Chou D, Kumta PN, Almarza AJ. 2014 "Magnesium Alloys as a Biomaterial for Degradable Craniofacial Screws" Acta Biomaterialia, May 2014, 10(5): 2323-2332. Epub 2013 Dec 30. DOI: 10.1016/j.actbio.2013.12.040, PMID: 24384125

profile than AZ31, however bone growth occurred around both screw types. The degradation rate of both Mg-alloy screw types in the bone marrow space and the muscle were faster than in the cortical bone space at 12 weeks. Furthermore, it was shown that by alloying Mg, the degradation profile could be changed. These results indicate the promise of using Mg-alloys for craniofacial applications.

7.2 INTRODUCTION

Magnesium (Mg) alloys have recently been a focus of degradable implant research. Results to date are demonstrating great promise for Mg-alloys to regenerate both hard and soft musculoskeletal tissues [21, 37, 39, 40, 50, 51, 61, 69, 73, 74, 78, 93, 127, 128, 137-140, 150-154, 156-159, 163, 167, 168], which is valuable due to the necessity for engineering degradable craniofacial implants. Craniofacial implants, such as plates and screws, are used in procedures such as osteotomies, bone graft stabilization during reconstructions, and for trauma reconstruction [133]. Previously, craniofacial bone plates and screws have been fabricated from stainless steel, vitallium, chromium-cobalt, and other metal alloys [133]. Titanium has become the preferred permanent metal of choice due to its ability to osteointegrate [92]. However, it is estimated that 10-12% of craniofacial implants are removed due to infection, exposure, pain, and discomfort [92]. Resorbable polymer plates and screws are becoming more popular to use for craniofacial implants because they allow for fixation and stabilization but are not permanent [92]. However, biodegradable polymers, such as poly-l-lactide, are biomechanically inferior to their metal counterparts [117]. Two other shortcomings of the polymer implants include the need for a heating device to provide implant malleability and the need to tap the bone prior to

screw placement [14]. Thus degradable metals have both the strength and the ability to degrade, unlike their polymer and permanent metal counterparts. In particular, much research has been done on the degradable metal Mg [21, 33, 34, 37, 39, 40, 50, 51, 61, 69, 73, 74, 78, 93, 127, 128, 137-140, 142, 150-159, 163, 167, 168].

Many previous studies have looked at the effect of Mg-alloys on long bones [21, 37, 39, 40, 50, 51, 61, 69, 73, 74, 78, 93, 127, 128, 137-140, 150-154, 156-159, 163, 167, 168], but the effect of Mg-alloys on craniofacial bone has not been thoroughly studied. Mg-alloy rods and cylinders have been implanted into guinea pig femurs [152, 154], rat femurs [159, 167], and rabbit femurs [69, 78, 137-140, 150, 153, 156-158, 163, 168] and tibias [21, 50, 51, 61, 74, 93, 127, 128]. Mg-alloy screws have been tested in-vitro [33, 34, 142, 155] and have also been implanted into rabbit femurs [138] and tibias [39, 40, 73], as well as sheep hip bones [37, 151]. Studies of inflammatory and immune response show that degrading Mg scaffolds show good biocompatibility and react in-vivo with an appropriate inflammatory host response [21, 40, 78, 150, 153, 157, 159, 167, 168]. It has been shown that degrading Mg implants promote bone formation [37, 39, 40, 50, 51, 69, 78, 93, 127, 128, 137, 138, 151, 152, 154, 156, 158, 159, 163, 167, 168] and osteoblastic activity [78, 151, 154, 156, 159, 167]. In these previous studies several different types of Mg-alloys have been implanted, specifically the commercially available alloy AZ31 (2.5-3.5 wt% aluminum, 0.6-1.4 wt% zinc, 0.2-1.0 wt% manganese) has been previously tested in bone in-vivo as rods [154, 163] and as screws [37, 151]. All four studies revealed new bone formation around the AZ31 implants [37, 151, 154, 163]. One of the studies showed that the corrosion behavior of the AZ31 screw differed depending on the location of the AZ31 in the original tissue [151]. Bone formation was noted around the Mg rods, but not

in the surrounding soft tissue [154]. There was also little change to the blood composition and no inflammation from the degrading implant [163].

Long bones and flat bones, such as the craniofacial bones, form differently during development resulting in differences in the organic and inorganic phases [135]. Long bones and craniofacial bones also undergo different loading. Long bones can undergo extensive loading, as can the mandible, but the skull normally undergoes minimal loading. The blood flow in various regions of the body is also different. All of these factors could affect the degradation rates of the Mg-alloys and also the bone regeneration in these areas. An investigation should be conducted to see if there are differences in how Mg behaves in the craniofacial region compared to the long bones.

As a first step towards improving degradable craniofacial plates and screws, this study aimed to evaluate the use of Mg as a degradable biomaterial. The objective of this study was therefore to implant screws fabricated from commercially available Mg-alloys (pure Mg and AZ31) in-vivo in a rabbit mandible. First the Mg-alloy screws were compared to commercially available stainless steel screws in an in-vitro pull-out test to determine the holding strength. A custom finite element code was then developed to simulate these pull-out tests on a computer. Factors contributing towards the pull-out strength were determined using this computational model. Then, the two Mg-alloys were implanted for three time periods (4, 8, or 12 weeks). The two controls consisted of only osteotomies (holes) with no implant or a stainless steel screw implanted for 12 weeks. MicroCT (computed tomography) was used to assess bone remodeling and Mg degradation for all time points, and histologic analysis was also used for the Mg-alloys at 12 weeks.

7.3 METHODS

7.3.1 Screw Fabrication

Bone screws were designed for the rabbit mandible and fabricated from commercially available pure Mg and a Mg aluminum zinc alloy (AZ31) purchased from Goodfellow (Oakdale, PA). The pure Mg was 99.9% pure, and the AZ31 alloy contained 2.5-3.5 wt% aluminum, 0.6-1.4 wt% zinc, and 0.2-1.0 wt% manganese with the remainder being Mg. Similarly sized, commercially available stainless steel screws were purchased from Small Parts (Seattle, WA). The screws were approximately 1 mm in diameter with M0.25 threads and the shaft was approximately 2 mm in length (Figure 28 A).

The Mg-alloy screws were fabricated by the University of Pittsburgh Swanson Center for Product Innovation (SCPI) using CNC (computerized numerical control) machining. After fabrication, the screws were sonicated in isopropanol to remove any residual debris. The screws then underwent a stress relief heat treatment at 205 °C for 90 minutes in an argon atmosphere. Next, the screws underwent 3 cycles of sonication in isopropanol for 3 minutes each following which they were allowed to air dry. All of the screws were stored in air tight containers until documentation and use in this study. Documentation included weighing and imaging each individual screw.

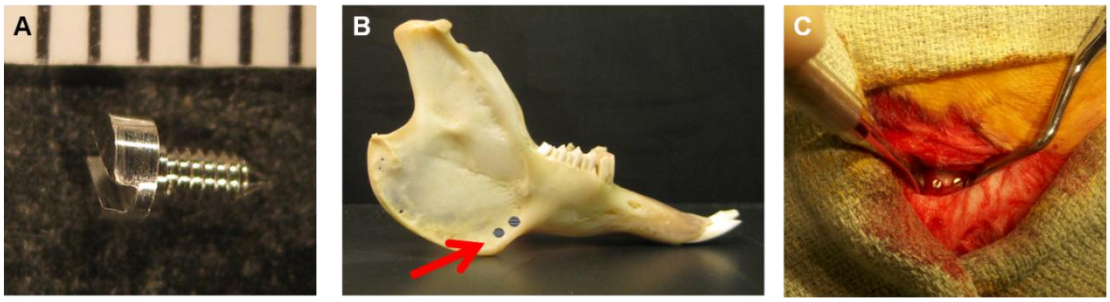

Figure 28. Mg-alloy craniofacial bone screws. A) Picture of a screw. The screws were machined from commercially available pure Mg and AZ31 stock rods. B) Screw implantation location in the rabbit mandible. The screws were placed along the lower edge of the mandible just posterior to the molars. C) View of two Mg-alloy screws implanted during surgery.

7.3.2 In-vitro Testing and Finite Element Modeling

7.3.2.1 Pull-Out Test

A mechanical test was designed to compare the holding strength of the pure Mg and AZ31 screws to stainless steel screws. A material testing system was set up for complete axial pull-out tests (Figure 29 A) (MTS Insight, MTS Systems, Eden Prairie, MN). Synthetic bone made of solid rigid polyurethane foam (ASTM F-1839-08) from Sawbones (a division of Pacific Research Laboratories, Inc. Vashon, WA) was used as the control material for the pull-out tests. Screws were placed in the foam after the holes were predrilled and tapped. A testing rate of 5 mm/min was used according to ASTM standard F543-07. The maximum force needed to release the screw from the foam was recorded for each screw. A one-way ANOVA with Tukey's post hoc test was used to compare the results with a statistical significance set at $p<0.05$.

7.3.2.2 Computational Techniques

Custom three-dimensional (3D) finite element (FE) software was developed to simulate experimental pull-out tests and study the effect of various mechanical properties on the observed pull-out strength. Synthetic bone was modeled as a cylinder with a diameter of 5 mm with the screw inserted along the longitudinal axis (Figure 29 Bi). The screw and the cylindrical bone were discretized with 3731 and 14254 four-noded tetrahedral finite elements, respectively. Details of the finite element discretization are shown in Figure 29 Bii. The outer surface of the bone was held rigidly in place with fixed boundary conditions. The diameter of the cylinder was chosen such that boundary effects on the stress field were minimal in the vicinity of the screw. All finite element nodes on the surface of the screw head were given a prescribed displacement Δ of 5 mm/min to mimic the experimental loading condition. Young's modulus of the synthetic bone was assumed to be 0.5 GPa while that for the screw was varied to simulate different materials. Interface of the screw and the synthetic bone was represented with novel zero thickness interfacial finite elements. A phenomenological interfacial constitutive law was developed to govern the mechanical response of the interfacial region (see Figure 29 Biii). This law takes into account the initial adhesion and interlocking of the bone and screw threads (initial rising region), onset of failure in surrounding bone material and subsequent softening of the interface (intermediate falling region), and ultimate frictional sliding (final horizontal region) leading to complete pull-out of the screw.

7.3.2.3 Calibration of FE model parameters

Our interfacial model possesses three parameters; maximum interfacial strength σ_c, relative sliding distance δ_c at which this strength is achieved, and a constant frictional traction τ_f. These parameters were calibrated using experimental data from the pull-out tests for pure Mg screws.

Modulus of the screw material was assigned to that of Mg (45 GPa). Parametric range for σ_c was taken to be lower than the yield strength of Mg (~21 MPa) so that the screw itself never failed, as observed in the experiments. The entire pull-out force versus applied displacement response was simulated and represented in Figure 29 C. A least square optimization technique was utilized to extract model parameters that fit the experimental curves best. A sensitivity analysis was performed to assess the effect of these parameters on the pull-out strength, *i.e.*, the peak of the pull-out curve.

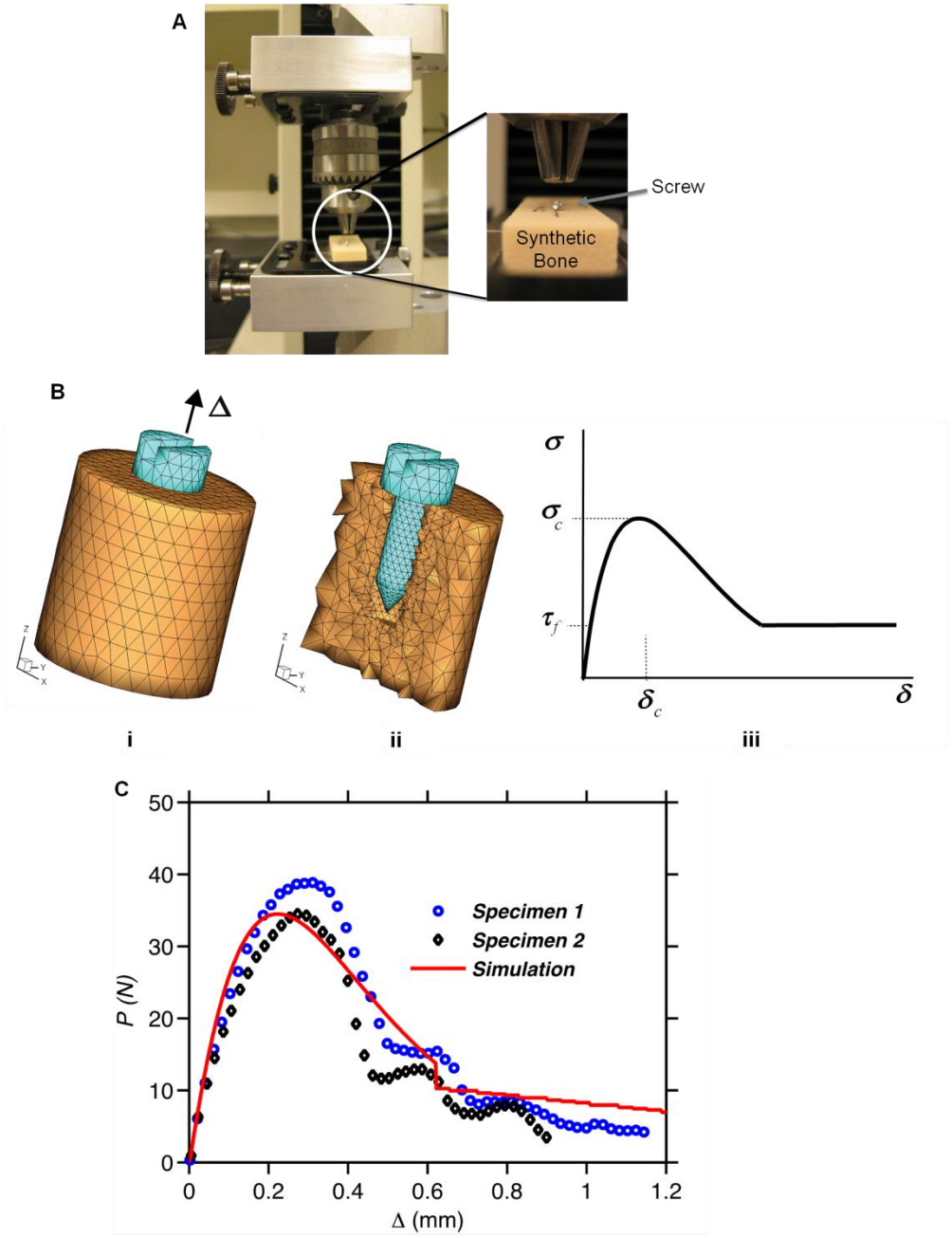

Figure 29. Pull-out testing. A) Pull-out tests were used to compare the pure Mg and AZ31 screws to stainless steel screws. Screws were placed in synthetic bone and the force required to remove the screw was recorded. B) (i) Pull-out experiment simulation domain. The bone is colored golden while the screw is blue. (ii) Details of the finite element discretization. (iii) Interfacial constitutive law used to simulate the pull-out tests with three model parameters indicated. C) Simulated pull-out force profile along with two representative experimental data for pure Mg. Experimental curves were utilized to extract the model parameters as shown in Biii.

7.3.3 Animal Procedures

Fifteen skeletally mature, female, New Zealand White rabbits approximately 1 year in age weighing between 5-7 kg were purchased from Myrtle's Rabbitry, Inc. (Thompsons Station, TN) and Charles River Laboratories International, Inc. (Wilmington, MA). All rabbits were examined by a veterinarian before surgery and were found to be in good health. All animal procedures were approved by the Institutional Animal Care and Use Committee at the University of Pittsburgh and in accordance with the National Institutes of Health guidelines for the use of laboratory animals.

Before the implantation surgery, all rabbits were sedated with ketamine and xylazine and intubated, and a surgical plane of anesthesia was maintained with isoflurane. The surgical site was shaved and scrubbed with betadine and sterilely draped. The incisure of facial vessels, located where the curve of the mandible and the posterior end of the molar region meet, was palpated and an incision was made slightly posterior to the incisure. An incision was made with a sterile scalpel, and the skin and muscle were reflected to reveal the bone. A sterile drill with a 0.85 mm drill bit was used to pre-drill holes and the holes were tapped. Two screws of the same material were placed on one side of the mandible (Figure 28 B, C). After implantation, the muscle and skin were sutured with resorbing sutures. Two screws of another material were placed on the opposite side of the mandible using the same procedure. Screw types were not mixed on a per side basis to avoid galvanic corrosion.

Following the surgical procedure the rabbits were extubated and observed until they had recovered from the anesthesia. The rabbits were monitored daily for the first week after surgery. The rabbits were given the option of soft food for the first few days after surgery and normal hard pellet food was available throughout the recovery period. Antibiotic injections were given

twice a day for five days post-op. Skin sutures were removed two weeks post-op. The Mg-alloy screws were not able to be visualized using X-rays, likely due to the size of the screws and the resolution of the X-rays, as well as the similarity in density between the bone and the Mg-alloy screws. Also, no hydrogen pockets were observed physically or in the X-rays. At the appropriate endpoint, the rabbits were sedated with ketamine and xylazine and euthanized with an intravenous injection of pentobarbital sodium. After death, the mandibles were collected, and assessed grossly, then wrapped in PBS soaked gauze and frozen until further processing and analysis.

The pure Mg and AZ31 screws were implanted in at least three different rabbits for each time point of 4, 8, and 12 weeks. Then after analysis of the longitudinal data, the control rabbits were implanted and incubated for 12 weeks. The control groups included a group with stainless steel screws implanted, and a group where osteomies (holes) were drilled into the mandible but no screws were placed. Naïve control bone was also examined.

7.3.4 In-Vivo Analysis

7.3.4.1 Qualitative MicroCT Assessment

First, all samples of the study were scanned with a 44.5 μm voxel size (80 kV, 500 μA) on an in-vivo Inveon micro computed tomography (CT) system (Siemens AG, Munich, Germany), referred to as Scan Set A. Set A scans were performed to obtain a global perspective of overall screw integrity. The entire left and right sides of the mandible were scanned in Set A, with only the condyles, incisors, and most of the molars removed, and at least three samples were scanned per type and time point. Three-dimensional (3D) volumes were generated from lateral projections for every scan using the Siemens reconstruction software, and exported as dicom

files for analysis using Mimics 12 software (Materialise, Leuven, Belgium). Regions of interest were user-defined around the screws for further analysis by generation of 3D renderings using a threshold initially set at the default software value for CT bone. New bone formation and the amount of residual magnesium were visually assessed.

Higher resolution microCT imaging was performed on a smaller subset of samples, referred to as Scan Set B (two screws per type and time point), using an in-vivo VivaCT 40 (Scanco Medical, Basselsdorf, Switzerland) or an ex-vivo SkyScan 1172 (Bruker-Skyscan, Contich, Belgium) system with a 10.5 μm (70 kV, 110 μA) or 12.9 μm (59 kV, 167 μA) voxel size, respectively. The whole mandible samples were cut down to only include the region around the screw implants. The 4 and 8 week samples from set B were scanned on the VivaCT 40 system, while the 12 week set B samples and the control samples were scanned on the Skyscan 1172 system. 3D volumes were generated as the respective file type for each system format (isq files for Scanco VivaCT 40 and a stack of bmp files from Skyscan 1172). These higher resolution set B scans and control scans were imported into Mimics 12 software for analysis. Bone remodeling and magnesium degradation were visually inspected in both the two-dimensional (2D) slices and 3D reconstructions from Mimics.

The higher resolution Set B screw scans were also qualitatively described by individual screw parts (Head, Shaft, Shaft in Cortical Bone, Shaft in Marrow Space) by calculating screw volume fraction using the Skyscan DataViewer and CTAn software. First, the scans were reoriented to align the standard x plane with the screw of interest. Regions of interest were subsequently defined around the screws extending to the boundary with the adjacent bone. As the peak representing the screw voxels mineral densities was distinct from the respective peak of background and degradation product voxels in distribution of mineral densities within the

regions of interest histograms, a threshold for segmentation of the residual Mg screw was set at the inflection point between the two peaks (Figure 30). The volume of the remaining Mg-alloy was calculated from the microCT and expressed as a bone volume fraction meaning the remaining screw volume fraction (referred to as volume fraction) of the theoretical initial screw volume of interest. First, the total volume fraction of the remaining screw alloy was determined. The theoretical total screw volume was determined by assuming the shaft of the screw was a solid cylinder 1 mm in diameter and 2 mm long, plus the volume of the screw head as described below. As a difference in the degradation rate of the screws in the different regions of the bone (cortical and bone marrow) and muscle was preliminarily assessed visually, the screws were for the purposes of the volume fraction measurements first divided into two parts, head and shaft. The shafts in turn were divided into two parts, the one inside cortical bone and the one inside the bone marrow space. The theoretical volume in the shaft, cortical bone, and bone marrow space measurements for volume fraction were calculated by assuming a theoretical cylinder with a diameter of 1 mm and a height that was equal to the height of the stack of images being analyzed. The theoretical volume of the head of the screw for volume fraction was calculated as the volume of a cylinder the size of the head (2 mm in diameter, 1 mm long) minus the volume of a rectangle from the drive slot in the screw.

7.3.4.2 Histology

The 12 week samples from the pure Mg and AZ31 screws were formalin fixed and sent to Alizeé Pathology (Thurmont, MD) for processing by embedding in 70/30 methylmethacralate (MMA). Sections were ground and polished to a thickness of approximately 65±15 μm. The slides were stained with hematoxylin and eosin and evaluated with light microscopy.

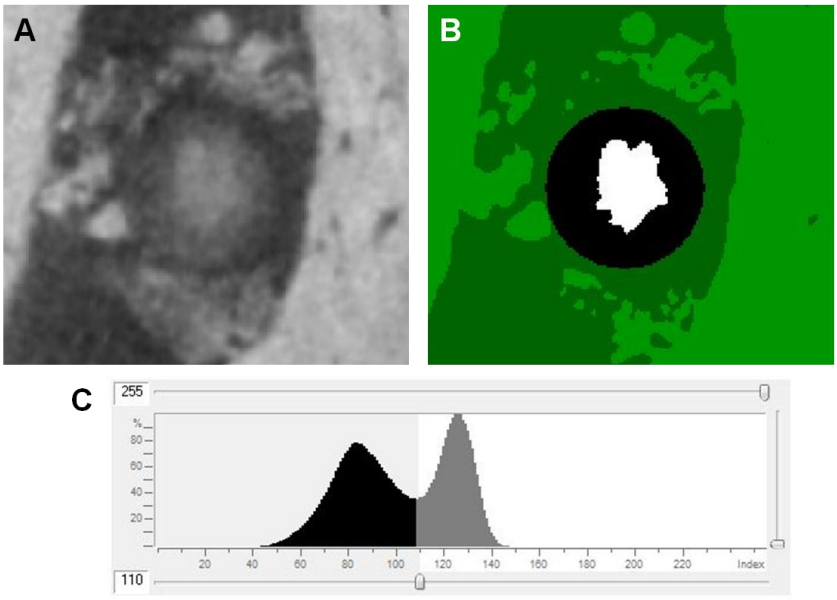

Figure 30. MicroCT processing. A) Reoriented slice of a 12 week AZ31 screw. B) Binarized image of the region of interest of the same slice. C) Histogram showing the threshold set at the inflection point in the curve.

7.4 RESULTS

7.4.1 Pull-Out Test and FE Modeling

Pure Mg and AZ31 screws exhibited pull-out forces similar to that for the stainless steel screws when pulled out of a synthetic bone material. The pull-out strength for all of these screw materials was approximately 40 N (Figure 31 A) with no statistical differences between the groups. This observation led us to believe that the threads of the Mg-alloy screws gripped the synthetic bone in the same manner as the stainless steel screws. A systematic computational study was then undertaken to gain further understanding of the mechanical parameters governing the pull-out strength. First the modulus of the individual screw material was taken as 1 GPa, 43.25 GPa (AZ31 alloy), 45 GPa (pure Mg), and 210 GPa (stainless steel), respectively, while all

other model parameters remained constant. Simulated pull-out force profiles for all these cases have been plotted, see Figure 31 B. These curves signify that for a constant diameter of the screw with similar interfacial conditions, *e.g.*, thread profile and depth of penetration, the pull-out strength remains essentially constant. Next the effect of the interfacial strength σ_c on the pull-out strength was examined keeping all other model parameters constant. The mean value of this parameter was found to be 4.5 MPa when calibrated against experimental pull-out forces for pure Mg screws. Figure 31 C presents simulated pull-out curves for σ_c = 2.25 MPa, 4.5 MPa, and 6.75 MPa. Observe from Figure 31 C that this variation of the interfacial strength resulted in more than a three-fold increase in the predicted pull-out strength. Thus it was concluded that pull-out strength is highly sensitive on the interfacial strength between the screw and the bone. Similar parametric studies were performed to examine the effect of remaining two interfacial parameters, δ_c and τ_f, on the pull-out strength (not reported here). However, we found that the pull-out strength did not exhibit any appreciable sensitivity to these parameters.

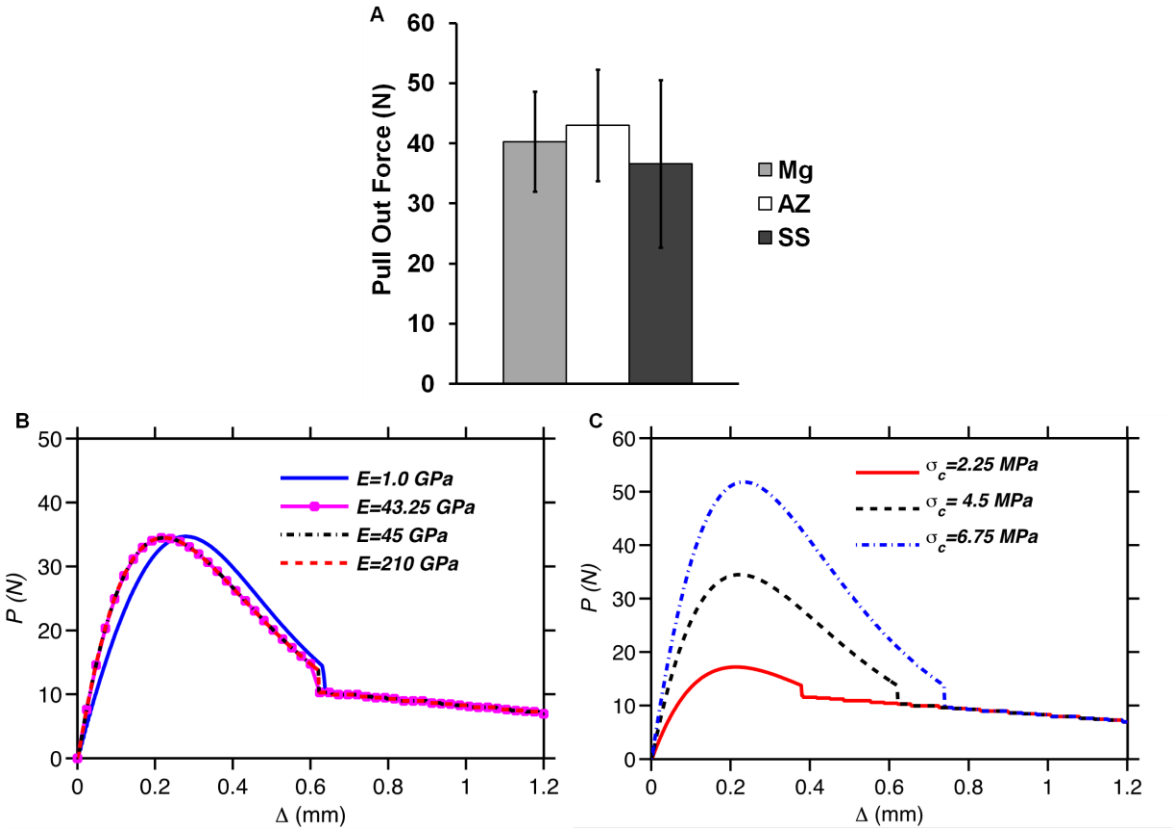

Figure 31. Experimental and simulated pull-out test results. A) Experimental pull-out test results. Both the pure Mg (Mg) and AZ31 (AZ) screws had a similar pull-out force to the stainless steel (SS) screws of approximately 40 N, with no statistical differences ($p<0.05$). B) Simulated pull-out profiles for different screw moduli corresponding to pure Mg (45 GPa), AZ31 (43.25 GPa), stainless steel (210 GPa), and a model very weak material (1 GPa). Interfacial parameters and synthetic bone modulus were kept constant for all these simulations. Yield strength for all these materials were more than the maximum interfacial strength of 4.5 MPa. C) Effect of maximum interfacial strength on the pull-out force profile. Other two interfacial parameters were kept constant. Screw material was taken as pure Mg.

7.4.2 Qualitative MicroCT Analysis

Signs of degradation were observed for the pure Mg screws at 4 weeks in scans from both sets A and B, Set B is shown in Figure 32, as evidenced by the reduced brightness in certain regions of these screws. Bone remodeling occurred in the area surrounding the screws. Any bone noted around and over the screw heads was considered new bone growth, as the heads of the screws were completely above the native bone at the time of implantation, while the bottom of the screw heads were placed flush with the bone. At 4 weeks, the pure Mg screws were in contact with the bone. Then at 8 weeks the shafts of the pure Mg screws appeared to be mostly degraded, as seen by the presence of holes within the screw bulk in the images, as well as major bone resorption with little new bone formation around the screws (Figure 32, Set B Scans). By 12 weeks, the bone resorption seemed to subside, and new bone appeared to be growing over the pure Mg screw in 71% of the screws imaged from both sets of scans, while at the same time bone resorption under the head of the screw was still noted in approximately 85% of the pure Mg screws.

The AZ31 screws, in both scan sets A and B, showed little sign of degradation at 4 weeks (Figure 32, Set B Scans), and the surrounding tissue seemed to remain intact. The AZ31 set A scans at 8 and 12 weeks continued to show little degradation; however, differences in degradation products were only visible in the higher resolution set B scans and not the set A scans. At 8 weeks, in set B, the AZ31 screws began to show signs of degradation, with regions of reduced brightness appearing in the shaft region of the screws (Figure 32, Set B Scans). The adjacent tissue continued to remodel around the screw, as seen by some new bone growth around the screws, and little bone resorption. At 12 weeks, the set B AZ31 screws continued to show signs of degradation with a larger area of decreased brightness in the shaft of the screw (Figure

32, Set B Scans). The surrounding tissue continued to remodel and grow around the screws. From both sets of scans, there were signs of bone resorption under the head of the screw in approximately 71% of the cases at 12 weeks. Bone grew around and over the head of the AZ31 screws in approximately 57% of the cases for the AZ31 screws at 12 weeks. An example of the bone overgrowth and the approximate location of the original bone line is shown in Figure 33 clearly showing the overgrowth of bone over the head of the AZ31 screw at 12 weeks.

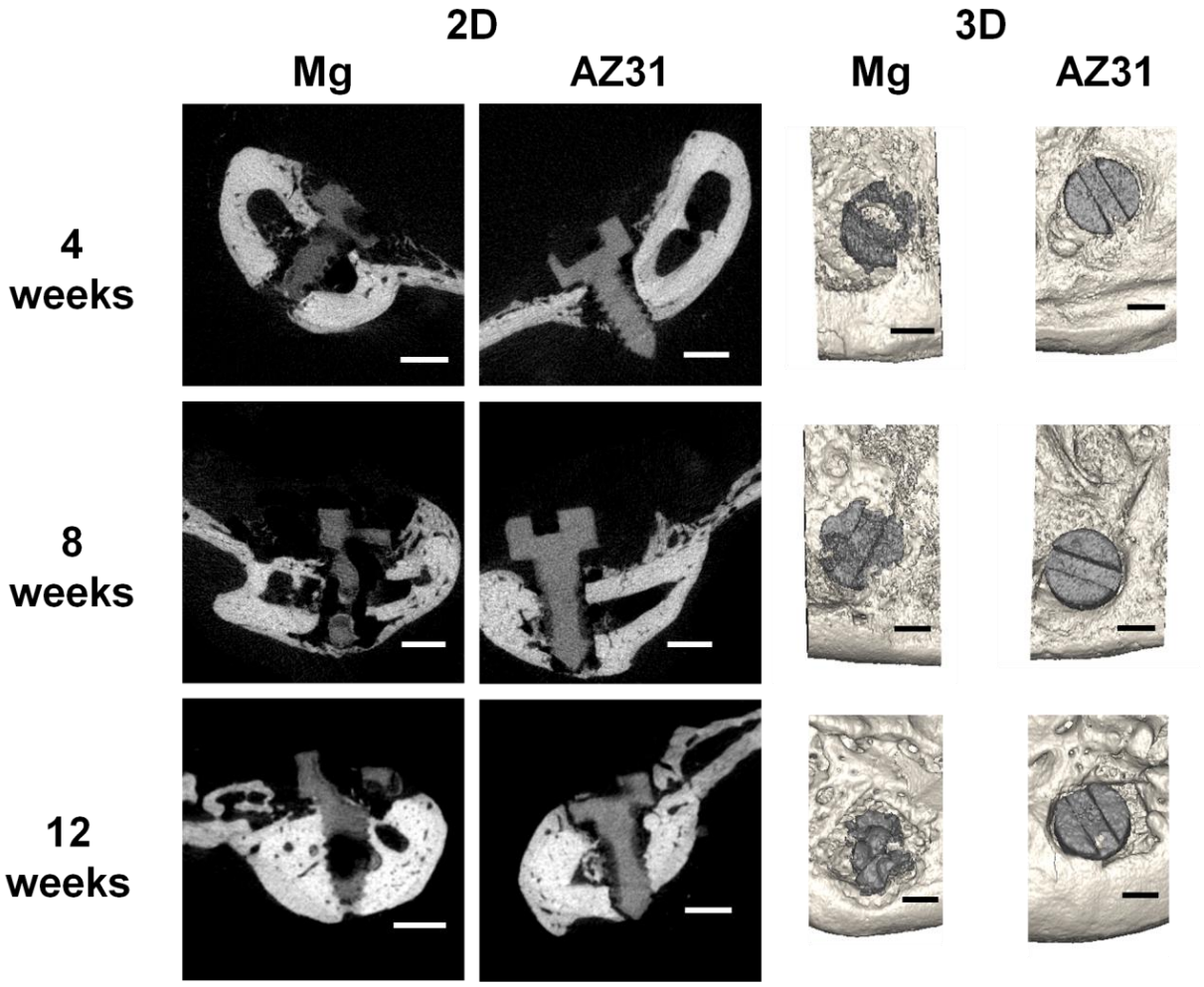

Figure 32. 2D slices and 3D reconstructions from the set B microCT scans. Pure Mg and AZ31 screws are shown at the full length of the screws at 4, 8 and 12 weeks. Scale bar =1 mm. Representative samples shown from n=2.

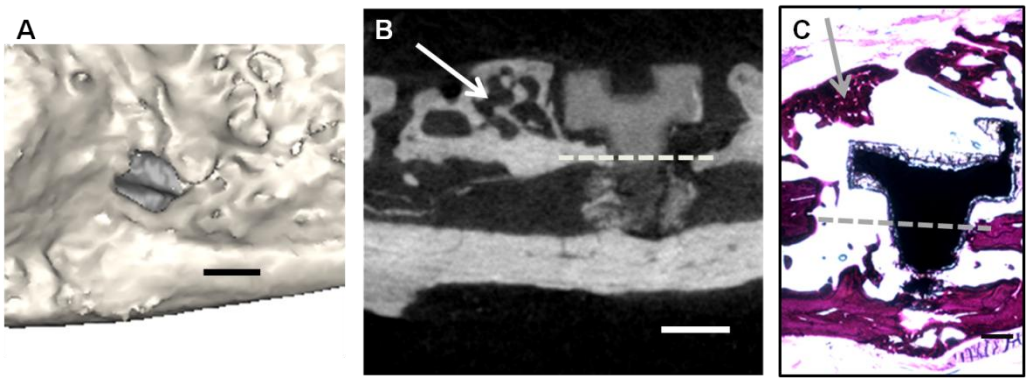

Figure 33. Example of bone overgrowth. A) 3D microCT reconstruction showing major bone overgrowth of an AZ31 screw at 12 weeks, from Scan Set A. (Scale bar =1mm) B) 2D microCT image showing the new bone growth around an AZ31 screw at 12 weeks, from Scan Set B. (Scale bar =1mm) The dashed lines in B) and C) show approximately where the original bone line was, anything above the line is new bone growth. The head of the screw was above the bone when the screws were implanted. C) Histological picture showing the overgrowth of bone over the head of an AZ31 screw at 12 weeks. (Scale bar =500µm)

Based on the results from the longitudinal portion of the study, the control samples included the empty holes (negative control), and stainless steel screws (external control) implanted in the rabbits for 12 weeks, scanned as part of the high resolution Set B Scans. On a qualitative basis, after 12 weeks, the mandibles with holes and without screws showed many signs of remodeling. The original holes were not apparent (Figure 34), and new bone growth was seen throughout the region where the holes existed. When compared to naïve control bone, the remodeled bone appeared to be rougher and thicker (Figure 34). After 12 weeks, the stainless steel screws were fully intact (Figure 34). Bone growth occurred around the stainless steel screws, but growth over the screws and bone resorption under the screws were not observed.

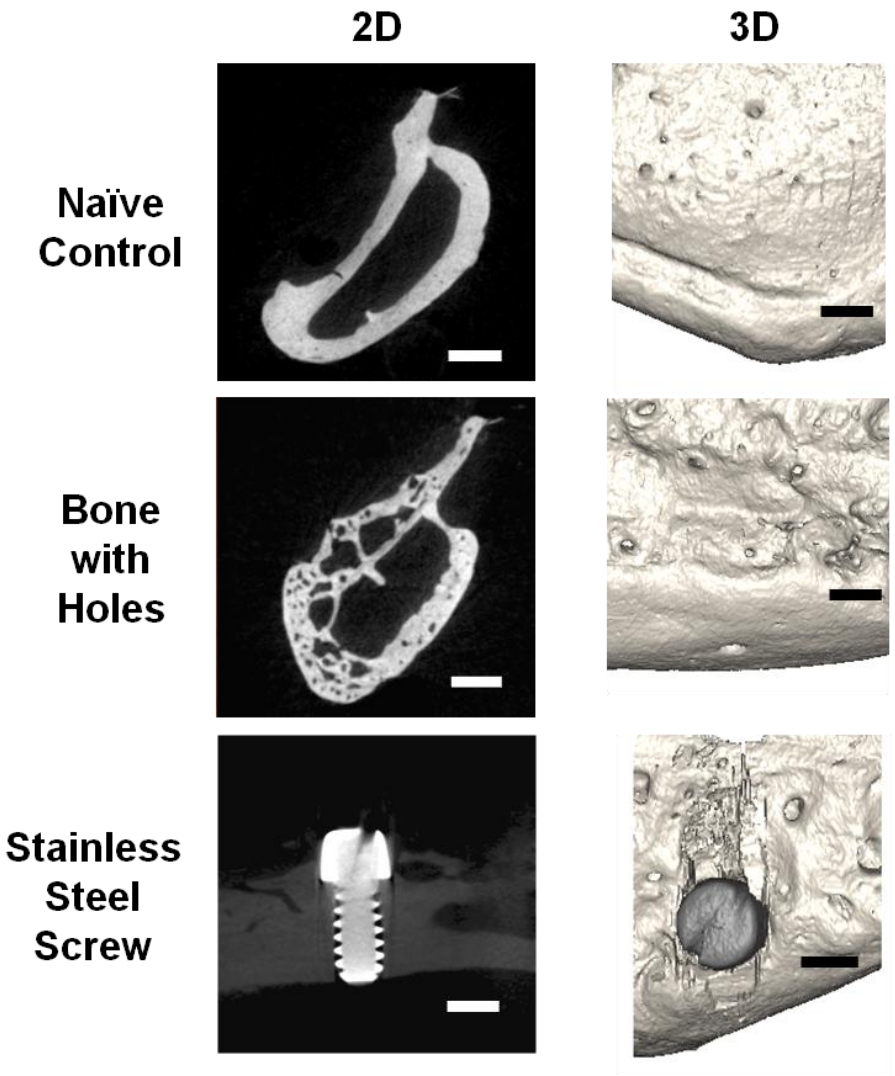

Figure 34. MicroCT control data at 12 weeks. 2D slices and 3D reconstructions from naïve control bone, bone with holes drilled but no screws placed after 12 weeks, and stainless steel screws placed for 12 weeks, from the higher resolution Set B Scans. (Scale bar =1 mm.) Note that the stainless steel screws were much more radiodense than the magnesium ones, resulting in increased beam hardening in the images. Representative samples shown from at least n=3.

For the longitudinal portion of the study, from the set B scans, the total volume fraction for both screw types seemed to decrease over time (Figure 35 A). The head of the screw remained fairly intact between 4 and 8 weeks, but not at 12 weeks (Figure 35 B). The volume fraction of the head at 12 weeks for the pure Mg was 31.3% and the AZ31 was 61.5%. In the Set B Scans, the screw shaft volume fraction seemed to decrease with time for both screw types (Figure 35 C). The degradation rate varied depending on the surrounding tissues. Separating the shaft into the cortical bone region and the bone marrow region, the volume fraction in the cortical space seemed to remain fairly constant over time (Figure 35 D), while the remaining volume fraction in the bone marrow space seemed to decrease with time for both screw types (Figure 35 E). The bone marrow space volume fraction for the AZ31 screws at 4 weeks was not calculated because the implanted screws did not penetrate the bone marrow space. By 8 weeks most of the pure Mg screw shaft in the bone marrow space seemed to be degraded with a volume fraction of approximately 12.0% (Figure 35 E), while the volume fraction in the cortical space was 43.4% (Figure 35 D). By 12 weeks, more material seemed to be degraded for both screws types in the bone marrow space, with a mean volume fraction value of 9.6% in the pure Mg and 20.0% in the AZ31 group (Figure 35 E), compared to 71.5% and 44.2% for the pure Mg and AZ31 groups, respectively, in the cortical bone (Figure 35 D).

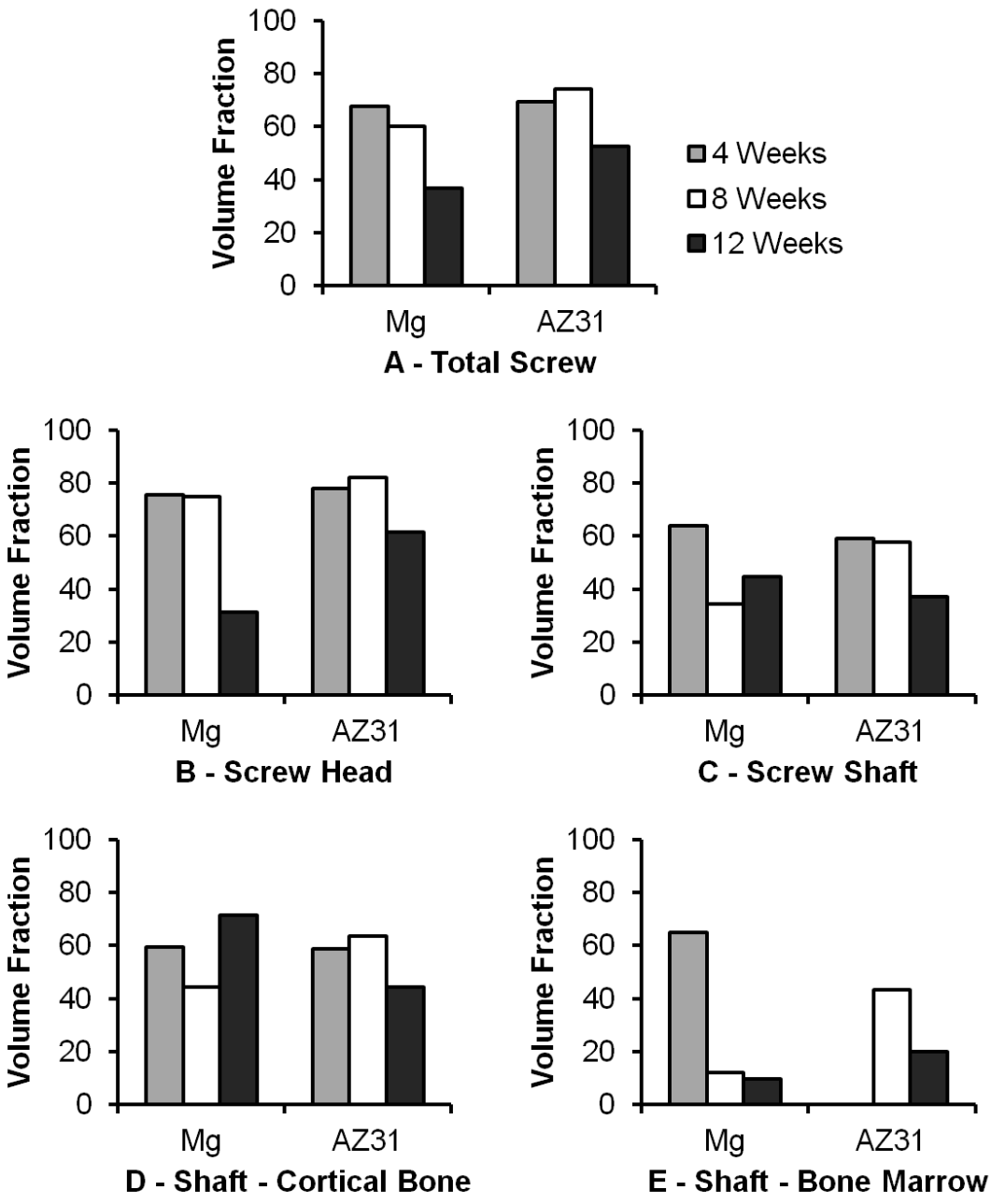

Figure 35. Volume fraction of the remaining Mg-alloys. Volume fractions were calculated from the set B scans for A) the whole screw, separating the screw into B) the head and C) the shaft, and for separating the shaft into D) the cortical space, and E) the bone marrow space calculated from the 10.5 and 12.9 µm voxel microCT scans, averaged for 2 screws per group. Note in E at 4 weeks the AZ31 screws were not included because the screws did not penetrate the bone marrow space.

7.4.3 Histology

Histology confirmed the findings noted in the microCT images for pure Mg and AZ31 groups at 12 weeks, identifying the brighter areas around the screws on these images as newly formed bone. The sections showed that in some locations the shafts of the pure Mg screws were completely degraded at 12 weeks (Figure 36 A). New bone was seen growing up next to the pure Mg screws and there was also new bone growing over the head of the screws. The AZ31 screws showed continuous bone to metal interfaces, as the bone was integrated with the threading, with little overall degradation of the AZ31 screws (Figure 36 B). New bone was seen growing up next to and in contact with the metal for both screw types. It should be noted that significant bone overgrowth was also observed around the AZ31 screws.

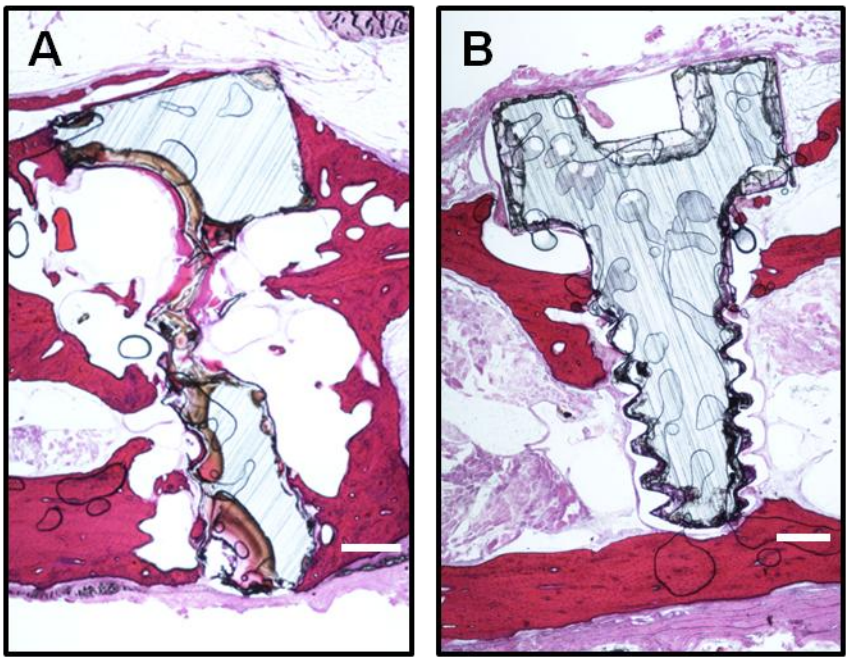

Figure 36. H&E histology at 12 weeks. A) Pure Mg and B) AZ31. Scale bar =500 µm. Note that the sectioning method resulted in sections of varying thickness, so the red colors vary between samples. Representative samples shown from at least n=3.

7.5 DISCUSSION

Over time, the two Mg-alloys behaved differently in-vivo. The degradation products for the pure Mg screws appeared to be removed, while the degradation products for the AZ31 screws appeared to remain at the site. In the AZ31 screws, two density levels were observed in the screw shaft, while the Mg screws only had one density level. Comparing the denser regions of the remaining material for both screws types, the screws were similar in volume. However, when including the lower density region of the AZ31 screws, the volume was much larger. The lower density region in the AZ31 screws could be the remaining degradation product, while the pure Mg screws degradation product might have been resorbed and not observed in microCT.

Bone remodeling and growth was observed around both screw types after 12 weeks of implantation. The degradation rate of the screws was site-dependent, as the shafts degraded faster in the marrow space compared to the cortical bone. More studies need to be performed to see how well the screws can anchor a plate for up to at least 8 weeks in-vivo. Ideally, the Mg-alloy screws would allow for initial stabilization and adequate strength to permit bone healing during function, and then decrease in strength with time so that the physiological force is then transferred to the bone [133]. The amount of time for craniofacial bone to heal and varies, but one study reported that after 4 weeks a mandible fracture with screw and plate fixation was at an advanced stage of bony union demonstrating functional stability, and by 8 weeks the fracture sites had fully remodeled [102]. If the degradation rate is not ideal, alloying Mg with Al, Zn, and Mn as is the case with AZ31, the degradation profile could be controlled. Thus, these results indicate the promise of using Mg-alloys for craniofacial applications.

Comparing the in-vitro pull-out test results to previous studies [33, 34, 39, 142, 155], similar pull-out forces were determined amongst screw types tested in each study, but the screws

studied herein were much smaller than other screws tested previously, so the absolute force values were expectedly lower in this study. It is therefore difficult to do a direct comparison between the studies because of several factors including different screw size, design, and material, different bone or synthetic bone materials properties, and the screw insertion technique [39]. Nevertheless, our data showed that the design of our Mg-alloy screws resulted in a holding strength similar to stainless steel screws of a comparable size. The results agree with the previous studies showing similar holding strengths between screws of varying types of similar sizes [33, 34, 39, 142, 155].

To gain a mechanistic insight into these pull-out experiments and the parameters that control the pull-out strength, this study resorted to a finite element based computational approach. The finite element algorithm, developed specifically for this purpose, allowed this study to examine separately the effects of mechanical properties of the screw material and the interface condition. The primary mechanical parameters investigated were the modulus of the screw material and the interface properties between screw and bone. Interface properties are in turn dependent on a number of factors such as thread profile, failure strength of the bone, coefficient of friction between the bone and the screw and the area of contact. The model allowed this investigation to lump all these effects together in a novel interfacial constitutive law. The pull-out strength indeed was determined to be insensitive to the modulus of the screw material. It only influenced the initial slope of the pull-out curve when its magnitude was comparable to that of the synthetic bone. Peak pull-out force was related to the onset of weakening of the interface and exhibited a strong correlation with the interfacial strength. These simulations along with these pull-out experiments point to an important conclusion that the pull-out strength can be controlled by initiating a proper design of the interface, for example by

choice of thread profiles, as long as failure strength of the screw material is higher than that of the surrounding bone.

These in-vivo Mg results were similar in the mandible as compared to the long bones. Bone formation occurred around the Mg-alloy screws. The Mg-alloy screws were also biocompatible, with no evident signs of inflammatory response and in general, a healthy profile of the surrounding tissues was observed on histological sections. However, the screws seemed to degrade much faster in the marrow space as compared to the cortical bone [137, 167]. The differences in the organic and inorganic phases of long bones compared to flat bones seemed to make little difference in the behavior of the Mg-alloy screws, at least in the mandible, which is loaded similar to long bones. Implanting Mg-alloys in the skull may however have different outcomes.

Comparing to the previous AZ31 screw studies, similar results were noted. New bone formation occurred around the implants [37, 151]. A difference in the degradation of the screws between the cortical bone and the marrow space or the head of the screw was seen, which agrees with the study that reported notable differences based on the location of the implant in the original tissue [151]. A limitation of this study was in the screw placement; some screws were placed in the region of the mandible with only cortical bone, so for some screws the marrow space could not be analyzed.

The Mg-alloys did not seem to inhibit bone remodeling around the holes created in the mandible. The bone with holes without screws was observed to remodel with excess bone growth. New bone was seen growing around the pure Mg, AZ31, and stainless steel screws; however, overgrowth was not observed with the stainless steel screws. It is possible that Mg helped the periosteum to promote bone growth over the heads of the screws. A previous study

supported the hypothesis that the major corrosion products of Mg-alloys are the major origin of enhanced bone growth around the implant [69], the current study seemed to agree with this previous study's findings. However, more studies and longer term studies are warranted to understand the benefits and drawbacks of new bone growth in the craniofacial region.

Future studies will be needed to specifically determine if the degrading Mg or any of the alloying elements have any beneficial or detrimental effect on the surrounding craniofacial tissues, as well as overall systemic health. Novel alloys will need to be developed and tested incorporating suitable alloy and device designs exhibiting optimal degradation characteristics while promoting bone regeneration without inducing any undesired effects on the surrounding tissues. FE modeling can be used to compare future screw designs to determine the most appropriate design for the specific application. Now, as this system is in place, consideration for a bone fixation device can begin, such as plates and screws. Evaluation of shear strength, torque, and other mechanical properties, as well as analysis of bone stabilization from the fixation device needs to be completed. In addition to using Mg-alloys to improve craniofacial plates and screws, these results are also beneficial for conducting research for improving other craniofacial and long bone prosthetics.

7.6 CONCLUSIONS

Mg degradation and bone remodeling occurred with both Mg-alloy screw types. The pure Mg degraded with a different profile than the AZ31. Mg-alloy screws degraded at varying rates throughout the length of the screw depending on its location within the bone, subject to whether the screw was in the cortical bone, in the marrow space, or in the muscle. Alloying of Mg will

allow for control of the degradation rates, which can then be adapted for site specific results. FE modeling can also be used to help design future screws for specific applications. The results of this study show promise for the future use of degradable Mg-alloys for craniofacial fixation applications.

7.7 CONTRIBUTIONS

I completed the in-vitro testing, helped with the screw design, assisted with the screw implant surgeries, collected and analyzed the low resolution microCT scans, analyzed the high resolution CT scans, analyzed data, and prepared and edited the manuscript. Dr. Verdelis advised on the microCT analysis method, helped collect the high resolution scans, and helped with editing the paper. Dr. Matai and Dr. Pal did the finite element model development and analysis, and wrote the sections about the model. Dr. Hagandora assisted with the mechanical testing development. Dr. Chung helped with the surgeries and the design of the screw. Mr. Holmes fabricated the screws in the University of Pittsburgh Swanson Center for Product Innovation. Mr. Chou helped with the screw fabrication and processing as well as manuscript editing. Dr. Kumta helped with the project design and manuscript editing. Dr. Almarza helped with project design, screw implantation surgeries, data analysis, and manuscript editing.

8.0 OVERALL DISCUSSION

8.1 SUMMARY

The long term goals from this dissertation include resolution of pain and restoring joint function for patients with various TMDs, and the studies presented in this dissertation worked towards beginning to address these goals. The first part of this dissertation used an altered occlusion TMD model in a rabbit and used various fibrocartilage assessments, pain assessments, and joint movement assessments to better understand the degeneration process. The second part of this dissertation looked at the potential for using a resorbable metal, magnesium, for a craniofacial implant.

These unilateral splint studies allowed for a unique combination of assessments to understand degeneration from an altered occlusion model in a rabbit. The altered occlusion should have affected the magnitude and distribution of loads in the joint, which led to the damage of the condylar fibrocartilage. These studies were unique in that they combined multidisciplinary assessments to provide a comprehensive examination of the TMJ. Placing unilateral splints also seemed to cause more damage to the contralateral side of the TMJ; however changes were noted on both sides. Trends for increased pain sensitivity were noticed in the behaviors of the splinted animals, and the anatomical approaches suggested increased pain through an increased number of c-Fos+ cells present. However, a possible compensatory change

was observed in the action potential behavior of the putative nociceptive afferents of the TMJ. The joint kinematics were also affected, where the total distance traveled by the condyles and incisors decreased after splinting. One reason the unilateral splint model was advantageous was that the joint capsule was not penetrated.

During the altered occlusion studies the rabbits' weights were monitored. The initial week or two after splint placement the rabbits lost some weight, but by the second or third weeks most of the rabbits were maintaining and/or gaining weight. During the first week after the splinting procedure, the rabbits had access to both soft and hard food, and then throughout the remainder of the study the rabbits continued to eat their normal hard pellets. The rabbits seemed fairly healthy by weight measurements, but the condyles showed signs of remodeling and degeneration, pain analyses showed nociception was present, and kinematics showed a change in joint motion. Thus, the rabbit model seems to provide useful information on the effects of altered occlusion without having too much measureable discomfort for the animals.

The dynamic function of the rabbit TMJ was analyzed through non-invasive three-dimensional skeletal kinematics, providing knowledge for understanding normal joint motion. The normal mechanics of the TMJ can be used in the future to compare and distinguish kinematics of injured/degenerated joints, as well as healing joints. Repeatable measurements were determined for both the distances in the joint space and the joint paths. The dynamic biplane x-ray imaging system we used was beneficial because it allowed for non-invasive measurement of normal rabbit chewing, both at the incisors and within the joint space.

Biodegradable metals such as magnesium have the potential to provide more options for craniofacial implants, by promoting bone growth and regeneration, and limiting the need for future procedures to remove the devices. The magnesium study showed that commercially

available pure Mg and AZ31 shaped as screws were biocompatible in the rabbit mandible, and bone growth occurred around both screw types. The degradation rate of both screw types were found to vary depending on the location of the material in the tissue, whether it was located in muscle, cortical bone, or bone marrow space. Furthermore, it was shown that by alloying Mg, the degradation profile could be changed. These results indicate the promise of using and developing Mg-alloys for craniofacial and other applications.

Overall, these studies were also beneficial for gaining better insight into the TMJ. The TMJ differs greatly from other more researched and well understood joints such as the knee or shoulder, so assumptions from studies on other joints should not be blindly applied to the TMJ. The TMJ is also a bilateral joint, so the left side affects the right side of the joint and vice versa, so each side cannot be analyzed alone or be the 'control' sample for an experiment. TMD symptoms may vary from side to side as our studies seemed to suggest. These studies were important for the furtherance of research and gaining a better understanding of the function of the TMJ and for a possible degeneration mechanism.

8.2 LIMITATIONS

There are also limitations of the studies that have been completed. TMD is a vague term as it covers almost as many problems as someone complaining of knee pain. In this dissertation, research was completed on only a focused area of one specific TMD. Also, animal models are often used to better understand a disease such as aspects of TMD, but can only provide specific information that is representative of the human condition.

For the splint model, one limitation was determining a method of splinting that would not fall off the teeth. Even with the current system, problems still arose with the splints falling off, or when the splints were to be removed, they were very easy to lift off the teeth. For longer term studies, better and stronger attachments for the splints will be necessary, while still remaining removable. This splint model could also be adapted to a larger animal model; however it would be difficult to adapt the pain assessments to an even larger animal. It proved difficult to adapt the current pain assessments to the rabbits, and though we got statistically significant results, the differences were small, and doing a long term multi-time point study might prove difficult to see differences between the groups.

Another limitation of the splint studies is that rabbits' teeth will continually erupt. At some point in time, the contralateral upper and lower molars will grow to meet. It is unknown how the splint would or would not continue to affect the rabbit after that point. Perhaps in the future, the rabbits' contralateral molars could be filed down to their original height at certain time points throughout the study. The incisors also continually grow, so the rabbits need to be monitored to make sure they are still able to eat throughout time.

We do not yet know if the changes we are seeing from the altered occlusion are truly degeneration of the tissue or if the tissue is just remodeling to a new 'normal' to adapt for the change in occlusion, which is a limitation. It is yet unknown if the changes would continue on the chronic degenerative pathway or if the changes would reach a new homeostasis that supports the change in loading. This is why studies with variable endpoints and checking for chronicity are important and required in the future.

For the behavioral testing a limitation was that rabbits are animals of prey, and are prone to hide their pain, making the assessments difficult. Steps were taken to make the rabbits

comfortable around the testers and in the testing situation; however the readings could have still been affected by the human presence in the room.

For the altered occlusion study, a limitation of the kinematic assessment was that we could only microCT the rabbits head after the final time point and the rabbit was euthanized. It would be more beneficial and ideal to have a CT scan of the head at every time point data is collected, to account for any changes in the bony structure of the joint. We had to assume there were no changes to the bony structures and ignored the teeth in the analysis, because the teeth did change from one data collection to the next. However, due to the limitations of the necessary resolution of the models and the equipment available, the rabbit's heads could only be scanned once the animal was deceased.

A limitation of the kinematic assessment is that it is currently very labor intensive, so there is a question of whether it would really be feasible and profitable to be adapted for clinical use. It would need to be determined that kinematic analysis greatly changes the diagnostic outcome and the overall outcome of the patients for it to be adapted to the clinic. Another limitation is that patients may not like having so much radiation directed at their skull, for both the data collection and the CT/MRI, though it has been shown to be within acceptable radiation limits. Training the animals, in our case rabbits, for the kinematics analysis was not an easy venture. Kinematic data collection should be easier for humans who can follow directions without much training and practice.

Another limitation of the kinematic analysis is that it is unknown how the rabbit chewing varies from day to day. The study compared multiple trials at one point in time, but did not collect data from the same rabbit over several days. A more thorough study should consider looking at the changes or lack of changes that occur day to day in chewing. Another limitation is

the lack of a standardized bolus size and composition. In human studies, chewing gum would be a good option to use to control both the composition of the bolus and the size of the bolus. In animal studies, using dried fruit, the pieces can be made to be similar in size, but the chewing patterns may be affected by the composition of the fruit and how fast the animal chews the fruit and is breaking it down, and where in that process the data is collected.

For the magnesium study, one limitation was that we were only testing screws, and not a whole device such as plates and screws to heal a fracture. Clinically, screws will mostly be used to attach some sort of device to the bone; however the study was a good first step and allowed for a better understanding to be gained of the biocompatibility of magnesium in the craniofacial region. Other limitations included that the screws were too small to be visualized by the x-rays taken throughout the healing/incubation time, with the current resolution of the clinical device. While the screws were small, at the same time they were almost too large for very high resolution microCT scans; it was difficult to get microCT scans that were reasonable in file size and dealt with time, budget, software, and hardware constraints and that were most importantly showing enough details.

8.3 FUTURE DIRECTIONS

There are various directions the studies in this dissertation could continue in order to work towards the overall goals. For the altered occlusion TMJ degeneration model future studies can adapt the length of time with the splints in place to shorter or longer periods, and also allow time for recovery after the splints have been removed for various amounts of time. Changing the timing of the study will allow for better understanding of when the degeneration and pain

becomes chronic and irreversible. This type of study would allow us to see how resilient the TMJ is to injury. It can be determined if there is a certain time point by which the problem is corrected, that the joint will heal and recover to a 'normal' original state, or if you are past that point, the problem will continue on the chronic pathway, or perhaps the joint will reach a new 'normal' state that is different from the original state. These future studies should continue to be multidisciplinary including the analysis of the joint tissues, pain analysis, and kinematic analysis. Another possibility would be to adapt the study to a larger animal model that is more similar to humans.

In the future for the kinematic analysis, it would be beneficial to begin collecting data on subsets of TMD patients at various stages of the disorder, as well as normal subjects, to determine if there is a certain signature in movement that arise from TMDs. The kinematic analysis could possibly be adapted to the clinic to detect motion problems sooner and allow for earlier treatment which could prevent the problem from becoming chronic. If a patient is in pain, which is the number one reason why patients present to clinicians, we have shown that there can also be a change in joint movement. Future steps will need to see if the joint movement can be returned to a 'normal' pattern and if that alleviates joint pain.

For the magnesium study, one future direction would be to try a fracture model in both the mandible and skull with magnesium plates and screws and compare to the titanium and/or polymer plates and screws. For a thorough analysis, the magnesium-alloy plates and screws should be studied in both the loaded mandible and the unloaded skull, because the loading may be a cause for varied results between locations. If magnesium is to be used in the skull, the effects of magnesium on the surrounding tissues, including the brain will need to be analyzed. Additional work will also need to be done to determine alloy compositions that degrade at the

proper rate for the desired application. The magnesium screws and devices will need to be mechanically tested in multiple test beds such as the pull out test, but also in torsion and bending. The devices need to be able to support the daily loading until the fracture/injury heals, then degrade away once the bone can again support the load.

8.4 CONCLUSIONS

Overall these studies begin to better understand one mechanism that could be behind the development of a TMD. There are many different development methods and types of TMDs that could be studied. The studies in this dissertation are a small step towards better understanding pain and degeneration from altered occlusion. With a better understanding of pain and degeneration from TMDs, hopefully better diagnostic and treatment methods can be developed to decrease the pain and restore joint function. These studies also begin to look at the use of magnesium for implants in the craniofacial region, which could help reduce the need for second procedures to remove implants and perhaps increase the lifespan of various implants into the skull and mandible.

APPENDIX A

STANDARD CURVES, ERROR PROPAGATION, AND POWER ANALYSIS

A.1 BIOCHEMICAL ANALYSIS

The biochemistry assays performed in Chapter 3.0 were all from established protocols. The total collagen content was measured using a hydroxyproline assay. The concentration of the collagen standards ranged from 50 μg/mL to 800 μg/mL. The absorbance of the standards was measured and a sample standard curve is shown in Figure 37. The assay is accurate to 50 μg of collagen content from the original sample. As such, collagen content is reported down to 0.05 mg.

The GAG content was measured using a dimethyl methylene blue assay kit for sulfated GAGs from Blyscan. The standards ranged from 0.25 μg to 4 μg per tube. The absorbance of the samples and the standards was measured and a sample standard curve is shown in Figure 38. The assay is accurate to 0.25 μg of sulfated GAG content from the original sample. As such, GAG content is reported down to 0.0025 mg.

The DNA content was measured using a PicoGreen fluorescence kit to measure double stranded DNA. The standards ranged from 7700 pg to 115500 pg and a sample fluorescence standard curve is shown in Figure 39. The PicoGreen assay is even more sensitive than the range

in which we use it. We do convert DNA to cell numbers by a conversion factor of 7.7 pg DNA/cell. Since that conversion is an approximation, we report cell number down to 1000 cells.

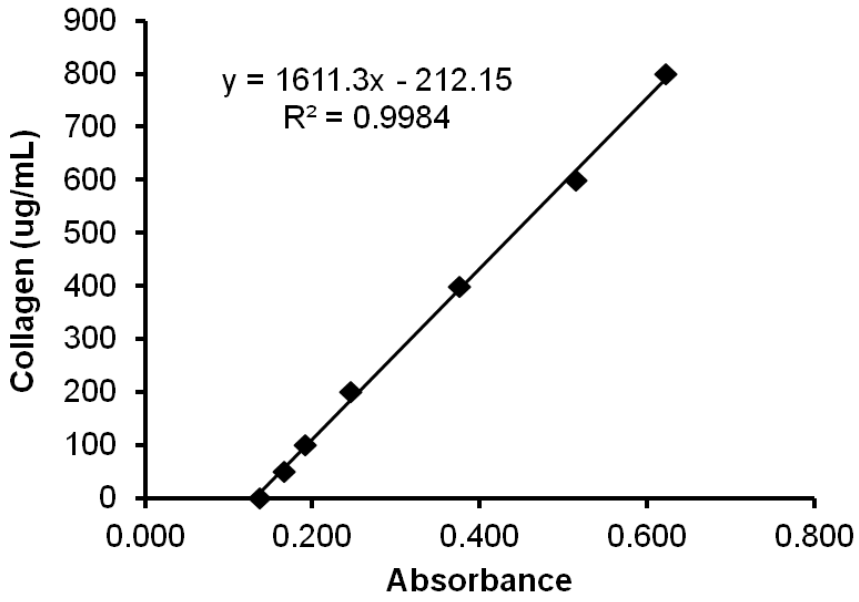

Figure 37. Representative hydroxyproline assay standard curve using collagen standards to measure total collagen content.

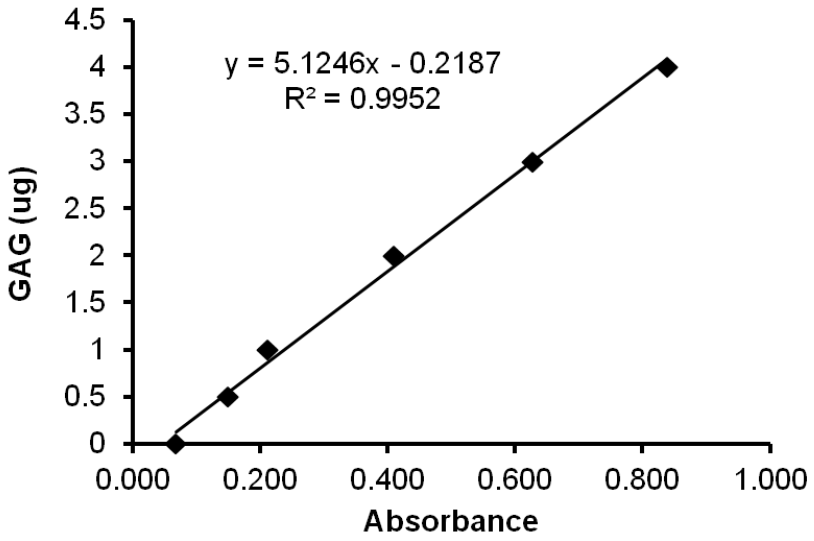

Figure 38. Representative dimethyl methylene blue GAG assay standard curve.

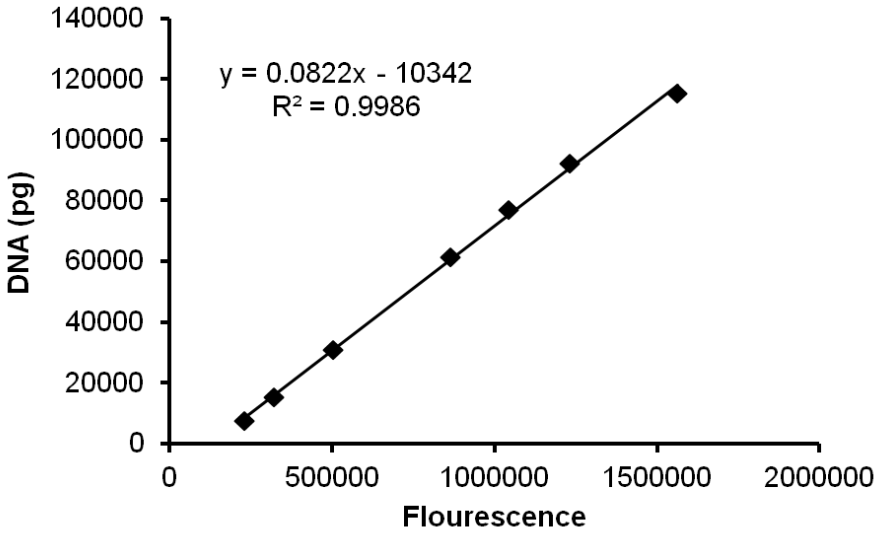

Figure 39. Representative PicoGreen DNA assay standard curve.

A.2 MECHANICAL ANALYSIS

The MTS Insight 1 used for the mechanical testing in Chapter 3.0 and Chapter 7.0 has a position resolution of 0.001 mm and a position accuracy to 0.01 mm, based on specifications in the instruction manual provided by MTS. For the soft tissue testing in Chapter 3.0 a 10 N load cell was used. The company calibration of the 10 N load cell claims that there is an estimated measurement uncertainty of 0.040% of the reading, and reports measurements to 0.0001 N. For the screw uniaxial pull out testing in Chapter 7.0 a 1 kN load cell was used. The calibration report for the 1 kN load cell claims the estimated measurement uncertainty is 0.030% of the reading, and reports measurements to 0.1 N. The diameter measurement of the TMJ disc samples has a resolution of around 0.01 mm. According to these errors the limitations to the error propagation for the soft tissue testing would rest on the diameter of the sample and the position and movement of the cross head, so the distance and strain of the mechanical tests. As to the repeatability of the measurement of mechanical properties of the TMJ fibrocartilage, we observed a standard deviation of +/- 30% from the means in native tissue. This is on par with what is observed to most soft musculoskeletal tissues.

A.3 POWER AND SAMPLE SIZE

Power analyses were performed to determine the sample size needed to see a statistically significant difference between groups for some of the experiments. In the altered occlusion studies there were trends that the contralateral and the treated sides of the splinted rabbits were different; however, there were no statistical differences observed. To complete the power

analyses, α was set at 0.05 and the power was set at 0.80. G*Power 3.1.2 was used to perform the power analysis, determining the effect size based on the differences in the means and the standard deviations.

One power analysis was completed on the splinted and contralateral sides for the condylar fibrocartilage compression test. To see a significant difference between the strain in the left and right sides of the posterior condyle, 12 samples per group would be needed.

A second power analysis was completed on the GAG biochemical analysis between the left and right condyles of the splinted rabbits. To see a significant difference between the percent GAG per dry weight, 51 samples per group would be required.

A third power analysis was done to see how many cells would be required to find a difference between the treated and contralateral sides for the electrophysiological analysis. Looking specifically at the after hyperpolarization decay time constant, 51 cells per group would be required to see a statistical difference.

For the TMJ disc no statistical differences between the control and the splinted samples were observed. At the 10% strain step to see a statistical difference between groups a sample size of 76 per group would be required.

BIBLIOGRAPHY

1. Al-Sukhun, J., Helenius, M., Lindqvist, C., and Kelleway, J., *Biomechanics of the Mandible Part I: Measurement of Mandibular Functional Deformation Using Custom-Fabricated Displacement Transducers.* Journal of Oral and Maxillofacial Surgery, 2006. **64**(7): p. 1015-1022.

2. Ali, A.M. and Sharawy, M.M., *Alteration in fibronectin of the rabbit craniomandibular joint tissues following surgical induction of anterior disk displacement: Immunohistochemical study.* Acta Anatomica, 1995. **152**(1): p. 49-55.

3. Allen, K.D. and Athanasiou, K.A., *A surface-regional and freeze-thaw characterization of the porcine temporomandibular joint disc.* Annals of Biomedical Engineering, 2005. **33**(7): p. 951-962.

4. Almarza, A.J., Bean, A.C., Baggett, L.S., and Athanasiou, K.A., *Biochemical analysis of the porcine temporomandibular joint disc.* British Journal of Oral and Maxillofacial Surgery, 2006. **44**(2): p. 124-128.

5. Almarza, A.J., Hagandora, C.K., and Henderson, S.E., *Animal models of temporomandibular joint disorders: Implications for tissue engineering approaches.* Annals of Biomedical Engineering, 2011. **39**(10): p. 2479-2490.

6. Anderst, W., Zauel, R., Bishop, J., Demps, E., and Tashman, S., *Validation of three-dimensional model-based tibio-femoral tracking during running.* Medical Engineering & Physics, 2009. **31**(1): p. 10-16.

7. Arnett, G.W., Milam, S.B., and Gottesman, L., *Progressive mandibular retrusion--idiopathic condylar resorption. Part I.* American journal of orthodontics and dentofacial orthopedics : official publication of the American Association of Orthodontists, its constituent societies, and the American Board of Orthodontics, 1996. **110**(1): p. 8-15.

8. Arnett, G.W., Milam, S.B., and Gottesman, L., *Progressive mandibular retrusion-idiopathic condylar resorption. Part II.* American journal of orthodontics and dentofacial orthopedics : official publication of the American Association of Orthodontists, its constituent societies, and the American Board of Orthodontics, 1996. **110**(2): p. 117-127.

9. Athanasiou, K.A., Almarza, A.J., Detamore, M.S., and Kalpakci, K.N., *Tissue Engineering of Temporomandibular Joint Cartilage*. Synthesis Lectures on Tissue Engineering, ed. K.A. Athanasiou. 2009: Morgan & Claypool.

10. Axelsson, S., Holmlund, A., and Hjerpe, A., *An experimental model of osteoarthrosis in the temporomandibular joint of the rabbit.* Acta Odontologica Scandinavica, 1992. **50**(5): p. 273-280.

11. Baird, D.N. and Rea, W.J., *The temporomandibular joint implant controversy: A review of autogenous/alloplastic materials and their complications.* Journal of Nutritional and Environmental Medicine, 1998. **8**(3): p. 289-300.

12. Baird, D.N. and Rea, W.J., *The temporomandibular joint implant controversy. Part II: Its clinical implications.* Journal of Nutritional and Environmental Medicine, 1999. **9**(3): p. 209-222.

13. Baltali, E., Zhao, K.D., Koff, M.F., Durmuş, E., An, K.N., and Keller, E.E., *Kinematic Assessment of the Temporomandibular Joint Before and After Partial Metal Fossa Eminence Replacement Surgery: A Prospective Study.* Journal of Oral and Maxillofacial Surgery, 2008. **66**(7): p. 1383-1389.

14. Bell, R.B. and Kindsfater, C.S., *The Use of Biodegradable Plates and Screws to Stabilize Facial Fractures.* Journal of Oral and Maxillofacial Surgery, 2006. **64**(1): p. 31-39.

15. Benson, C.J., Eckert, S.P., and McCleskey, E.W., *Acid-evoked currents in cardiac sensory neurons: A possible mediator of myocardial ischemic sensation.* Circulation Research, 1999. **84**(8): p. 921-928.

16. Bereiter, D.A., Okamoto, K., and Bereiter, D.F., *Effect of persistent monoarthritis of the temporomandibular joint region on acute mustard oil-induced excitation of trigeminal subnucleus caudalis neurons in male and female rats.* Pain, 2005. **117**(1-2): p. 58-67.

17. Bey, M.J., Kline, S.K., Tashman, S., and Zauel, R., *Accuracy of biplane x-ray imaging combined with model-based tracking for measuring in-vivo patellofemoral joint motion.* Journal of Orthopaedic Surgery and Research, 2008. **3**(1): p. 38.

18. Bey, M.J., Zauel, R., Brock, S.K., and Tashman, S., *Validation of a new model-based tracking technique for measuring three-dimensional, in vivo glenohumeral joint kinematics.* Journal of Biomechanical Engineering, 2006. **128**(4): p. 604-609.

19. Bey, M.J., Zauel, R., Brock, S.K., and Tashman, S., *Validation of a new model-based tracking technique for measuring three-dimensional, in vivo glenohumeral joint kinematics.* J Biomech Eng, 2006. **128**(4): p. 604-9.

20. Bibb, C.A., Pullinger, A.G., and Baldioceda, F., *Serial variation in histological character of articular soft tissue in young human adult temporomandibular joint condyles.* Archives of Oral Biology, 1993. **38**(4): p. 343-352.

21. Bondarenko, A., Hewicker-Trautwein, M., Erdmann, N., Angrisani, N., Reifenrath, J., and Meyer-Lindenberg, A., *Comparison of morphological changes in efferent lymph nodes after implantation of resorbable and non-resorbable implants in rabbits.* BioMedical Engineering Online, 2011. **10**: p. 32.

22. Bosshardt-Luehrs, C.P.B. and Luder, H.U., *Cartilage matrix production and chondrocyte enlargement as contributors to mandibular condylar growth in monkeys (Macaca fascicularis).* American Journal of Orthodontics and Dentofacial Orthopedics, 1991. **100**(4): p. 362-369.

23. Brainerd, E.L., Baier, D.B., Gatesy, S.M., Hedrick, T.L., Metzger, K.A., Gilbert, S.L., and Crisco, J.J., *X-Ray reconstruction of moving morphology (XROMM): Precision, accuracy and applications in comparative biomechanics research.* Journal of Experimental Zoology Part A: Ecological Genetics and Physiology, 2010. **313 A**(5): p. 262-279.

24. Carlsson, G.E., *Epidemiology and Treatment Need for Temporomandibular Disorders.* Journal of Orofacial Pain, 1999. **13**(4): p. 232-237.

25. Charra, R., Datiche, F., Gigot, V., Schaal, B., and Coureaud, G., *Pheromone-induced odor learning modifies Fos expression in the newborn rabbit brain.* Behavioural Brain Research, 2013. **237**(0): p. 129-140.

26. Chaves, K., Munerato, M.C., Ligocki, A., Lauxen, I., and De Quadros, O.F., *Microscopic Analysis of the Temporomandibular Joint in Rabbits (Oryctolagus cuniculus L.) Using An Occlusal Interference.* Cranio, 2002. **20**(2): p. 116-124.

27. Chen, D.C., Lai, Y.L., Chi, L.Y., and Lee, S.Y., *Contributing factors of mandibular deformation during mouth opening.* Journal of Dentistry, 2000. **28**(8): p. 583-588.

28. Cholasueksa, P., Warita, H., and Soma, K., *Alterations of the rat temporomandibular joint in functional posterior displacement of the mandible.* Angle Orthodontist, 2004. **74**(5): p. 677-683.

29. Coggeshall, R.E., *Fos, nociception and the dorsal horn.* Prog Neurobiol, 2005. **77**(5): p. 299-352.

30. Cohen, B., Lai, W.M., and Mow, V.C., *A transversely isotropic biphasic model for unconfined compression of growth plate and chondroepiphysis.* Journal of Biomechanical Engineering, 1998. **120**(4): p. 491-496.

31. Craig, M., Bir, C., Viano, D., and Tashman, S., *Biomechanical response of the human mandible to impacts of the chin.* Journal of Biomechanics, 2008. **41**(14): p. 2972-2980.

32. Cutrer, F.M., Limmroth, V., Ayata, G., and Moskowitz, M.A., *Attenuation by valproate of c-fos immunoreactivity in trigeminal nucleus caudalis induced by intracisternal capsaicin.* British Journal of Pharmacology, 1995. **116**(8): p. 3199-3204.

33. Denkena, B., Podolsky, C., Lucas, A., Hassel, T., Witte, F., and Palm, O., *Processing of degradable surgical implants made of magnesium alloys.* Biomaterialien, 2005. **6**(3): p. 171.

34. Denkena, B., Witte, F., Podolsky, C., and Lucas, A. *Degradable implants made of magnesium alloys*. in *Proceedings of the 5th Euspen International Conference*. 2005. Montpellier, France.

35. Detamore, M.S., Orfanos, J.G., Almarza, A.J., French, M.M., Wong, M.E., and Athanasiou, K.A., *Quantitative analysis and comparative regional investigation of the extracellular matrix of the porcine temporomandibular joint disc.* Matrix Biol, 2005. **24**(1): p. 45-57.

36. Dolwick, M.F., *The temporomandibular joint: normal and abnormal anatomy*, in *Internal Derangements of the Temporomandibular Joint*, C.A. Helms, R.W. Katzberg, and M.F. Dolwick, Editors. 1983, Radiology Research and Education Foundation: San Francisco, CA. p. 1-14.

37. Duygulu, O., Alper Kaya, R., Oktay, G., and Arslan Kaya, A., *Investigation on the potential of magnesium alloy AZ31 as a bone implant.* Materials Science Forum, 2007. **546-549**: p. 421-424.

38. Dym, H. and Israel, H., *Diagnosis and Treatment of Temporomandibular Disorders.* Dental Clinics of North America, 2012. **56**(1): p. 149-161.

39. Erdmann, N., Angrisani, N., Reifenrath, J., Lucas, A., Thorey, F., Bormann, D., and Meyer-Lindenberg, A., *Biomechanical testing and degradation analysis of MgCa0.8 alloy screws: A comparative in vivo study in rabbits.* Acta Biomaterialia, 2011. **7**(3): p. 1421-1428.

40. Erdmann, N., Bondarenko, A., Hewicker-Trautwein, M., Angrisani, N., Reifenrath, J., Lucas, A., and Meyer-Lindenberg, A., *Evaluation of the soft tissue biocompatibility of MgCa0.8 and surgical steel 316L in vivo: A comparative study in rabbits.* BioMedical Engineering Online, 2010. **9**: p. 63.

41. Farndale, R.W., Sayers, C.A., and Barrett, A.J., *A direct spectrophotometric microassay for sulfated glycosaminoglycans in cartilage cultures.* Connect Tissue Res, 1982. **9**(4): p. 247-8.

42. Farrar, W.B. and McCarty, W.L., Jr., *The TMJ dilemma.* J Ala Dent Assoc, 1979. **63**(1): p. 19-26.

43. Flake, N.M., Bonebreak, D.B., and Gold, M.S., *Estrogen and inflammation increase the excitability of rat temporomandibular joint afferent neurons.* Journal of Neurophysiology, 2005. **93**(3): p. 1585-1597.

44. Fuentes, M.A., Opperman, L.A., Buschang, P., Bellinger, L.L., Carlson, D.S., and Hinton, R.J., *Lateral functional shift of the mandible: Part I. Effects on condylar cartilage thickness and proliferation.* American Journal of Orthodontics and Dentofacial Orthopedics, 2003. **123**(2): p. 153-159.

45. Gallo, L.M., *Modeling of Temporomandibular Joint Function Using MRI and Jaw-Tracking Technologies -- Mechanics.* Cells Tissues Organs, 2005. **180**(1): p. 54-68.

46. Goldstein, B.H., *Temporomandibular disorders: A review of current understanding.* Oral Surgery, Oral Medicine, Oral Pathology, Oral Radiology, and Endodontology, 1999. **88**(4): p. 379-385.

47. Gonzalez, Y.M., Greene, C.S., and Mohl, N.D., *Technological Devices in the Diagnosis of Temporomandibular Disorders.* Oral and Maxillofacial Surgery Clinics of North America, 2008. **20**(2): p. 211-220.

48. Gray, R.J.M., Davies, S.J., and Quayle, A.A., *Temporomandibular Disorders: A Clinical Approach*. 1995, London: British Dental Association.

49. Hagandora, C.K., Chase, T.W., and Almarza, A.J., *A Comparison of the Mechanical Properties of the Goat Temporomandibular Joint Disc to the Mandibular Condylar Cartilage in Unconfined Compression.* Journal of Dental Biomechanics, 2011. **2**(1).

50. Hampp, C., Angrisani, N., Reifenrath, J., Bormann, D., Seitz, J.M., and Meyer-Lindenberg, A., *Evaluation of the biocompatibility of two magnesium alloys as degradable implant materials in comparison to titanium as non-resorbable material in the rabbit.* Materials Science and Engineering C, 2013. **33**(1): p. 317-326.

51. Hampp, C., Ullmann, B., Reifenrath, J., Angrisani, N., Dziuba, D., Bormann, D., Seitz, J.M., and Meyer-Lindenberg, A., *Research on the biocompatibility of the new magnesium alloy LANd442-An in vivo study in the rabbit tibia over 26 weeks.* Advanced Engineering Materials, 2012. **14**(3): p. B28-B37.

52. Hansson, T. and Nordström, B., *Thickness of the soft tissue layers and articular disk in temporomandibular joints with deviations in form.* Acta Odontologica Scandinavica, 1977. **35**(6): p. 281-288.

53. Hansson, T., Oberg, T., Carlsson, G.E., and Kopp, S., *Thickness of the soft tissue layers and the articular disk in the temporomandibular joint.* Acta Odontologica Scandinavica, 1977. **35**(2): p. 77-83.

54. Haque, M.A., Anderst, W., Tashman, S., and Marai, G.E., *Hierarchical model-based tracking of cervical vertebrae from dynamic biplane radiographs.* Medical Engineering and Physics, 2013. **35**(7): p. 994-1004.

55. Harriott, A.M. and Gold, M.S., *Electrophysiological properties of dural afferents in the absence and presence of inflammatory mediators.* Journal of Neurophysiology, 2009. **101**(6): p. 3126-3134.

56. Harris, J.A., *Using c-fos as a Neural Marker of Pain.* Brain Research Bulletin, 1998. **45**(1): p. 1-8.

57. Henderson, S.E., Desai, R., Tashman, S., and Almarza, A.J., *Functional Analysis of the Rabbit Temporomandibular Joint Using Dynamic Biplane Imaging.* Journal of Biomechanics, 2014. **47**(6): p. 1360–1367.

58. Henderson, S.E., Tudares, M.A., Gold, M.S., and Almarza, A.J., *Analysis of Pain in the Rabbit Temporomandibular Joint after Unilateral Splint Placement.* Journal of Oral and Facial Pain and Headache, 2014. (Accepted).

59. Henderson, S.E., Verdelis, K., Maiti, S., Pal, S., Chung, W.L., Chou, D.-T., Kumta, P.N., and Almarza, A.J., *Magnesium Alloys as a Biomaterial for Degradable Craniofacial Screws.* Acta Biomaterialia, 2014. **10**(5): p. 2323-2332.

60. Hoskin, K.L., Zagami, A.S., and Goadsby, P.J., *Stimulation of the middle meningeal artery leads to Fos expression in the trigeminocervical nucleus: a comparative study of monkey and cat.* Journal of Anatomy, 1999. **194**(4): p. 579-588.

61. Huehnerschulte, T.A., Reifenrath, J., von Rechenberg, B., Dziuba, D., Seitz, J.M., Bormann, D., Windhagen, H., and Meyer-Lindenberg, A., *In vivo assessment of the host reactions to the biodegradation of the two novel magnesium alloys ZEK100 and AX30 in an animal model.* BioMedical Engineering Online, 2012. **11**: p. 14.

62. Huff, K.D., Asaka, Y., Griffin, A.L., Berg, W.P., Seager, M.A., and Berry, S.D., *Differential mastication kinematics of the rabbit in response to food and water: Implications for conditioned movement.* Integrative Physiological and Behavioral Science, 2004. **39**(1): p. 16-23.

63. Ikeda, T., Terayama, R., Jue, S.-S., Sugiyo, S., Dubner, R., and Ren, K., *Differential rostral projections of caudal brainstem neurons receiving trigeminal input after masseter inflammation.* The Journal of Comparative Neurology, 2003. **465**(2): p. 220-233.

64. Ingawalé, S. and Goswami, T., *Temporomandibular joint: Disorders, treatments, and biomechanics.* Annals of Biomedical Engineering, 2009. **37**(5): p. 976-996.

65. Inoue, M., Harasawa, Y., Yamamura, K., Ariyasinghe, S., and Yamada, Y., *Effects of food consistency on the pattern of extrinsic tongue muscle activities during mastication in freely moving rabbits.* Neuroscience Letters, 2004. **368**(2): p. 192-196.

66. Inoue, T., Kato, T., Masuda, Y., Nakamura, T., Kawamura, Y., and Morimoto, T., *Modifications of masticatory behavior after trigeminal deafferentation in the rabbit.* Experimental Brain Research, 1989. **74**(3): p. 579-591.

67. Jagger, R.G., Bates, J.F., and Kopp, S., *Temporomandibular Joint Dysfunction: Essentials*. 1994, Oxford: Butterworth-Heinemann Ltd.

68. Jankowski, M.P., Lawson, J.J., McIlwrath, S.L., Rau, K.K., Anderson, C.E., Albers, K.M., and Koerber, H.R., *Sensitization of Cutaneous Nociceptors after Nerve Transection and Regeneration: Possible Role of Target-Derived Neurotrophic Factor Signaling.* The Journal of Neuroscience, 2009. **29**(6): p. 1636-1647.

69. Janning, C., Willbold, E., Vogt, C., Nellesen, J., Meyer-Lindenberg, A., Windhagen, H., Thorey, F., and Witte, F., *Magnesium hydroxide temporarily enhancing osteoblast activity and decreasing the osteoclast number in peri-implant bone remodelling.* Acta Biomaterialia, 2010. **6**(5): p. 1861-1868.

70. Kalpakci, K.N., Willard, V.P., Wong, M.E., and Athanasiou, K.A., *An interspecies comparison of the temporomandibular joint disc.* Journal of Dental Research, 2011. **90**(2): p. 193-198.

71. Keller, E.E., Baltali, E., Liang, X., Zhao, K., Huebner, M., and An, K.N., *Temporomandibular custom hemijoint replacement prosthesis: Prospective clinical and kinematic study.* Journal of Oral and Maxillofacial Surgery, 2012. **70**(2): p. 276-288.

72. Kessler, W., Kirchhoff, C., Reeh, P.W., and Handwerker, H.O., *Excitation of cutaneous afferent nerve endings in vitro by a combination of inflammatory mediators and conditioning effect of substance P.* Experimental Brain Research, 1992. **91**(3): p. 467-476.

73. Kim, S.-M., Jo, J.-H., Lee, S.-M., Kang, M.-H., Kim, H.-E., Estrin, Y., Lee, J.-H., Lee, J.-W., and Koh, Y.-H., *Hydroxyapatite-coated magnesium implants with improved in vitro and in vivo biocorrosion, biocompatibility, and bone response.* Journal of Biomedical Materials Research Part A, 2014. **102**(2): p. 429-441

74. Krause, A., Von Der Höh, N., Bormann, D., Krause, C., Bach, F.W., Windhagen, H., and Meyer-Lindenberg, A., *Degradation behaviour and mechanical properties of magnesium implants in rabbit tibiae.* Journal of Materials Science, 2010. **45**(3): p. 624-632.

75. Langenbach, G.E.J., Weijs, W.A., Brugman, P., and Van Eijden, T.M.G.J., *A longitudinal electromyographic study of the postnatal maturation of mastication in the rabbit.* Archives of Oral Biology, 2001. **46**(9): p. 811-820.

76. Lawson, J.J., McIlwrath, S.L., Woodbury, C.J., Davis, B.M., and Koerber, H.R., *TRPV1 Unlike TRPV2 Is Restricted to a Subset of Mechanically Insensitive Cutaneous Nociceptors Responding to Heat.* The Journal of Pain, 2008. **9**(4): p. 298-308.

77. Leiggener, C.S., Erni, S., and Gallo, L.M., *Novel approach to the study of jaw kinematics in an alloplastic TMJ reconstruction.* International Journal of Oral and Maxillofacial Surgery, 2012. **41**(9): p. 1041-1045.

78. Li, Z., Gu, X., Lou, S., and Zheng, Y., *The development of binary Mg–Ca alloys for use as biodegradable materials within bone.* Biomaterials, 2008. **29**(10): p. 1329-1344.

79. Linsen, S.S., Reich, R.H., and Teschke, M., *Mandibular kinematics in patients with alloplastic total temporomandibular joint replacementa prospective study.* Journal of Oral and Maxillofacial Surgery, 2012. **70**(9): p. 2057-2064.

80. Liu, C., Kaneko, S., and Soma, K., *Glenoid fossa responses to mandibular lateral shift in growing rats.* Angle Orthodontist, 2007. **77**(4): p. 660-667.

81. Lu, Y., McNearney, T.A., Wilson, S.P., Yeomans, D.C., and Westlund, K.N., *Joint capsule treatment with enkephalin-encoding HSV-1 recombinant vector reduces inflammatory damage and behavioural sequelae in rat CFA monoarthritis.* European Journal of Neuroscience, 2008. **27**(5): p. 1153-1165.

82. Mao, J.J., Rahemtulla, F., and Scott, P.G., *Proteoglycan expression in the rat temporomandibular joint in response to unilateral bite raise.* Journal of Dental Research, 1998. **77**(7): p. 1520-1528.

83. Markolf, K.L., Bargar, W.L., Shoemaker, S.C., and Amstutz, H.C., *The role of joint load in knee stability.* Journal of Bone and Joint Surgery - Series A, 1981. **63**(4): p. 570-585.

84. Matsuka, Y., Kitada, Y., Mitoh, Y., Adachi, A., and Yamashita, A., *Effects of a bite-raising splint on the duration of the chewing cycle and the EMG activities of masticatory muscles during chewing in freely moving rabbits.* Journal of Oral Rehabilitation, 1998. **25**(2): p. 159-165.

85. McNeill, C., *Management of temporomandibular disorders: Concepts and controversies.* The Journal of Prosthetic Dentistry, 1997. **77**(5): p. 510-522.

86. Mejersjo, C. and Hollender, L., *Radiography of the temporomandibular joint in female patients with TMJ pain or dysfunction. A seven year follow-up.* Acta Radiologica - Series Diagnosis, 1984. **25**(3): p. 169-176.

87. Mercuri, L.G., *Re: Dimitroulis, G. The role of surgery in the management of disorders of the temporomandibular joint: a critical review of the literature. Part 2. Int J Oral Maxillofac Surg 2005: 34: 231-237.* Int J Oral Maxillofac Surg, 2006. **35**(3): p. 284-6.

88. Mercuri, L.G., *Surgical management of TMJ arthritis*, in *TMDs, an evidence-based approach to diagnosis and treatment*, D.M. Laskin, C.S. Greene, and W.L. Hylander, Editors. 2006, Quintessence: Chicago. p. 455-468.

89. Mercuri, L.G., *A rationale for total alloplastic temporomandibular joint reconstruction in the management of idiopathic/progressive condylar resorption.* J Oral Maxillofac Surg, 2007. **65**: p. 1600-1609 erratum.

90. Mercuri, L.G. and Giobbie-Hurder, A., *Long-term outcomes after total alloplastic temporomandibular joint reconstruction following exposure to failed materials.* J Oral Maxillofac Surg, 2004. **62**(9): p. 1088-96.

91. Mercuri, L.G., Wolford, L.M., Sanders, B., White, R.D., and Giobbie-Hurder, A., *Long-term follow-up of the CAD/CAM patient fitted total temporomandibular joint reconstruction system.* J Oral Maxillofac Surg, 2002. **60**(12): p. 1440-8.

92. Meslemani, D. and Kellman, R.M., *Recent advances in fixation of the craniomaxillofacial skeleton.* Current Opinion in Otolaryngology and Head and Neck Surgery, 2012. **20**(4): p. 304-309.

93. Meyer-Lindenberg, A., Thomann, M., Krause, A., Bormann, D., Von Rechenberg, B., and Windhagen, H., *Investigation on the use of a magnesium alloy as a new resorbable implant material for orthopaedic surgery.* Kleintierpraxis, 2010. **55**(7): p. 349-363.

94. Mizumura, K., *Natural history of nociceptor sensitization: the search fora peripheral mechanism of hyperalgesia.* Pain Reviews, 1998. **5**(2): p. 59.

95. Morimoto, T., Inoue, T., Nakamura, T., and Kawamura, Y., *Characteristics of rhythmic jaw movements of the rabbit.* Archives of Oral Biology, 1985. **30**(9): p. 673-677.

96. Morita, T., Fujiwara, T., Negoro, T., Kurata, C., Maruo, H., Kurita, K., Goto, S., and Hiraba, K., *Movement of the mandibular condyle and activity of the masseter and lateral pterygoid muscles during masticatory-like jaw movements induced by electrical stimulation of the cortical masticatory area of rabbits.* Archives of Oral Biology, 2008. **53**(5): p. 462-477.

97. Naeije, M., *Local kinematic and anthropometric factors related to the maximum mouth opening in healthy individuals.* Journal of Oral Rehabilitation, 2002. **29**(6): p. 534-539.

98. Nakano, H., Maki, K., Shibasaki, Y., and Miller, A.J., *Three-dimensional changes in the condyle during development of an asymmetrical mandible in a rat: A microcomputed tomography study.* American Journal of Orthodontics and Dentofacial Orthopedics, 2004. **126**(4): p. 410-420.

99. NIH and NIDCR. *TMJ Disorders*. 2010; Available from: http://www.nidcr.nih.gov/OralHealth/Topics/TMJ/TMJDisorders.htm.

100. Nitzan, D.W., *The process of lubrication impairment and its involvement in temporomandibular joint dics displacement. A theoretical concept.* Journal of Oral and Maxillofacial Surgery, 2001. **59**(1): p. 36-45.

101. Palla, S., Gallo, L.M., and Gössi, D., *Dynamic stereometry of the temporomandibular joint.* Orthodontics & Craniofacial Research, 2003. **6 Suppl 1**: p. 37-47.

102. Poon, C.C.H. and Verco, S., *Evaluation of fracture healing and subimplant bone response following fixation with a locking miniplate and screw system for mandibular angle fractures in a sheep model.* International Journal of Oral and Maxillofacial Surgery, 2013. **42**(6): p. 736-745.

103. Proff, P., Gedrange, T., Franke, R., Schubert, H., FanghÃ¤nel, J., Miehe, B., and Harzer, W., *Histological and histomorphometric investigation of the condylar cartilage of juvenile pigs after anterior mandibular displacement.* Annals of Anatomy, 2007. **189**(3): p. 269-275.

104. Pullinger, A.G., Baldioceda, F., and Bibb, C.A., *Relationship of TMJ articular soft tissue to underlying bone in young adult condyles.* Journal of dental research, 1990. **69**(8): p. 1512-1518.

105. Rees, L.A., *The structure and function of the mandibular joint.* Br Dent J, 1954. **96**(6): p. 125-33.

106. Ren, K., *An improved method for assessing mechanical allodynia in the rat.* Physiology and Behavior, 1999. **67**(5): p. 711-716.

107. Sato, C., Muramoto, T., and Soma, K., *Functional lateral deviation of the mandible and its positional recovery on the rat condylar cartilage during the growth period.* Angle Orthodontist, 2006. **76**(4): p. 591-597.

108. Schipplein, O.D. and Andriacchi, T.P., *Interaction between active and passive knee stabilizers during level walking.* Journal of Orthopaedic Research, 1991. **9**(1): p. 113-119.

109. Schwartz, G., Enomoto, S., Valiquette, C., and Lund, J.P., *Mastication in the rabbit: A description of movement and muscle activity.* Journal of Neurophysiology, 1989. **62**(1): p. 273-287.

110. Sergerie, K., Lacoursière, M.O., Lévesque, M., and Villemure, I., *Mechanical properties of the porcine growth plate and its three zones from unconfined compression tests.* Journal of Biomechanics, 2009. **42**(4): p. 510-516.

111. Sergl, H.G. and Farmand, M., *Experiments with unilateral bite planes in rabbits.* Angle Orthodontist, 1975. **45**(2): p. 108-114.

112. Shaw, R.M. and Molyneux, G.S., *The effects of induced dental malocclusion on the fibrocartilage disc of the adult rabbit temporomandibular joint.* Archives of Oral Biology, 1993. **38**(5): p. 415-422.

113. Sindelar, B.J., Evanko, S.P., Alonzo, T., Herring, S.W., and Wight, T., *Effects of intraoral splint wear on proteoglycans in the temporomandibular joint disc.* Arch Biochem Biophys, 2000. **379**(1): p. 64-70.

114. Singh, M. and Detamore, M.S., *Stress Relaxation Behavior of Mandibular Condylar Cartilage Under High-Strain Compression.* Journal of Biomechanical Engineering, 2009. **131**(6): p. 061008-1-5.

115. Solberg, W., Woo, M., and Houston, J., *Prevalence of mandibular dysfunction in young adults.* J Am Dent Assoc, 1979. **98**(25).

116. Stegenga, B., De Bont, L.G.M., and Boering, G., *Osteoarthrosis as the cause of craniomandibular pain and dysfunction: A unifying concept.* Journal of Oral and Maxillofacial Surgery, 1989. **47**(3): p. 249-256.

117. Suuronen, R., Pohjonen, T., Tech, L., Vasenius, J., and Vainionpaa, S., *Comparison of absorbable self-reinforced multilayer poly-l-lactide and metallic plates for the fixation of mandibular body osteotomies: An experimental study in sheep.* Journal of Oral and Maxillofacial Surgery, 1992. **50**(3): p. 255-262.

118. Swann, A.C. and Seedhom, B.B., *Improved techniques for measuring the indentation and thickness of articular cartilage.* Proceedings of the Institution of Mechanical Engineers, Part H: Journal of Engineering in Medicine, 1989. **203**(3): p. 143-150.

119. Takeda, M., Tsuboi, Y., Kitagawa, J., Nakagawa, K., Iwata, K., and Matsumoto, S., *Potassium channels as a potential therapeutic target for trigeminal neuropathic and inflammatory pain.* Molecular Pain, 2011. **7**.

120. Tanaka, E., Detamore, M.S., and Mercuri, L.G., *Degenerative disorders of the Temporomandibular joint: etiology, diagnosis, and treatment.* Journal of Dental Research, 2008. **87**(4): p. 296-307.

121. Tanaka, E., Iwabe, T., Dalla-Bona, D.A., Kawai, N., Van Eijden, T., Tanaka, M., Kitagawa, S., Takata, T., and Tanne, K., *The effect of experimental cartilage damage and impairment and restoration of synovial lubrication on friction in the temporomandibular joint.* Journal of Orofacial Pain, 2005. **19**(4): p. 331-336.

122. Tanaka, E., Iwabuchi, Y., Rego, E.B., Koolstra, J.H., Yamano, E., Hasegawa, T., Kawazoe, A., Kawai, N., and Tanne, K., *Dynamic shear behavior of mandibular condylar cartilage is dependent on testing direction.* Journal of Biomechanics, 2008. **41**(5): p. 1119-1123.

123. Tanaka, E., Rego, E.B., Iwabuchi, Y., Inubushi, T., Koolstra, J.H., Van Eijden, T.M.G.J., Kawai, N., Kudo, Y., Takata, T., and Tanne, K., *Biomechanical response of condylar cartilage-on-bone to dynamic shear.* Journal of Biomedical Materials Research - Part A, 2008. **85**(1): p. 127-132.

124. Tashman, S. and Anderst, W.J., *In-vivo measurement of dynamic joint motion using high speed biplane radiography and CT: application to canine ACL deficiency.* Journal of Biomechanical Engineering, 2003. **125**(2): p. 238-45.

125. Tashman, S. and Anderst, W.J., *In-vivo measurement of dynamic joint motion using high speed biplane radiography and CT: application to canine ACL deficiency.* J Biomech Eng, 2003. **125**(2): p. 238-45.

126. Tashman, S., Kolowich, P., Collon, D., Anderson, K., and Anderst, W.J., *Dynamic Function of the ACL-reconstructed Knee during Running.* Clinical Orthopaedics and Related Research, 2007. **454**(January): p. 66-73.

127. Thomann, M., Krause, C., Angrisani, N., Bormann, D., Hassel, T., Windhagen, H., and Meyer-Lindenberg, A., *Influence of a magnesium-fluoride coating of magnesium-based implants (MgCa0.8) on degradation in a rabbit model.* Journal of Biomedical Materials Research - Part A, 2010. **93**(4): p. 1609-1619.

128. Thomann, M., Krause, C., Bormann, D., Von Der Höh, N., Windhagen, H., and Meyer-Lindenberg, A., *Comparison of the resorbable magnesium alloys LAE442 und MgCa0.8 concerning their mechanical properties, their progress of degradation and the bone-implant-contact after 12 months implantation duration in a rabbit model.* Materialwissenschaft und Werkstofftechnik, 2009. **40**(1-2): p. 82-87.

129. Timmis, D.P., Aragon, S.B., Van Sickels, J.E., and Aufdemorte, T.B., *Comparative study of alloplastic materials for temporomandibular joint disc replacement in rabbits.* Journal of Oral and Maxillofacial Surgery, 1986. **44**(7): p. 541-554.

130. Tominaga, K., Alstergren, P., Kurita, H., and Kopp, S., *Serotonin in an antigen-induced arthritis of the rabbit temporomandibular joint.* Archives of Oral Biology, 1999. **44**(7): p. 595-601.

131. Tominaga, K., Yamada, Y., and Fukuda, J., *Changes in chewing pattern after surgically induced disc displacement in the rabbit temporomandibular joint.* Journal of Oral and Maxillofacial Surgery, 2000. **58**(4): p. 400-405.

132. Travers, K.H., Buschang, P.H., Hayasaki, H., and Throckmorton, G.S., *Associations between incisor and mandibular condylar movements during maximum mouth opening in humans.* Archives of Oral Biology, 2000. **45**(4): p. 267-275.

133. Turvey, T.A., Proffit, W.P., and Phillips, C., *Biodegradable fixation for craniomaxillofacial surgery: A 10-year experience involving 761 operations and 745 patients.* International Journal of Oral and Maxillofacial Surgery, 2011. **40**(3): p. 244-249.

134. Ueki, K., Takazakura, D., Marukawa, K., Shimada, M., Nakagawa, K., Takatsuka, S., and Yamamoto, E., *The use of polylactic acid/polyglycolic acid copolymer and gelatin sponge complex containing human recombinant bone morphogenetic protein-2 following condylectomy in rabbits.* Journal of Cranio-Maxillofacial Surgery, 2003. **31**(2): p. 107-114.

135. van den Bos, T., Speijer, D., Bank, R.A., Brömme, D., and Everts, V., *Differences in matrix composition between calvaria and long bone in mice suggest differences in biomechanical properties and resorption: Special emphasis on collagen.* Bone, 2008. **43**(3): p. 459-468.

136. Voiner, J., Yu, J., Deitrich, P., Chafin, C., and Giannakopoulos, H., *Analysis of mandibular motion following unilateral and bilateral alloplastic TMJ reconstruction.* International Journal of Oral and Maxillofacial Surgery, 2011. **40**(6): p. 569-571.

137. Von Der Höh, N., Bormann, D., Lucas, A., Denkena, B., Hackenbroich, C., and Meyer-Lindenberg, A., *Influence of different surface machining treatments of magnesium-based resorbable implants on the degradation behavior in rabbits.* Advanced Engineering Materials, 2009. **11**(5): p. B47-B54.

138. Von Der Höh, N., Bormann, D., Lucas, A., Thorey, F., and Meyer-Lindenberg, A., *Comparison of the in vivo degradation progress of solid magnesium alloy cylinders and screw-shaped magnesium alloy cylinders in a rabbit model.* Materials Science Forum, 2010. **638-642**: p. 742-747.

139. Von Der Höh, N., Krause, A., Hackenbroich, C., Bormann, D., Lucas, A., and Meyer-Lindenberg, A., *Influence of different surface machining treatments of resorbable implants of different magnesium alloys - A primary study in rabbits.* Deutsche Tierarztliche Wochenschrift, 2006. **113**(12): p. 439-446.

140. Von Der Höh, N., Von Rechenberg, B., Bormann, D., Lucas, A., and Meyer-Lindenberg, A., *Influence of different surface machining treatments of resorbable magnesium alloy implants on degradation – EDX-analysis and histology results.* Materialwissenschaft und Werkstofftechnik, 2009. **40**(1-2): p. 88-93.

141. Wadhwa, S. and Kapila, S., *TMJ disorders: future innovations in diagnostics and therapeutics.* Journal of Dental Education, 2008. **72**(8): p. 930-947.

142. Waizy, H., Weizbauer, A., Maibaum, M., Witte, F., Windhagen, H., Lucas, A., Denkena, B., Meyer-Lindenberg, A., and Thorey, F., *Biomechanical characterisation of a degradable magnesium-based (MgCa0.8) screw.* Journal of Materials Science: Materials in Medicine, 2012. **23**(3): p. 649-655.

143. Ware, W.H., *Clinical presentation*, in *Internal Derangements of the Temporomandibular Joint*, C.A. Helms, R.W. Katzberg, and M.F. Dolwick, Editors. 1983, Radiology Research and Education Foundation: San Francisco, CA. p. 15-30.

144. Watanabe, A., Yamaguchi, M., Utsunomiya, T., Yamamoto, H., and Kasai, K., *Histopathological changes in collagen and matrix metalloproteinase levels in articular condyle of experimental model rats with jaw deformity.* Orthodontics and Craniofacial Research, 2008. **11**(2): p. 105-118.

145. Wattanachai, T., Yonemitsu, I., Kaneko, S., and Soma, K., *Functional lateral shift of the mandible effects on the expression of eCM in rat temporomandibular cartilage.* Angle Orthodontist, 2009. **79**(4): p. 652-659.

146. Weijs, W.A., Brugman, P., and Grimbergen, C.A., *Jaw movements and muscle activity during mastication in growing rabbits.* Anatomical Record, 1989. **224**(3): p. 407-416.

147. Weijs, W.A. and Dantuma, R., *Functional anatomy of the masticatory apparatus in the rabbit (Oryctolagus cuniculus L.).* Netherlands Journal of Zoology, 1980. **31**(1): p. 99-147.

148. Weijs, W.A., Korfage, J.A.M., and Langenbach, G.J., *The functional significance of the position of the centre of rotation for jaw opening and closing in the rabbit.* Journal of Anatomy, 1989. **162**: p. 133-148.

149. Wilkes, C.H., *Internal derangements of the temporomandibular joint. Pathological variations.* Archives of Otolaryngology - Head and Neck Surgery, 1989. **115**(4): p. 469-77.

150. Willbold, E., Kalla, K., Bartsch, I., Bobe, K., Brauneis, M., Remennik, S., Shechtman, D., Nellesen, J., Tillmann, W., Vogt, C., and Witte, F., *Biocompatibility of rapidly solidified magnesium alloy RS66 as a temporary biodegradable metal.* Acta Biomaterialia, 2013. **9**(10): p. 8509-8517.

151. Willbold, E., Kaya, A.A., Kaya, R.A., Beckmann, F., and Witte, F., *Corrosion of magnesium alloy AZ31 screws is dependent on the implantation site.* Materials Science and Engineering: B, 2011. **176**(20): p. 1835-1840.

152. Witte, F., Fischer, J., Nellesen, J., Crostack, H.-A., Kaese, V., Pisch, A., Beckmann, F., and Windhagen, H., *In vitro and in vivo corrosion measurements of magnesium alloys.* Biomaterials, 2006. **27**(7): p. 1013-1018.

153. Witte, F., Fischer, J., Nellesen, J., Vogt, C., Vogt, J., Donath, T., and Beckmann, F., *In vivo corrosion and corrosion protection of magnesium alloy LAE442.* Acta Biomaterialia, 2010. **6**(5): p. 1792-1799.

154. Witte, F., Kaese, V., Haferkamp, H., Switzer, E., Meyer-Lindenberg, A., Wirth, C.J., and Windhagen, H., *In vivo corrosion of four magnesium alloys and the associated bone response.* Biomaterials, 2005. **26**(17): p. 3557-3563.

155. Witte, F., Podolsky, C., Hassel, T., and Lucas, A., *Fertigung von magnesium-implantaten.* Werkstattstechnik, 2004. **94**: p. 692-696.

156. Witte, F., Ulrich, H., Palm, C., and Willbold, E., *Biodegradable magnesium scaffolds: Part II: Peri-implant bone remodeling.* Journal of Biomedical Materials Research - Part A, 2007. **81**(3): p. 757-765.

157. Witte, F., Ulrich, H., Rudert, M., and Willbold, E., *Biodegradable magnesium scaffolds: Part I: Appropriate inflammatory response.* Journal of Biomedical Materials Research - Part A, 2007. **81**(3): p. 748-756.

158. Xu, L., Pan, F., Yu, G., Yang, L., Zhang, E., and Yang, K., *In vitro and in vivo evaluation of the surface bioactivity of a calcium phosphate coated magnesium alloy.* Biomaterials, 2009. **30**(8): p. 1512-1523.

159. Xu, L., Yu, G., Zhang, E., Pan, F., and Yang, K., *In vivo corrosion behavior of Mg-Mn-Zn alloy for bone implant application.* Journal of Biomedical Materials Research - Part A, 2007. **83**(3): p. 703-711.

160. Yamada, Y. and Haraguchi, N., *Reflex changes in the masticatory muscles with load perturbations during chewing hard and soft food.* Brain Research, 1995. **669**(1): p. 86-92.

161. Yamada, Y., Haraguchi, N., Oi, K., and Sasaki, M., *Two-dimensional jaw tracking and EMG recording system implanted in the freely moving rabbit.* Journal of Neuroscience Methods, 1988. **23**(3): p. 257-261.

162. Yamada, Y., Uchida, K., and Sato, T., *Mandibular movement trajectories and masticatory muscle activities in the rabbit in the sleep and wake states.* Dentistry in Japan, 1990. **27**(1): p. 35-39.

163. Yang, J.X., Cui, F.Z., Lee, I.S., Zhang, Y., Yin, Q.S., Xia, H., and Yang, S.X., *In vivo biocompatibility and degradation behavior of Mg alloy coated by calcium phosphate in a rabbit model.* Journal of Biomaterials Applications, 2012. **27**(2): p. 153-164.

164. Yoon, H.J., Baltali, E., Zhao, K.D., Rebellato, J., Kademani, D., An, K.N., and Keller, E.E., *Kinematic Study of the Temporomandibular Joint in Normal Subjects and Patients Following Unilateral Temporomandibular Joint Arthrotomy With Metal Fossa-Eminence Partial Joint Replacement.* Journal of Oral and Maxillofacial Surgery, 2007. **65**(8): p. 1569-1576.

165. You, B.M., Siy, P., Anderst, W., and Tashman, S., *In vivo measurement of 3-D skeletal kinematics from sequences of biplane radiographs: Application to knee kinematics.* IEEE Transactions on Medical Imaging, 2001. **20**(6): p. 514-525.

166. Zarb, G.A. and Carlsson, G.E., *Temporomandibular Disorders: Osteoarthritis.* Journal of Orofacial Pain, 1999. **13**(4): p. 295-306.

167. Zhang, E., Xu, L., Yu, G., Pan, F., and Yang, K., *In vivo evaluation of biodegradable magnesium alloy bone implant in the first 6 months implantation.* Journal of Biomedical Materials Research Part A, 2009. **90A**(3): p. 882-893.

168. Zhang, S., Zhang, X., Zhao, C., Li, J., Song, Y., Xie, C., Tao, H., Zhang, Y., He, Y., Jiang, Y., and Bian, Y., *Research on an Mg–Zn alloy as a degradable biomaterial.* Acta Biomaterialia, 2010. **6**(2): p. 626-640.

169. Zhou, Q., Imbe, H., Dubner, R., and Ren, K., *Persistent Fos protein expression after orofacial deep or cutaneous tissue inflammation in rats: Implications for persistent orofacial pain.* Journal of Comparative Neurology, 1999. **412**(2): p. 276-291.